UNIVERSITAT DE BARCELONA

The role of microtubule nucleation during neural development

Ricardo Silva dos Santos Vais

UNIVERSITAT DE BARCELONA

FACULTAT DE FARMÀCIA I CIÈNCIES DE L'ALIMENTACIÓ

Programa de Doctorat en Biomedicina

The role of microtubule nucleation during neural development

Ricardo Viais

2019

UNIVERSITAT DE BARCELONA

FACULTAT DE FARMÀCIA I CIÈNCIES DE L'ALIMENTACIÓ

Programa de Doctorat en Biomedicina

The role of microtubule nucleation during neural development

Memòria presentada per: Ricardo Silva dos Santos Viais per optar al títol de doctor per la Universitat de Barcelona

Jens Lüders
(Director de la tesis)

Ricardo Silva dos Santos Viais
(Doctorando)

Albert Tauler Girona
(Tutor de la tesis)

Ricardo Viais, 2019

About the cover: Fixed mouse hippocampal neurons cultured *in vitro* and stained with an α-tubulin antibody (blue) that labels microtubules. Acknowledgement to Victor Neves for his help with the design.

Aos meus pais, à minha irmã e aos meus avós
por serem os meus pilares e pelo seu amor e exemplo constantes

(To my parents, my sister and my grandparents
for being my cornerstone and for their constant love and good examples)

ACKNOWLEDGEMENTS

Developing the work presented in this thesis and reaching this important moment in my life have just been possible with the contribution and support of many people who are part of my life. Even though it is impossible to list all of them, I would like to dedicate the next pages to acknowledge some of the people who made this moment possible.

First, I would like to thank Isabelle Vernos, Sebastian Pons, Niels Galjart, Joan Roig and Sebastian Maurer who dedicated some of their time and energy to evaluate and discuss the present work. I hope you enjoy it and that your comments allow me to improve both this project and my qualities as a scientist.

I would also like to thank Travis Stracker, Eduardo Soriano and Marco Milán who, as members of my Thesis Advisory Committee, contributed with valuable critics and suggestions during the last five years.

To Jens Lüders who, apart from being my thesis director, has been a true mentor. Thank you for allowing me to develop my PhD thesis in your laboratory and for trusting and supporting my work. Furthermore, thank you for your constant availability to embrace long discussions which always started late and ended up too late. It was and it is a pleasure to be part of your team.

To Joan Roig for your advices and for making our lab meetings more challenging (and longer).

And because the success of a PhD starts long before the PhD I would like to dedicate part of this thesis to all these teachers who willingly or unwillingly contributed to my love for science and for me to follow a scientific career. Specially, I must thank Marcel Jimenez, my Master thesis director who I admire and who is a great mentor, scientist and communicator.

Like the γTuRC needs its GCPs its GCPs, this thesis would have been impossible without all the former and current members of the Microtubule Nucleation Laboratory. To all of you, thank you! Specially to Carlos Sanchez for being by first tutor at IRB. Even though sometimes we may have different working methods, it was a pleasure working with you and taking you as an example of critical thinking, accuracy and as a scientist and friend.

To Rosita whose heart is of the size of the world. I really enjoyed the time we spent together and all these spontaneous visits to Tacos Tacos when WBs, IFs or IPs did, or did not, work. To Francisco for building up the Portuguese team in the lab and for his advices.

To Cristina for your technical help and, particularly, for the thousands of PCRs which I was always asking you, “with a bit of urgency”.

To Artur Ezquerra whose presence in the lab is really missed (until I took your sunny spot next to the window 😊). Muchas gracias por ser un gran compañero de PhD, por enseñarme que culturas y cultivos no es lo mismo, que es más fácil decir nevera que “jefjijerador” (refrijerador) y por estar siempre en desacuerdo solo porque estamos de acuerdo.

To Nina and Aamir for their help and experience as Lüders Lab Post-Docs and to Ilaria for her constant availability to help us, PhD students, and for the funny moments surfing.

To Fabian because it is very important to brainstorm good (or not so good) jokes all day and for your great scientific contribution to the lab.

A Martita por su gran corazón, apoyo y amistad y por todos los buenos momentos pasados jugando partiditas de cartas, viajando, escalando o simplemente tomando un té y hablando de la vida.

Al papa frita de Joel por darle su nombre a Joelin like-protein, por su amistad, por “ultrapasarme” escalando y por enseñarme que se pueden intentar las azules y las rojitas y que el bodyboard sí que mola más.

I would also like to thank Dr. Sadanori Watanabe and Dr. Goshima for sharing with us their floxed-*Haus6* mouse model and Dr. Étienne Coyaud and Dr. Brian Raught for their collaboration in analysing the GCP3 pulldowns by mass spectrometry.

In addition, I wish to thank to Toni (Antoni Parcerisas) for his availability and for his great help in solving many problems with neuron primary cultures and with the experiments with CamKIIα-Cre mice which, in the end, were not included in this thesis.

Furthermore, developing this work would have been impossible without the support of the IRB and PCB core facilities to which teams I am very thankful.

To the Advanced Microscopy Facility members, and particularly to Lidia, Anna and Niko for their help and for not getting mad at me when I ask 1000 times the same thing.

To the team of the Histopathology facility for their great work and kindness and, particularly, to Neus, Monica and Anna with whom I worked for often. Aquí tengo que hacer un agradecimiento especial a Anais por su preciosa ayuda y por entenderme cuando le pido bloques de OCT y cortes raros, siempre “para ayer”.

To the members of the Animal Facility. Thank you for your efficiency, kindness and for allowing us to make sure that our research is done with the minimal impact on animal welfare. Your work is essential for making ethical science at the highest level.

During the last 5 years IRB allowed me to grow, not only as scientist, but also as a person learning how to manage different projects and contributing to our community. Being part of the Student council and organising the 1st ENABLE conference were both a big challenge and great experiences. I would like to thank all my colleagues and friends who joined me in these projects. Here I must give a special acknowledgement to Clara Caminal for always being so kind and patient.

To Leyre Caracuel for taking care of us, PhD students and for your impeccable work. Pero, sobre todo gracias por tu amistad, por nuestras conversaciones, viajes, por ser la única

persona que me corrige el castellano (¡muy bien!) y por tu fantástica terraza. Y venga, a entrenar para los próximos 21 Km.

To those friendships which I built during these last five years at IRB, which in some cases started already when I came here for the interviews. I would like to specially thank Susana, Alexandra, Ernest, Gemma, Helena Martin, Gianmarco y Jordi Badia for making the PhD life much nicer and happier. Furthermore, to Craig, thanks for keep trying to say frango, or pão, for knowing how to share Welcome Party tickets and for our conversations. To Jürgen, thank you for walking with me "El Camino" and for introducing me to the world of climbing and surfing.

Here, I must give a special "thank you" to Laura for all the great moments that we passed during the thesis and for these awful moments we passed while writing this thesis. "Esk" sobrevivir a todo el estrés de la escrita fue mucho más fácil teniendo la mejor compañera de escrita del mondo. Y celebrar la tesis será aún mejor porque defendemos en la misma semana 😊

I would also like to thank Leyre (again), Jürgen and Craig (also again) and Cristina Füster, Helena Roura, Enric Ros and Marina for building up the "Cadiz teams" and, in some cases, the "Zarautz team", "Sallent team", "Canarias team", "Nijmegen team" or "NOS Alive team". Those were all great moments and I wish the list of these great travels keep growing.

También me gustaría agradecer a Silvana por su amistad y por contribuir, junto con Cata, Caro y muchos otros, para mi formación Chilena. A Pedro y a Freixo, gracias por los buenos momentos mientras escribía la tesis y por apoyarme intentado siempre convencerme de que "mejor quedar que escribir demasiado".

To my long-time friend Fabiana, obrigado por seres uma boa copiloto (é discutível) e uma fala barato como eu. Agora é a tua vez, fico à espera da tua tese e levarei uma sopinha de legumes 😊

To my best friend and brother Miguel, obrigado por dizeres que já não sei falar português e pela eterna amizade.

Y porque en estos cinco años vivir en Calle Padua trajo muy buenos compañeros de piso y amistades quiero dejar un agradecimiento especial a Andrea, a Jenny (que me hace siempre tan feliz por quedarse feliz cuando yo cocino) a Arianna y a Simone (por ser como un hermanito pequeño que deja sus cosas por todas partes pero que cocina como un verdadero chef, insiste que puedo cantar y que me enseñó a hacer el 8).

Y porque quedarme en calle Padua solo fue posible porque dos angelitos me aceptaron "solamente por 3 meces" (¡eso decían!). Muchas gracias a Catalina de los Ángeles (Cata) y Carolina Beltrán (Caro) y a sus familias. Es imposible imaginar estos años sin vosotras de la misma manera que es imposible agradecer a una, sin agradecer a la otra. ¡Gracias por contaminar mi castellano con vuestro chileno poh! Gracias por todos los momentos que pasamos como una verdadera familia.

And at last, but not least, I would like to tell you how grateful I am for having the family I have. To all of them, I dedicate this thesis.

Obrigado aos meus avós (Mimi, João, Deolinda e António) pelo seu eterno e incondicional amor e por tudo o que me ensinaram. E que um dia eu represente para alguém o que vocês representam para mim.

À Marianolas por ser a irmã mais linda e mais fixe do mundo. Tenho muito orgulho em ti.

Aos meus pais pelo exemplo que são e porque apesar da distância é como se estivessem sempre comigo. Quaisquer palavras são insuficientes para descrever a minha gratidão.

Thank you very much…
Muchas Gracias…
Moltes Gràcies…
Muito obrigado.

ABSTRACT

The γ-tubulin ring complex (γTuRC) is required to efficiently generate new microtubules (MT) in a process known as MT nucleation. In mitotic cells, MT nucleation by γTuRC occurs from the centrosome, in vicinity of the chromosomes and from the lattice of pre-existing MTs in a process additionally involving the augmin complex. In neurons, the centrosome loses its MT nucleation capacity, while the γTuRC can still promote nucleation elsewhere. Still, it remains unclear how the γTuRC is regulated in these cells and whether other non-centrosomal sites function as microtubule-organizing centre in neurons.

The aim of this thesis is to understand how MT nucleation mediated by augmin and γTuRC contributes to brain development and how nucleation is regulated during this process.

In this thesis we show that the augmin complex is required for both axonal and dendritic development *in vitro*. In the axon, augmin guarantees that MTs are nucleated with the correct orientation, ensuring uniform axonal MT polarity. On the other hand, augmin depletion leads to an overall decrease in MT density in dendrites with no major effect on their polarity. Surprisingly, despite our findings, analysis of augmin function by other groups *in vivo* in flies and zebrafish has not revealed any dramatic defects.

Strikingly, we show that, in conditional KO mice with gene deletion in the augmin subunit *Haus6* in neural progenitors, brain development is halted before embryonic day 13 and the animals die at birth. These major brain defects are caused by impaired mitosis and massive cell death in neuroprogenitors, indicating significant, species-specific differences in the requirement for augmin function.

In the last part of this thesis we identified KIF2A and CEP170 as γTuRC interactors in *in vitro* cultured mouse cortical neurons and we show that, in agreement with published data on KIF2A function, CEP170 seems to inhibit growth of axon collateral branches. We speculate that KIF2A and CEP170 may function as negative regulators of microtubule nucleation by γTuRC.

Together these results establish augmin-mediated nucleation as essential for mammalian brain development and provide first insight in the regulation of microtubule nucleation in neurons by γTuRC interactors.

RESUMEN

El complejo de anillo gamma-tubulina (γTuRC) es necesario para generar microtúbulos de manera eficiente en un proceso conocido como nucleación de microtúbulos. En células mitóticas, la nucleación a partir del γTuRC tiene lugar en el centrosoma, en regiones próximas a los cromosomas y en la superficie de microtúbulos previamente formados, en un proceso que requiere adicionalmente la presencia del complejo de augmina. A pesar de que en neuronas el centrosoma pierde su capacidad nucleadora de microtúbulos, el γTuRC aún puede inducir la nucleación en otros lugares. Sin embargo, aún se desconoce cómo se regula el γTuRC en estas células y si, aparte del centrosoma, existen otros lugares que puedan funcionar como centros organizadores de microtúbulos.

El objetivo de esta tesis doctoral es entender cómo la nucleación de microtúbulos dependiente de augmina y del γTuRC contribuyen al desarrollo cerebral y cómo se regula la nucleación de microtúbulos durante este proceso.

En esta tesis hemos demostrado que el complejo de augmina es necesario para el desarrollo de axones y dendritas *in vitro*. En el axón, augmina garantiza que los microtúbulos se nucleen en una orientación adecuada, asegurando una polaridad microtubular uniforme a lo largo del axón. Por otro lado, la ausencia de augmina causa una disminución general en la densidad de microtúbulos de las dendritas, sin afectar a su polaridad. Sorprendentemente, a pesar de nuestros descubrimientos, otros grupos han analizado la función de augmina *in vivo* (en moscas y pez cebra) sin encontrar ningún defecto significativo.

Curiosamente, hemos observado que, en ratones *knockout* condicionales en los que la subunidad *Haus6* de augmina ha sido delecionada de progenitores neuronales, el desarrollo cerebral se interrumpe antes del decimotercer día del desarrollo embrionario. Adicionalmente, esta condición resulta letal para los animales, que mueren durante el nacimiento. Se ha encontrado que las causas de estos dramáticos defectos cerebrales son problemas en mitosis y una muerte masiva de neuroprogenitores. Estos resultados indican que existen diferencias en el requerimiento de augmina entre diferentes especies.

En la última parte de esta tesis identificamos KIF2A y CEP170 como interactores del γTuRC en neuronas corticales de ratones cultivadas *in vitro*. También demostramos que, en concordancia con datos publicados sobre KIF2A, CEP170 parece inhibir el crecimiento de

ramificaciones laterales en axones. Nuestra hipótesis es que tanto KIF2A como CEP170 podrían actuar como reguladores negativos de la nucleación de microtúbulos dependiente de γTuRC.

En conclusión, estos resultados demuestran que la nucleación dependiente de augmina es un proceso esencial en el desarrollo cerebral humano, y proporcionan una primera visión de cómo interactores del γTuRC pueden regular la nucleación de microtúbulos en neuronas.

LIST OF ABBREVIATIONS

γTuNA – γTuRC-mediated nucleation activator

γTuRC – γ-Tubulin ring complex

γTuSC – γ-Tubulin small complex

Aa – Amino acid

ALS – Amyotrophic lateral sclerosis

ATP – Adenosine triphosphate

cKO – conditional knock-out

CLASP - Cytoplasmatic-linker associated proteins

CP – Cortical plate

CPC – Chromosomal passenger complex

DIV – Days *in vitro*

DNA – Deoxyribonucleic acid

ECT – Ectoderm

ER – Endoplasmic Reticulum

Fl - Flox

GCP - γ-Tubulin complex protein

GDP – Guanosine diphosphate

GFP – Green fluorescence protein

GO – Gene ontology

GTP – Guanosine triphosphate

HAUS – Homologous to augmin subunit

IKM – inter-kinetic nuclear movement

IgG – Immunoglobulin G

IP – Intermediate precursor

IP – Immunoprecipitation

IZ – Intermediate zone

k-MT – Kinetochore microtubule

KO – knock-out

MAP – Microtubule associated protein

MCPH – Recessive primary microcephaly

MT – Microtubule

MTOC – Microtubule organising centre

MS – Mass spectrometry

MZ – Marginal zone

NEC – Neuroepithelial cell

NECT – Neuroectoderm

NF – Neural folds

NG – Neural groove

nk-MT – Non-kinetochore microtubule

NT – Neural tube

OCT – Optimal cut temperature compound

PBS – Phosphate-buffered saline, pH7.4

PCM – Pericentriolar material

PCR – Polymerase chain reaction

PFA – Paraformaldehyde

PTM – Posttranslational modification

qRT-PCR – Quantitative real-time PCR

RanGTP – GTP-bound Ras-related nuclear protein

RGC – Radial glial cell

RNA – Ribonucleic acid

RNAi – RNA interference

SAC – Spindle assembly checkpoint

SAF – Spindle assembly factor

SAINT – Significance Analysis of INTeractome

shRNA – short-hairpin RNA

SVZ – Subventricular zone

VZ – Ventricular zone

VS – Ventricular surface

WB – Western blot

WT – Wild type

INDEX

LIST OF FIGURES

INTRODUCTION

1. THE BASIS OF MICROTUBULE CYTOSKELETON REGULATION

The cytoskeleton is essential for regulating cellular organization in a scale much larger than individual proteins. Major cytoskeleton functions include (1) driving locomotion, (2) maintenance and regulation of cell shape, (3) ensuring cell division and (4) regulating the positions of organelles and macromolecules by trafficking.

The eukaryotic cytoskeleton comprises four main components: microtubules (MTs), actin, septins and intermediate filaments. Apart from intermediate filaments, which are made of fibrous proteins and are very stable, microtubules, septins and actin filaments are formed by globular proteins that assemble into very dynamic polymeric structures. Strong cross talk between cytoskeleton components is also essential for regulating cell shape, mechanics and locomotion[1] and, particularly, several studies have shown the clear relevance of this cross talk to ensure a proper neuronal development and function[2–4].

1.1 Microtubule structure, polarity and dynamics

Microtubules are long hollow cylindrical polymers with 25 nm of diameter and are composed of α-tubulin-β-tubulin heterodimers (α/β-tubulin dimers) that interact longitudinally and laterally (**Figure 1a,b**). Tubulin was first identified around 50 years ago by Gary Borisy (at the time a graduate student in the lab of Edwin Taylor, University of Chicago) while he was trying to identify the molecular target of the spindle-assembly inhibitory drug colcemid[5].

In order to form MTs α/β-tubulin dimers bind longitudinally to form protofilaments, which are arranged to generate the typical cylindrical structure of MTs (**Figure 1c**). *In vitro* assembled MTs have a number of protofilaments which varies from twelve to sixteen, while *in vivo*, the number of protofilaments per MT is restrained to thirteen[6,7]. However, some exceptions can also be found.

The fact that α/β-tubulin dimers in the MT are arranged in a head-to-tail fashion results in an intrinsic MT polarity with β-tubulin exposed at the (+)-end and α-tubulin facing the (−)-end. MT (+)-ends are very dynamic, whereas (-)-ends are more stable being either capped or anchored to other structures in the cell[8] (**Figure 1c**).

α-Tubulin and β-tubulin monomers have an identical size, are highly similar in their amino acid sequence and share a highly conserved structure. On top of that, both can bind a guanine nucleotide with α-tubulin containing a nonexchangeable GTP binding site (known as N-site) and β-tubulin having an exchangeable binding site for GTP (known as E-site), which can be hydrolysed into GDP[9] (**Figure 1b**). Incorporation of an α/β-tubulin dimer into the MT requires the presence of GTP bound to β-tubulin at the E-site[10]. However, after the α/β-tubulin dimer is incorporated into the (+)-end of the MT and as the lattice ages, this GTP is progressively hydrolysed into GDP. Thus, the older region of the lattice contains β-tubulin in the GDP-bound form, whereas a zone at the growing (+)-end contains β-tubulin in the GTP-bound state. This "GTP cap" confers structural stability to the (+)-end of growing MTs. When the kinetics of GTP-hydrolysis overcomes the kinetics of MT growth (which can be limited for example by the amount of free tubulin available or by the action of proteins that affect MT growth rates), the GTP cap is lost. Consequently, the (+)-end becomes structurally unstable and protofilaments peel off from the MT, leading to MT shrinkage (catastrophe). Therefore, depending on the MT polymerisation rate and on the rate of GTP hydrolysis at the (+)-end, MTs can oscillate between phases of growth and shrinkage. This property of MT (+)-ends is known as dynamic instability and has been demonstrated both *in vitro* and *in vivo*, allowing cells to quickly reshape their MT network[11,12] (**Figure 1d**).

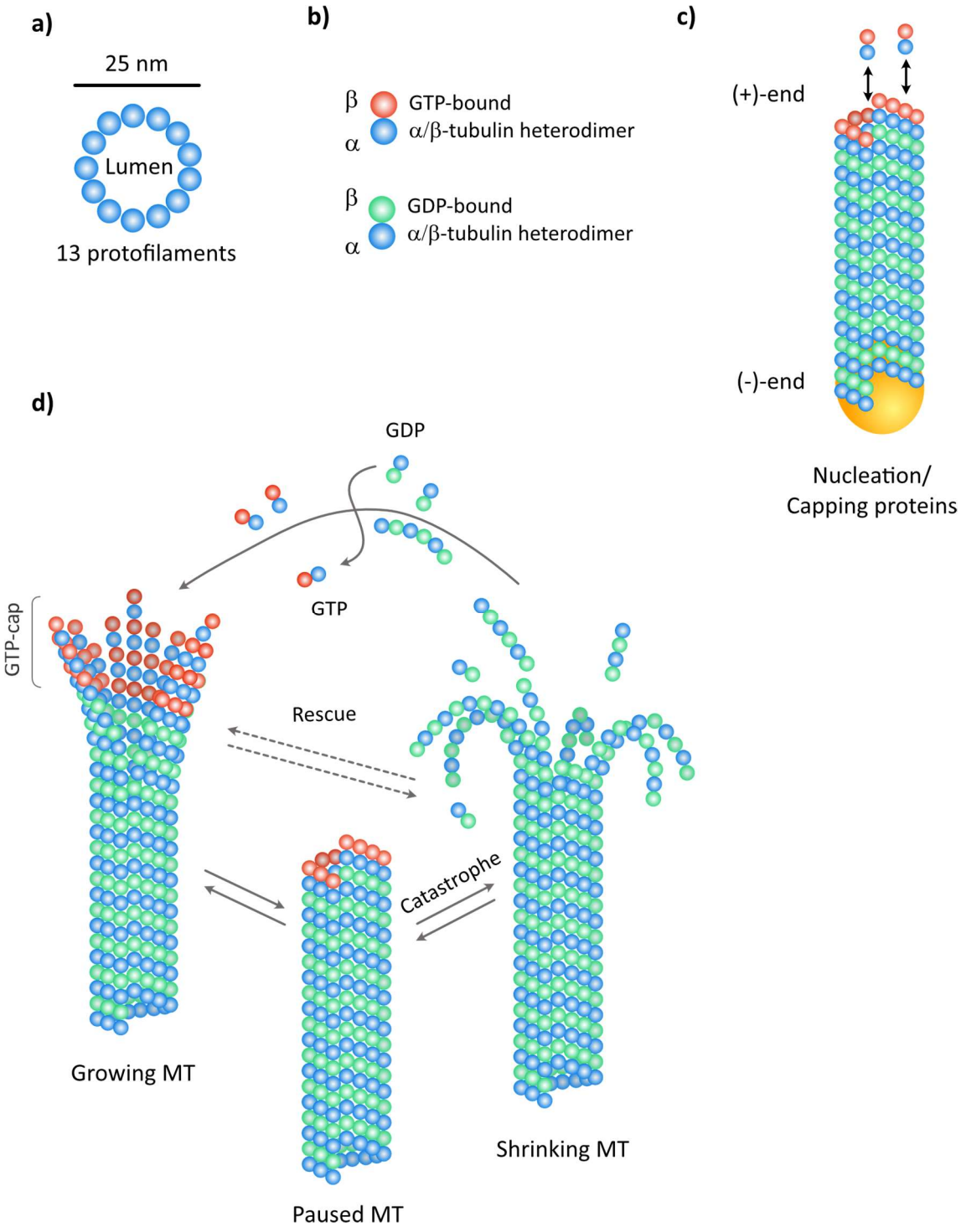

Figure 1 – Microtubule structure, polarity and dynamic instability. **(a)** Representation of a transversal section of a microtubule (MT) and its 13 protofilaments. **(b)** Representation of α/β-tubulin heterodimers with β-tubulin bound either to GTP (red sphere) or GDP (green sphere). α-Tubulin is represented by a blue sphere. **(c)** Representation of a MT and MT polarity with its dynamic (+)-end and its capped (-)-end. **(d)** Representation of the dynamic instability properties of MTs. Adapted from: [13].

1.2. Regulation of microtubule dynamics

Microtubule dynamics are crucial for the cytoskeleton to fulfil its cellular functions. Regulation of MT properties can occur through the activity of different proteins classified as microtubule-associated proteins (MAPs) or activity of motor proteins and MT severing enzymes (like the broadly studied katanin and spastin[14]). Different mechanisms involved in the regulation of MT dynamics are summarised in **Figure 2**.

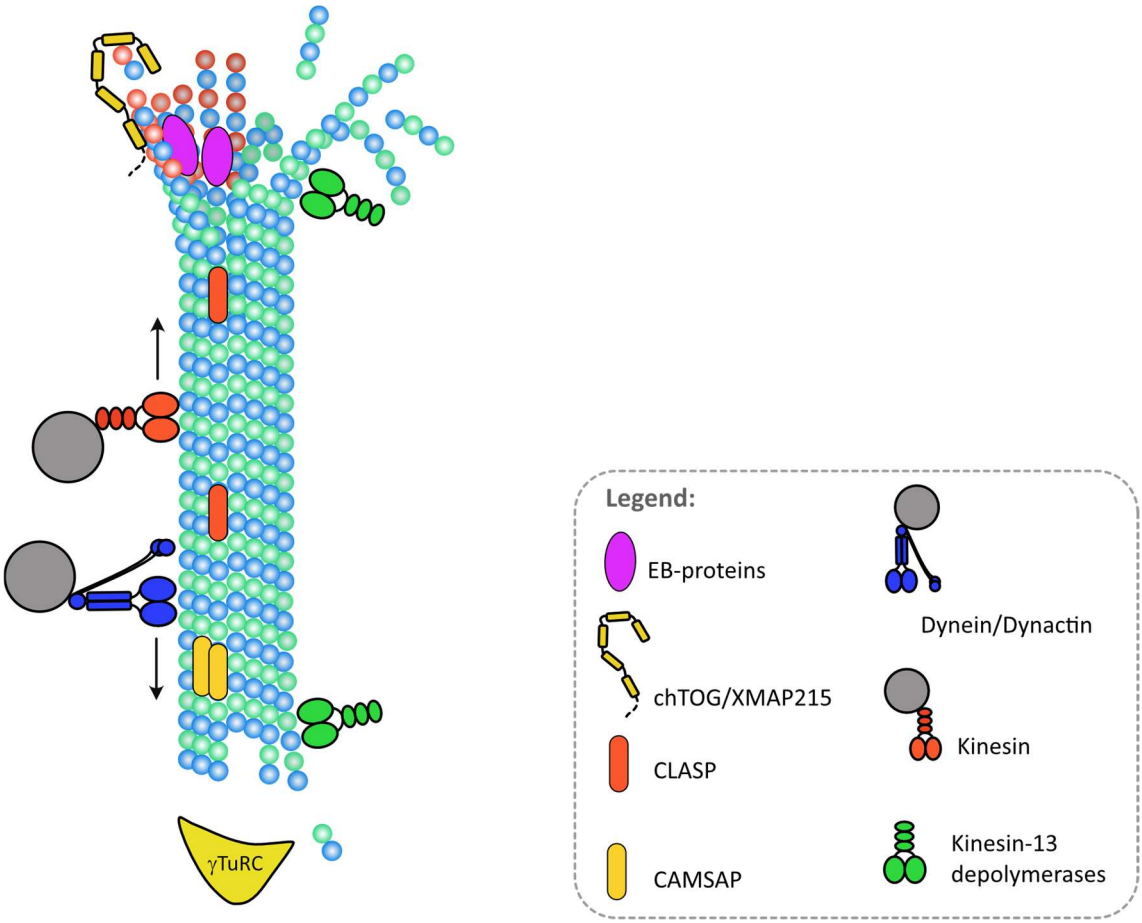

Figure 2 – Regulation of microtubule dynamics. (a) Representation of MT structure and MT-associated proteins (MAPs) that regulate microtubule dynamics. The legend of this figure is presented next to it (*bottom, right*) **(b)** Representation of the MT posttranslational modifications described for α and β-tubulins.

1.2.1. Microtubule-associated proteins

Microtubule associated proteins (MAPs) that interact with the MT (+)-end are commonly known as (+)TIP proteins (**Figure 2**). These proteins act either by promoting MT polymerisation or by inducing catastrophe. EB proteins specifically bind to growing MT (+)-ends. *In vitro* studies show that they bind close to the GTP-cap promoting lateral protofilament interaction[15–19]. Furthermore, EBs can also recruit other MAPs to the (+)-end. This is the case for XMAP215 which recruits α/β tubulin dimers, promoting MT elongation[20,21]. Additionally, cytoplasmatic-linker associated proteins (CLASPs) have also been implicated in MT growth by inhibiting catastrophe[21–23].

There are also proteins, like the members of the kinesin-13 protein family (KIF2A, KIF2B, MCAK/KIF2C) that act on the (+)-end by promoting catastrophic events[24]. As an example, MCAK/KIF2C was shown to form oligomers that promote dissociation of α/β-tubulin from MT ends in an ATP-dependent manner[25] (**Figure 2**).

Other proteins can affect MT dynamics through binding to the MT lattice. This is the case of the already mentioned CLASPs that, apart from binding to the (+)-end, can promote stabilisation of the MT lattice[26] (**Figure 2**). Other examples are MAP2 or tau, whose role in neuronal development will be discussed later.

Microtubule (-)-ends are more stable and are the place where MTs start forming. The role of the γ-tubulin ring complex in the generation of new MTs and regulation of (-)-ends will be discussed later. Still, there are other proteins that act on the MT (-)-end, stabilising or destabilising it. In this context, CAMSAPs are well described as a group of proteins that bind the (-)-end and protect it from depolymerisation[8,27] (**Figure 2**). Apart from acting at the (+)-end, members of the kinesin-13 protein family can also induce MT depolymerisation at the (-)-end[25].

1.2.2. Motor proteins

Motor proteins move along the MT lattice through hydrolysis of ATP and not only able to transport cargos (e.g. vesicles, organelles) to specific intracellular location, but also to reshape the entire MT network of the cell. Therefore, it is through the activity of motor proteins that MTs can accomplish their role as intracellular highways, ensuring a correct intracellular trafficking, essential for cellular function and morphogenesis.

Microtubule-based motor proteins are classified into two main categories: (1) motors that move towards the MT (+)-end (anterograde transport) and (2) motors that move towards the MT (-)-end (retrograde transport) (**Figure 2**). Motors that move towards the (+)-end include most members of the kinesin superfamily. The best example of a (-)-end directed motor is dynein, which assembles into a dynein/dynactin complex to move along MTs. In both cases, these proteins are able, on one hand, to bind to the MT lattice and, on the other hand, to bind to adaptor proteins that interact with a cargo.

There are also examples of MT motor proteins that can regulate MT dynamics. One example is the already discussed kinesin-13 protein family, whose members can induce MT depolymerisation. Kinesin-8 member KIF18A is also able to depolymerise MTs during mitosis[28]. Interestingly, recent work suggests that, apart from sliding antiparallel MTs, Eg5 can also induce MT polymerisation and stabilise MTs[29,30].

1.2.3. Tubulin isotypes and posttranslational modifications

In most organisms both α- and β-tubulin are encoded by multiple genes giving rise to different tubulin isotypes with a highly conserved structure. In mammals, 9 genes have been identified for α-tubulin and 9 genes for β-tubulin[31].

Initially, it was thought that tubulin isotypes were able to form individual MTs with specialised functions[32]. However, it quickly became clear that MTs display tubulin mosaicism, being simultaneously formed by α and β-tubulin monomers encoded by different genes[33]. Some of these tubulin isotypes, like the highly neuronal specific

β-tubulin isotype 3 (β3-tubulin), are expressed in specific tissues whereas others are more ubiquitously expressed.

Incorporation of different tubulin isotypes may have an influence on MT dynamics [34,35] and binding of MAPs and motor proteins. However, because most *in vitro* studies use tubulin isolated from the cow brain (which is composed of a mix of tubulin isotypes), little is known about the specific contributions of different tubulin isotypes on MT properties.

Posttranslational modifications (PTMs) on MTs have also been shown to regulate MT behaviour both directly and indirectly by affecting the binding of MAPs[36,37].

Tubulins are globular proteins with a flexible C-terminal tail that, once an α/β-tubulin dimer is incorporated into the MT, it stays exposed at the MT lattice surface and is susceptive to different types of posttranslational modifications (PTMs) (**Figure 3**). For example, once incorporated into the MT, the C-terminal tail of α-tubulin (which in most cases terminates in a tyrosine) can be enzymatically detyrosinated. This truncation can be reverted by the activity of a tyrosine ligase. Detyrosination becomes irreversible if the preceding amino acid (glutamine) is also removed, giving rise to Δ2-tubulin. The C-terminal tails of α and β-tubulin can also undergo poly-glutamylation and poly-glycylation, respectively.

Once incorporated into the polymer, α-tubulin can also be modified by acetylation. In contrast to the other PTMs, MT acetylation occurs at lysine-40 in a region that localises at the inner surface of the MT.

High levels of detyrosination and acetylation are a hallmark of “long lived” stable MTs. Yet, accumulation of these PTMs seems to be a consequence, rather than the cause of MT stability[36].

The role of microtubule PTMs during neuronal development will be discussed below.

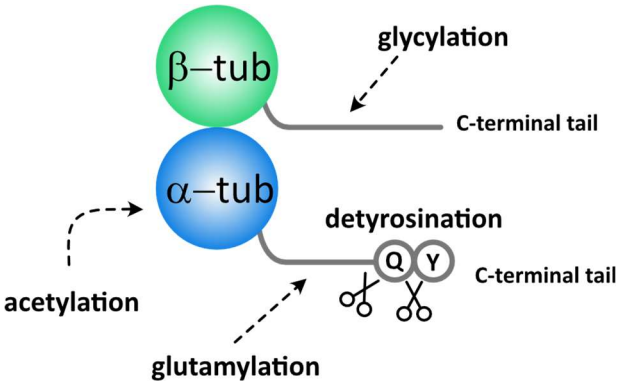

Figure 3 – Summary of the posttranslational modifications described in α/β-tubulin dimers. In this figure glycylation of the C-terminal tail of β-tubulin, detyrosination and glutamylation of the C-terminal tail of α-tubulin and acetylation of α-tubulin in a region that lies at the lumen of the MT are represented.

1.3. Microtubule nucleation

The first step in generating a new MT from free tubulin is known as MT nucleation. *In vitro,* MT nucleation occurs spontaneously in the presence of sufficiently high concentrations of soluble tubulin. In these conditions, MT nucleation occurs through spontaneous assembly of small MT seeds in a process kinetically less favourable than MT polymerisation[38]. *In vivo*, MT nucleation takes place at lower tubulin concentrations in conditions where spontaneous assembly of new MTs is highly disfavoured. Therefore, cells have evolved mechanisms to overcome this kinetically unfavourable mechanism and, at the same time, control where and when new MTs are generated. In cells, MT nucleation occurs mostly at sites known as MT organizing centres (MTOCs) by a mechanism requiring the presence of a nucleator that mimics or stabilises small MT seeds (reviewed in[39]).

The most well-established MT nucleator is γ-tubulin. γ-Tubulin was originally identified as a member of the tubulin superfamily in 1989 in *Aspergillus nidulans* by Elizabeth and Berl Oakley[40]. Since then, γ-tubulin was shown to be an ubiquitous protein in all eukaryotes and to be an essential component of MTOCs[41,42]. In *Drosophila melanogaster* and in vertebrates two different γ-tubulin genes have been identified[43]. In mice, only

one isoform, TUBG1 was found to be essential and ubiquitously expressed. On the other hand, another isoform TUBG2 is highly expressed in the mouse brain[44].

In order to act as a MT nucleator, γ-tubulin forms multi-subunit complexes by interaction with a conserved family of proteins known as γ-tubulin complex proteins (GCPs). Two different types of γ-tubulin complexes have been identified according to their size and protein composition[45] (**Figure 4**): (1) the "γ-tubulin small complex" (γTuSC), with a size of ~300 kDa is a hetero tetramer of two laterally associated GCP proteins (one GCP2 and one GCP3) with each binding longitudinally one molecule of γ-tubulin; (2) the larger "γ-tubulin ring complex" (γTuRC), with a size of ~2 MDa, is an assembly of several γTuSCs plus the GCP proteins GCP4, 5 and 6. In the γTuRC all the GCPs interact laterally and most likely each one of them binds a γ-tubulin protein longitudinally, leading to a circular, helical arrangement that, when viewed from the top, resembles a ring with 13 γ-tubulins (reviewed in [46,47,42,39,43]).

Whereas γ-TuSC components can be found in all eukaryotes, GCP4, 5 and 6 are missing in organisms like budding yeast or *Caernorhabditis elegans*. *In vitro*, nucleation activity of the γTuRC is estimated to be about 150-fold higher than that of γTuSC [45].

At least *in vitro*, GCP2-6 are essential for γTuRC structure and depletion of any of these proteins causes disruption of the complex in sucrose gradients. In addition, GCP2-6 seem to be structurally related, sharing the same core protein folding that contains two conserved γ-tubulin complex grip motifs, one in the N-terminal region and another one in the C-terminal region of the proteins. Several studies suggest that, whereas the N-terminal conserved region of GCP2-6 mediates lateral bindings between GCPs, their C-terminal region directly binds γ-tubulin [48–51].

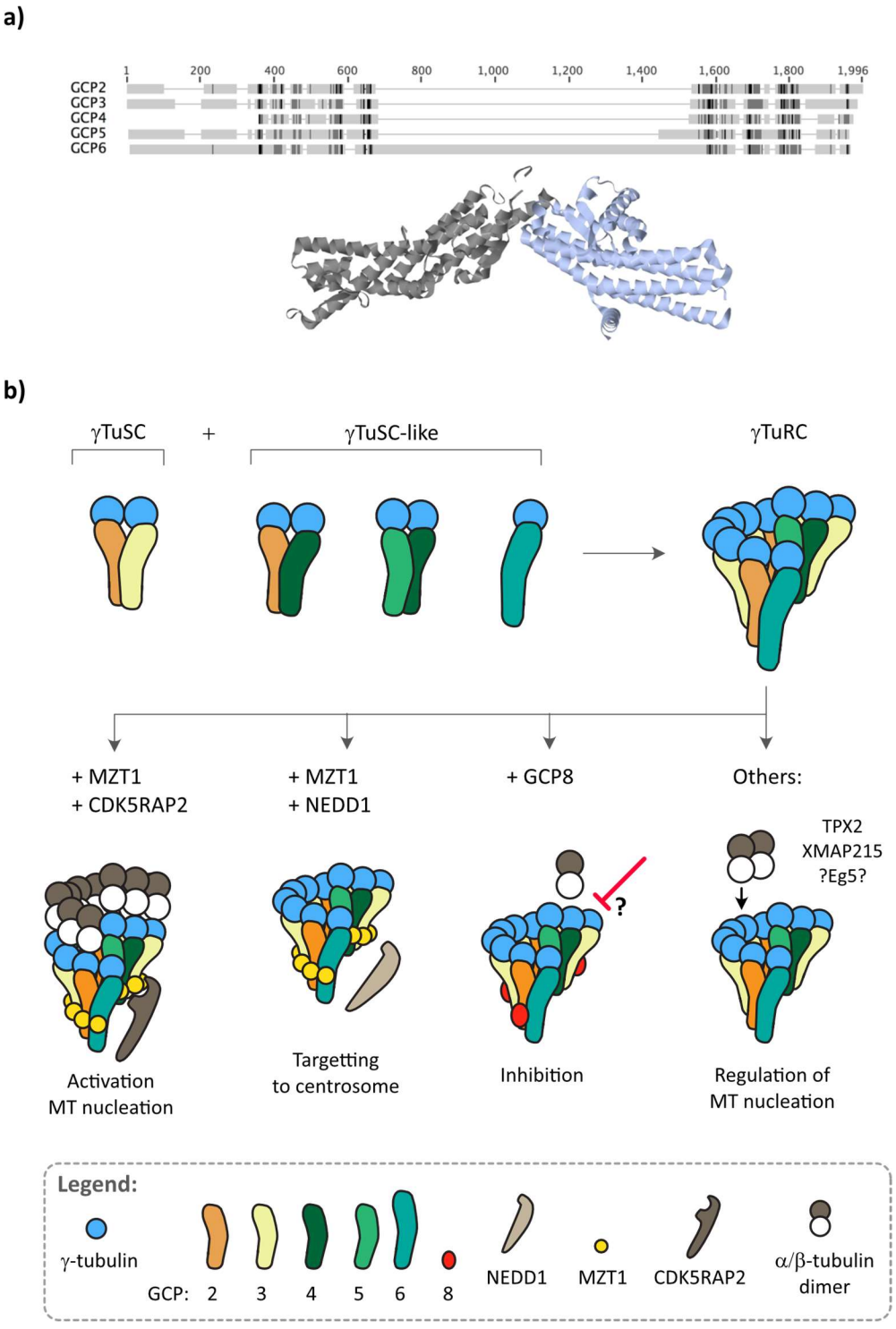

Figure 4 – γ-Tubulin ring complex structure and regulation. (a) Alignment of human γ-tubulin complex proteins (GCPs) GCP2,3,4,5 and 6 using MUSCLE algorithm within Geneious software. Conserved regions are indicated by grey shading with the darker regions corresponding to a higher degree of conservation. Below the alignment, GCP4 crystal structure is represented. Image taken from[52]. **(b)** Scheme showing how γ-tubulin complex proteins (GCPs) associate laterally with each other and longitudinally with γ-tubulin to assemble the γ-tubulin small complex (γTuSC) and γ-tubulin

ring complex (γTuRC). This scheme also representes how different proteins (MZT1, CDK5RAP2, GCP-WD/NEDD1, GCP8, TPX2, XMAP215, Eg5) associate with the γTuRC, promoting activation/inhibition of MT nucleation or targeting it to microtubule organizing centres (MTOC). Abbreviations: γ-tubulin small complex (γTuSC); γ-tubulin ring complex (γTuSC). Adapted from: **[53]**.

In addition to GCP2-6 using mass spectrometry analysis of purified γTuRC, the Luders group and others have identified GCPWD/NEDD1, MZT1 and GCP8/MZT2 as additional γTuRC subunits (**Figure 4**). Even though these subunits, based on RNA interference (RNAi), do not seem to be essential for the assembly and/or stability of human γTuRC, they have important roles in regulating γTuRC targeting and activity. NEDD1 serves as a targeting factor for γTuRC to mediate centrosomal, augmin-dependent and chromatin-mediated MT nucleation during cell division and is required for mitotic spindle assembly[54–57]. MZT1 binds to assembled γTuRC by interacting with the N-terminal regions of GCP3, 5 and 6 and potentially also GCP2. It mediates both targeting and activation of the γTuRC. On one hand, MZT1 promotes the interaction of the γTuRC with NEDD1 and, on the other hand, it serves as a positive regulator of nucleation by promoting the binding of γ-TuRC activating factor CDK5RAP2[53,58,59]. Unpublished data from Artur Ezquerra, a former PhD student in our laboratory, show that GCP8/MZT2 interacts with the N-terminal region of GCP2 and that it has a role as a negative regulator of the γ-TuRC during interphase in both the centrosome and the Golgi apparatus.

It is important to mention that, in addition to MT nucleation, the γ-TuRC has also been implicated in MT stabilisation by capping (-)-ends and modulating (+)-end dynamics [60–62]. However, these functions are much less characterized.

The most widely accepted model for how the γTuRC nucleates MTs is the template model. This model proposes that the helical arrangement of the 13 γ-tubulin molecules, which matches the geometry of a MT in cross-section, serves as a template for binding of α/β-tubulin dimers. According to this model, γ-tubulin in the γTuRC directly binds to α-tubulin, promoting lateral contacts between α/β-tubulin dimers and therefore kinetically favouring the formation of small MT seeds (revised in [39,47]). This model can

also explain how the γTuRC is able to control formation of MTs with 13 protofilaments *in vitro*[63].

Cytosolic γ-tubulin complexes are relatively week MT nucleators and the percentage of active complexes may be as low as 1%, concentrated at MTOCs[64]. Therefore, both γTuRC targeting and activation are required to induce proper MT nucleation. Few proteins have been implicated in γTuRC activation and most of them carry a CM1 sequence motif (also known as γTuNA, which stands for γTuRC-nucleation activator motif). Through its CM1 domain, human CDK5RAP2 has been shown to increase γTuRC nucleation activity *in vitro* by approximately five-fold. This mechanism is also relevant in a cellular context and overexpression of the CM1 domain of CDK5RAP2 induces ectopic MT nucleation in the cytoplasm[65]. As mentioned before, the γTuRC subunit MZT1 is involved in priming the complex for activation by CDK5RAP2[53] (**Figure 4**).

In addition to activation of the complex, other factors stimulate γTuRC-dependent MT nucleation by stabilising nascent MTs and/or promoting tubulin incorporation. This is the case of the TPX2 and of the MT polymerase XMAP215. TPX2 is an anti-catastrophe factor that, recently, was also shown to contain a CM1-like domain capable of inducing branched MT nucleation[66]. In *Xenopus* egg extracts and in *in vitro* experiments, XMAP215 was shown to interact with the γTuRC and, through its TOG domains, stimulate MT nucleation by polymerisation of tubulin subunits on the γTuRC template[67]. More recently, Eg5 has also been proposed to induce curved-to-straight transition of tubulin, promoting lateral interactions between tubulin heterodimers and facilitating MT nucleation[68]. On the other hand, negative regulators like the kinesin-related MT depolymerase MCAK may act on nucleation by impairing tubulin incorporation into nascent MTs[69].

The function of γ-tubulin complexes as main MT nucleators and their roles in spindle assembly and proliferation are well stablished across species. However, while impairing γ-tubulin function severely disrupts spindle formation and slows down MT nucleation from the centrosome, it does not completely abolish MT assembly[70–74]. This suggests

that other mechanisms may be able to compensate for γ-tubulin loss or act in parallel with γ-tubulin. In fact, several MAPs have been suggested to display MT nucleation activity. These proteins include members of the XMAP215 family and the spindle assembly factor TPX2. *In vitro* experiments proved that TPX2 can trigger spontaneous MT nucleation. Furthermore, TPX2 can act synergistically with XMAP215, or its human homologue chTOG/CKAP5, to stimulate MT nucleation[39].

1.4. Microtubule Organizing Centres

Inside the cell, MT nucleation occurs at specific sites known as microtubule organising centres (MTOCs).

The most well established MTOC in eukaryotic cells is the centrosome. Since its discovery over 100 years ago by Theodor Boveri and Edouard van Beneden[75], great advances were made in understanding centrosome structure and its function in cell division, motility and signalling. Animal centrosomes are composed of a pair of perpendicularly arranged, barrel-shaped centrioles and a surrounding electron-dense proteinaceous matrix, the pericentriolar material (PCM), which contains γ-tubulin and nucleates MTs (**Figure 5**). Each centriole has a cylinder-like structure composed of nine triplets of stable MTs arranged in a radial symmetry. One of the two centrioles (the older, mother centriole) is decorated with distal and subdistal appendages, critical for the function of centrosomes as MTOCs and signalling platforms[76].

Cycling cells in G1 have one centrosome with two centrioles (a mother and a daughter) that are kept together by the centrosome linker (**Figure 5a**). Centrosomes duplicate once every cell cycle (in parallel with DNA replication) as part of a process known as the centrosome cycle. In most cells, a complex cellular machinery ensures that centrosome duplication occurs only once every cell cycle, avoiding alterations in centrosome number[77–79]. During S-phase, each of the two centrioles serves as template for the formation of a new daughter centriole which grow from the proximal part of their lateral surface so that in G2 each cell has two centrosomes (with two centrioles each) (**Figure**

5b,c) [80]. These two centrosomes remain tethered together and act as a single MTOC until they reach mitosis. At the entry of mitosis, the centrosomal linker is degraded and the PCM and its MT nucleation capacity is dramatically enlarged (**Figure 5d,e**). In mitosis, each centrosome lies at one of the spindle poles organising the bipolar spindle and promoting proper chromosome segregation [80]. After mitosis, each of the daughter cells inherits one of the centrosomes and the centriole cycle is restarted[78].

Apart from its role as MTOC, the centrosome can also serve as basal body, building the foundations for cilia and flagella which are involved in chemical and mechano-sensing and cell locomotion (**Figure 5a1**). Cilia can be either motile or immotile, such as primary cilia which exist in most of the cells. Both types have sensory functions and are involved in cell signalling [81–83].

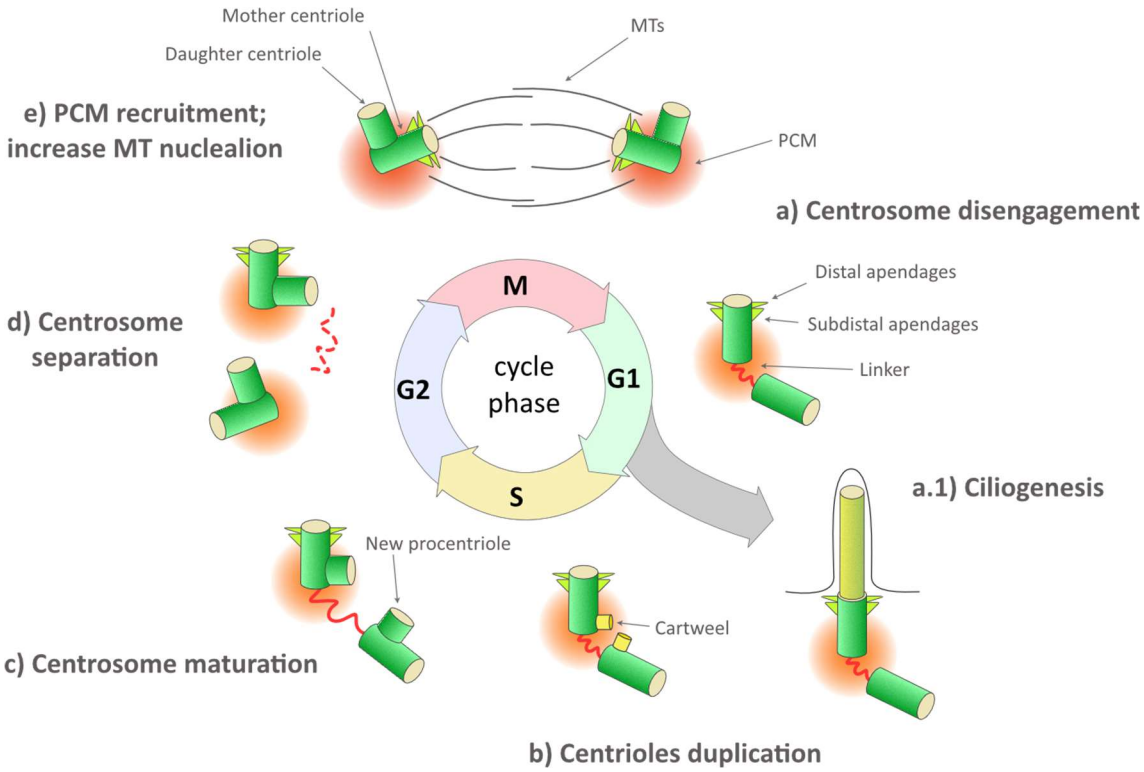

Figure 5 – Centrosome cycle. Scheme representing centriole configurations during centrosome duplication, separation and maturation during different stages of the cell cycle. Adapted from[79].

Most cells have only one or two pairs of centrioles, depending on the cell cycle phase. However, there are exceptions like multi-ciliated epithelial cells, which can grow 30 to 300 motile cilia on their apical surface. One example are the ependymal cells which lie at the surface of brain ventricles and, through the coordinated beating motion of their multiple motile cilia, are responsible for moving the cerebrospinal fluid in the brain[84].

Thus, tight regulation of centrosome biogenesis and duplication is highly important and defects in controlling centriolar number and structure have been linked to cancer, dwarfism, microcephaly and a group of diseases known as ciliopathies[85–87].

Apart from the centrosome there are other cellular structures that recruit γ-tubulin and serve as MTOCs in both cells with and without centrosomes. The Golgi apparatus is one well-known example, where MT nucleation and anchoring at Golgi membranes is important for reshaping the MT network during cell migration[88,89]. In plant cells, as well as in some differentiated animal cells like muscle cells, the nuclear envelope also serves as an active MTOC. Microtubule nucleation by the γTuRC can also occur in the vicinity of the chromatin during mitosis or from the lattice of pre-existing MTs in a process mediated by the augmin complex (reviewed in[90,91]).

The relative importance of these MTOCs in nucleating MTs in both mitotic cells and postmitotic neurons will be discussed below.

1.5. Mechanisms of microtubule nucleation during mitotic spindle assembly

Cell division in animal cells comprises different stages, the mitotic phases prophase, prometaphase, metaphase, anaphase and telophase, followed by cytokinesis. Each of them is marked by rearrangements in the MT network.

At the entrance of mitosis, in prophase, the relatively stable interphasic MTs disassemble and the centrosome recruits a high amount of PCM components, increasing its nucleation activity. By the action of motor proteins like Eg5, the two centrosomes are

separated to opposite poles of the cell, forming two independent MT asters. After breakdown of the nuclear envelope, in prometaphase, the two centrosome asters contribute to the establishment of the mitotic spindle, an antiparallel bipolar MT array with one centrosome at each pole. By metaphase, MTs emanating from both poles have been captured and bind to the chromosomes through the kinetochore, aligning them at the metaphase plate. During this process, MTs must be very dynamic to allow correction of attachment errors. Not surprisingly, treatments with drugs that either destabilise of stabilise MTs cause a mitotic delay by prolonging the time that cells spend in prometaphase.

If we take a closer look at the architecture of the mitotic spindle in animal cells, three categories of MTs can be found (**Figure 6**): **kinetochore MTs** (k-MTs), which build up the k-fibers (MT bundles involved in the attachment of chromosomes to the spindle poles through interaction with the kinetochores); **astral MTs** which radiate from the spindle poles and, through interaction with the cellular cortex, help in spindle positioning and **non-kinetochore MTs** (nK-MTs). nK-MTs originated from opposite poles meet at the central spindle region. Sliding of these antiparallel nK-MTs by molecular motors like Eg5 helps to separate the poles and to stabilise the spindle. (Reviewed in [92,93]).

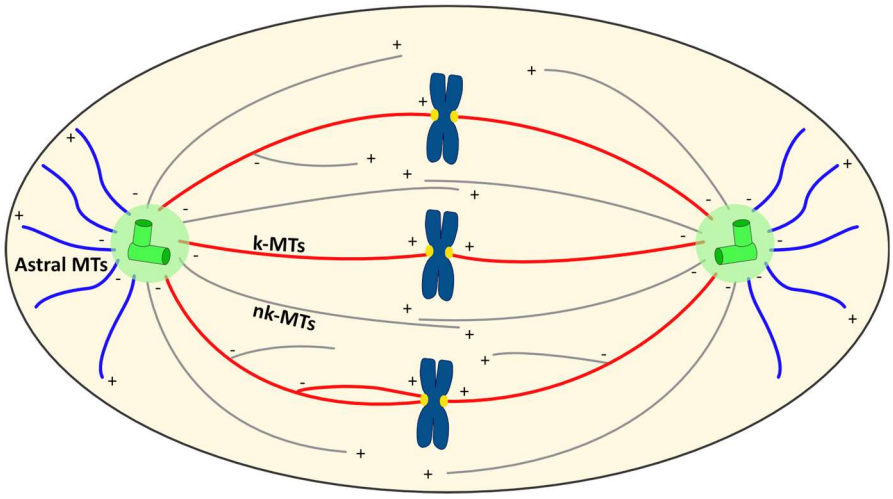

Figure 6 – Categories of microtubules found in metaphasic animal cells. In this scheme, the three categories of microtubules in metaphase spindles are represented: in red, bundles of kinetochore-microtubules (k-MTs) that are generated through nucleation at the chromatin, the centrosome and from within the spindle and that connect the chromosomes (through the kinetochore) to the spindle poles (in green); in blue, the astral MTs originated at the centrosome and that play an important role in spindle positioning; in grey, the non-kinetochore-microtubules (nk-MTs) that are originated from the centrosome or from within the spindle and contribute to robust spindle architecture.

After metaphase, anaphase starts with each pair of chromatids using spindle MTs as guides to migrate towards opposite poles of the cell. In order to avoid chromosome segregation defects, progression from metaphase to anaphase only occurs once all the kinetochores are properly attached to mitotic spindle MTs. With that purpose, cells have developed an accurate quality control mechanism that measures MT-kinetochore attachment and tension. This mechanism is known as the spindle assembly checkpoint (SAC) and a defective SAC leads to chromosome mis-segregation, aneuploidy and tumorigenesis. During early prometaphase, SAC proteins (like Mad1, Mad2 and Mps1) are recruited to kinetochores, signalling it as being non-attached to spindle MTs. The SAC allows mitotic progression to occur only once a group of 20-30 MT (+)-ends (known as k-fibers) is correctly attached to the kinetochore. In parallel, another mechanism ensures that each pair of kinetochores is attached to MTs from opposite poles (which generates tension between the kinetochores). This mechanism is important to ensure correct chromosome segregation since kinetochore attachments that are not under

tension activate the error correction pathway, which depends on Aurora B kinase substrate phosphorylation. This leads to MT detachment from the kinetochores which, in turn, activates the SAC. Once the SAC has been satisfied, anaphase is triggered by activation of the anaphase-promoting-complex/Cyclosome (APC/C)[94–97].

During anaphase, another antiparallel MT array, known as the central spindle, is formed between the chromosomes. Motor proteins promote sliding of these antiparallel MTs helping to further separate chromosomes. Once the duplicated chromatids reach each of the poles, chromosome attached MTs depolymerise, the chromatin decondenses and the nuclear envelope is reformed. Cytokinesis starts during late anaphase through the formation of an actomyosin ring that contracts the cellular membrane in the region of the central spindle and continues through telophase until abscission, when the two daughter cells are fully separated.

Tight regulation of MT nucleation during cell division is essential for the establishment of a robust mitotic spindle. Three major MT nucleation pathways have been described for mitotic spindle assembly (**Figure 7**): a centrosome-mediated, a chromatin-mediated and a MT amplification pathway. There is evidence suggesting both redundancy and synergy between the three[17,98,99]. On top of that, different cell types may require a different balance of these nucleation pathways to ensure proper assembly of the mitotic spindle.

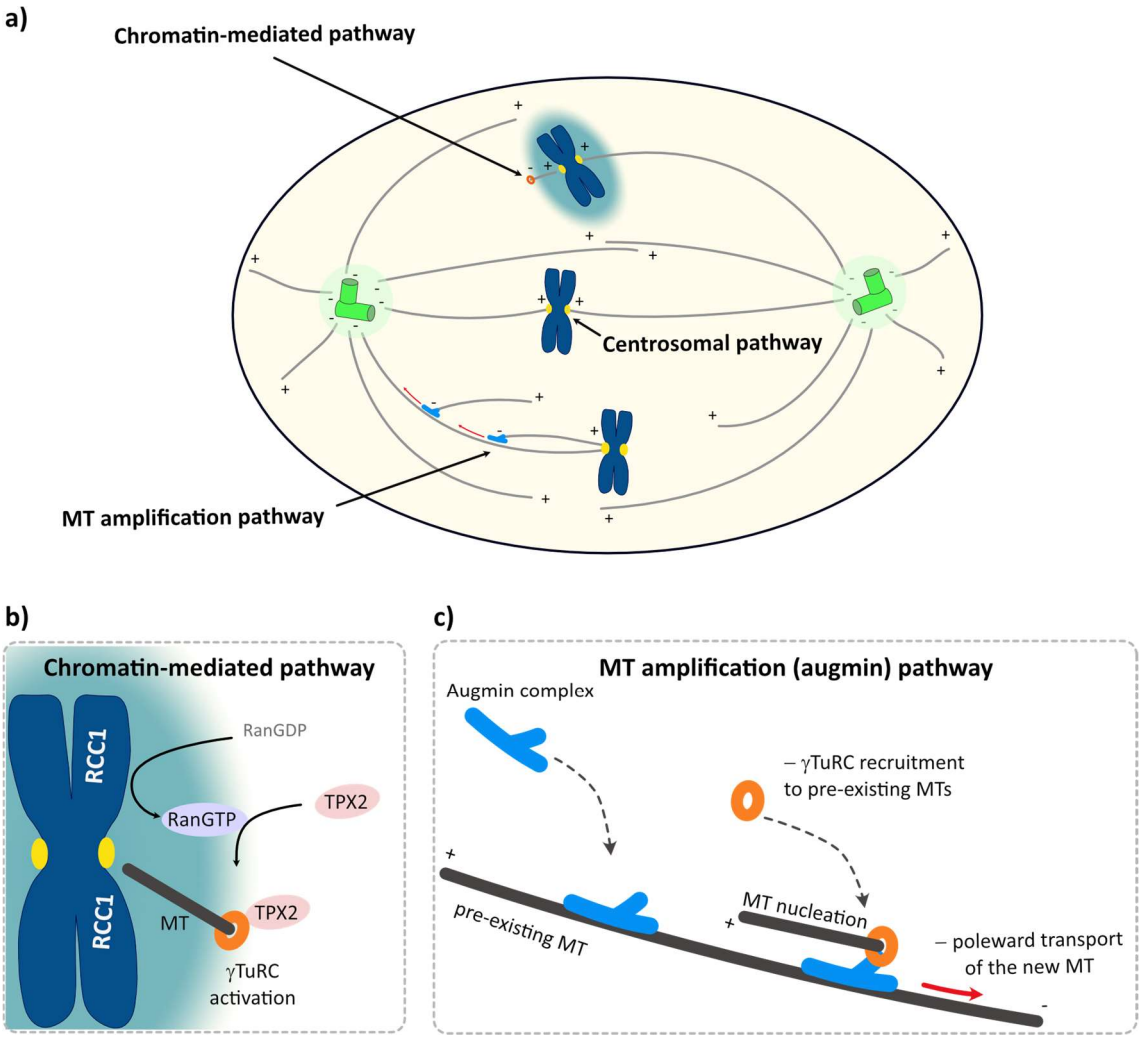

Figure 7 – Microtubule nucleation pathways in mitotic cells. (a) Scheme of a prometaphase cell where the three main pathways of microtubule (MT) nucleation are represented: Centrosome-mediated pathway; Chromatin-mediated pathway; MT amplification or augmin pathways.
(b) Details of the mechanism involved in the chromatin-mediated pathway. The generation of a RanGTP gradient around the chromosomes (here shown in blue) promotes the release of spindle assembly factors (SAFs) from importin. An example of a SAF that is released from importins as a consequence of the activity of the RanGTP pathway is TPX2. Interaction of TPX2 with the γTuRC (orange) induces MT nucleation. **(c)** Mechanistic details of the augmin-mediated pathway. The augmin complex (in light blue) targets the γTuRC (orange) to pre-existing MTs of the mitotic spindle, promoting MT nucleation with the newly formed MT having the same polarity as the "mother" MT. Newly formed MTs are then moved towards the poles in a process mediated by the activity of motor proteins.

1.5.1. The centrosome-mediated pathway

From the description of the mechanisms involved in cell division it becomes evident that the centrosome is a key mitotic player, due to its ability to nucleate MTs and organise the mitotic spindle poles. Its importance for mitosis is indicated by the fact that abnormalities in centrosome number have been linked to tumorigenesis and developmental defects. Mice lacking centrioles are not viable since acentriolar spindles assemble less efficiently, causing a short delay in prometaphase, and leading to massive cell death through activation of a p53-dependent pathway[100]. The specific brain developmental defects caused by centrosome aberrations, such as microcephaly, will be discussed in more detail later.

For a long time, a well-established model describing how MTs can find and bind to the kinetochores has been the "search-and-capture model". According to this model, MTs growing from the centrosome search the cellular space as they grow and shrink due to their dynamic instability, changing their trajectory in each growth phase. Once a MT is "captured" by a kinetochore it becomes stabilised by a phosphorylation-dependent mechanism involving Aurora B within the chromosomal passenger complex (CPC). However, mathematical models have demonstrated that if human cells would use only this random search-and-capture strategy to promote k-MT attachment, the duration of mitosis would be much longer than what is typically observed[65]. This suggests the existence of other mechanisms to achieve MT-kinetochore attachment.

1.5.2. The chromatin-mediated pathway

Microtubule nucleation can also occur in the vicinity of the chromosomes in a pathway mediated by Ras-related nuclear protein (Ran)-GTP (RanGTP) complex (reviewed in[90]). In summary, the existence of a RanGTP gradient centred on the mitotic chromatin promotes the release of spindle assembly factors (SAFs) from importins which induce MT nucleation in the vicinity of the chromosomes. An example of a SAF protein is TPX2 which, after release from importins, interacts with the GCP-WD/NEDD1 subunit of the

γTuRC triggering MT nucleation. If these MTs reach the kinetochore they are stabilised by the CPC and favour the assembly of k-fibres (**Figure 7b**).

1.5.3. The microtubule amplification or augmin pathway

During mitosis, γ-tubulin associates with the mitotic spindle in a process dependent on phosphorylation of the γ-TuRC subunit GCP-WD/NEDD1 at the serine-418. Expression of this S418D GCP-WD/NEDD1 mutant in cells depleted of endogenous NEDD1 leads, not only to removal of γ-tubulin from the spindle, but also to a reduction in the amount of spindle MTs and an increase in the mitotic index[54]. These observations, together with the fact that growing MT (+)-ends emerge from within the spindle[101] suggested that MT nucleation could most likely occur from pre-existing spindle MTs.

In 2007, an RNAi screen in *Drosophila melanogaster* S2 cells identified 5 previously uncharacterized proteins required for γ-tubulin localization to the mitotic spindle[102]. These proteins were named Dgt2 to 6 ("Dgt" referring to dim γ-tubulin). In a follow-up study it was found that these 5 proteins can form a complex that is able to bind both the γTuRC and MTs. This complex was named augmin complex due to its ability to augment MT density within the spindle[103].

Subsequent work by several groups identified the full set of 8 augmin **s**ubunits, which in human cells were named HAUS1 to HAUS8[104,105] (standing to **h**omologous to **au**gmin **s**ubunit). Depletion of any of the augmin subunits leads to disruption of the complex[104,105] in human cells and causes: (1) increase in mitotic index due to a prolonged mitosis; (2) increase in abnormal spindles; (3) reduction in the amount of MTs in the spindle; (4) reduction in kinetochore MT attachment as observed by increased levels of Mad2 on misaligned chromosomes; (5) centrosome fragmentation. In addition, augmin depletion also causes defects in cytokinesis and a reduction in the amount of MTs at the central spindle[105]. These phenotypes are much more severe than the ones observed in *Drosophila melanogaster* S2 cells and in the non-cancer cell line RPE1[106].

Since then, many studies have implicated the augmin complex in ensuring the robustness of the meiotic and/or mitotic spindle in mice, drosophila, zebra fish, plants and fungi [99,107–114].

Unlike the initial work done in cells, the use of *Xenopus* egg extracts allowed to directly visualize nucleation from the lattice of pre-existing MTs (and demonstrated the dependency of this process on γTuRC)[110]. It was observed that daughter MTs grow with a shallow angle and with the same polarity as the mother MT[111,115] with an architecture that resembles the formation of MT branching. Therefore, augmin-mediated MT nucleation is sometimes referred to as branching MT nucleation. It was further shown that RanGTP and its effector TPX2 stimulate augmin-dependent MT branching *in vitro*, suggesting that factors of both chromatin and MT amplification pathways may act cooperatively to nucleate MTs in mitosis. On the other hand, spindle assembly in *Drosophila* S2 cells is largely unperturbed following D-TPX2 depletion when compared to augmin depletion and TPX2 does not seem to have a prominent role in MT branching at the central spindle[116,117]. This suggests that the mechanisms involved in augmin-dependent nucleation are probably species or cell type dependent.

Information on the detailed structure of the augmin complex is still limited. Two independent studies (one using reconstituted human augmin[118] and another using *Xenopus* augmin purified from insect cells[119]) propose that the augmin complex has a Y-shaped structure, composed of two tetrameric subcomplexes. However, the two studies diverge in the description of the composition of these subcomplexes.

Recruitment of γ-tubulin to the mitotic spindle occurs through interaction between HAUS6 with the γTuRC subunit GCP-WD/NEDD1[105,120,121]. Experiments performed in our laboratory showed that, after MT nucleation within the spindle, MT (-)-ends are transported towards the poles in a process mediated both by the direct action of (-)-end directed motors dynein and HSET, and sliding of antiparallel MTs at the central spindle mediated by Eg5[122]. The relevance of this (-)-end poleward transport in building up a proper bipolar spindle is relevant not only in the context of MTs nucleated by the augmin pathway, but also for MTs nucleated by the chromatin pathway (**Figure 7c**).

More recently, an interesting study used mathematical modelling combined with live microscopy in HeLa cells in order to get more insight into how the cooperation of different spindle assembly pathways contributes to k-fibre formation[123]. The authors proposed that once pioneer MTs originated at the centrosome are captured by the kinetochores during early prometaphase, they are stabilised. This generates long-lived templates for augmin-driven amplification. During late prometaphase and metaphase, distribution of growing MT (+)-ends can be almost entirely explained by augmin-dependent amplification of these long-lived MTs.

In vivo, the augmin-mediated pathway may play an even more important role in cells that divide in the absence of centrosomes. During oocyte development in *Drosophila melanogaster* meiosis I occurs in the absence of centrosomes[124]. Indeed, *Drosophila melanogaster* carrying mutations in different augmin subunits are viable and don't present major defects apart from female infertility[107,114]. In mammals, full *Haus6* knockout (KO) mice are not viable and do not survive the blastocyst stage[99]. Similarly, to meiosis I in *Drosophila* females, the first rounds of mitosis during mouse development occur without centrosomes. In these cells augmin is required to cluster the multiple acentrosomal MTOCs, allowing the formation of a bipolar mitotic spindle. So far, no function has been described for augmin during later developmental stages, where centrosomes are present.

2. MICROTUBULES IN BRAIN DEVELOPMENT AND DISEASE

Brain development is a very complex process that relies on proper mitotic expansion of neuroprogenitors followed by different events involving neuronal differentiation which include neuronal specification, polarization, migration, maturation and wiring, among others. All these processes are highly dependent on the establishment of an ordered MT network and its dynamic remodelling. Thus, not surprisingly, brain development is very sensitive to defects in the MT network.

In this section I will summarise the main cellular events that occur during brain and neuronal development and highlight the functions of the MT cytoskeleton in most of them. I will mostly focus on mouse brain development as it is the animal model used in this thesis. Furthermore, special focus will be given to the available information on how new MTs are generated in neurons.

2.1. Histology of embryonic mouse brain development

A very complete brain atlas published in 2017 describes the main histological events occurring during brain development in the mouse embryo[125]. In this section, I will summarize these events in order to facilitate the understanding of the results presented in this thesis.

Mouse brain development starts around day embryonic day 7.0 (e7.0) of gestation with the formation of the neural plate, which consists in a thickened region of the embryonic ectoderm, the neuroectoderm (**Figure 8a**). Folding of the neural plate leads to formation of the neural tube, around e8.5 (**Figure 8a**). Neural tube formation starts by fusion of the neural folds in the boundary between the future hindbrain and spinal cord and proceeds both rostrally and caudally in a zipper-like fashion. Formation of the neural tube concludes with the physical separation of the neuroectoderm (the future central nervous system) from the surface ectoderm (the future skin). The inner ventricular zone

(VZ) of the neural tube is composed of the neuroepithelial progenitor cells that ultimately give rise to the great majority of the neural cell populations in the central nervous system (neurons, astrocytes and oligodendrocytes).

Progressively, the cephalic (more rostral) region of the neural tube dilates and at e9.0 three major brain vesicles are prominent: prosencephalon (forebrain), mesencephalon (midbrain) and rhombencephalon (hindbrain) (**Figure 8b**).

At e9.5, remodelling of the prosencephalon occur through folding of its rostral region. This leads to the division of the prosencephalon into 3 brain ventricles: the two more rostral constitute the telencephalon and will give rise to the two lateral ventricles of the cerebral hemisphere; the other one, more caudal, constitutes the diencephalon and will give rise to the third ventricle, surrounded by the thalamus and hypothalamus (**Figure 8b**).

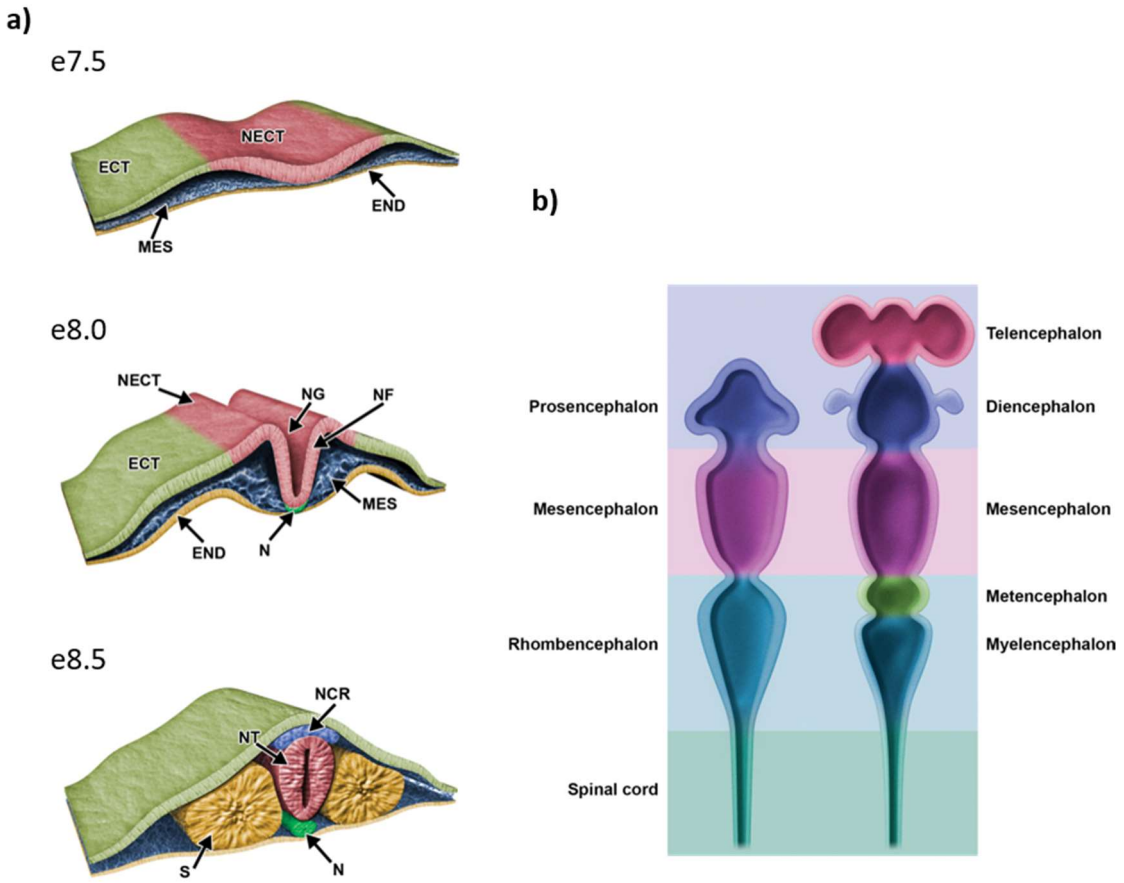

Figure 8 – Main events occurring during early development of the mouse embryonic brain. (a) Around embryonic day e7.0-e7.5 takes place the formation of the neural plate (in red) which

consists in a thickened region of the ectoderm (ECT), the neuroectoderm (NECT). At e8.0 the NECT starts folding, forming a neural groove (NG) surrounded by the neural folds (NF). Neural folds fuse with each other leading to the formation of the neural tube (NT). **(b)** Originally, the neural tube originates three main ventricles in the embryonic brain. At e9.5, remodelling of the prosencephalon, leads to the division of the prosencephalon into three ventricles: two lateral ventricles that correspond to the telencephalon and will give rise to the cortex and another ventricles (more caudal), the diencephalon, from where the thalamus and hypothalamus will be originated**.** Other abbreviations: END (endoderm), MES (mesoderm), N (notchord), NCR (neural crest cells), S (somite pairs). Image from: [125].

At e11.5 the fundamental topology of the brain is established with 5 individual brain ventricles formed. Rapid expansion of the brain results in the formation of larger and more defined subdivisions within the neuroectoderm. At this stage 3 morphologically distinct layers can be identified: The inner ventricular zone (VZ) close to the lumen and harbouring the neuroprogenitors, an intermediate zone and an outer marginal zone.

The cortical plate progressively enlarges, with neurogenesis occurring close to the lumen in the ventricular zone and both at ventricular and subventricular zones later in development.

Cortical neurogenesis occurs in a fast and sustained manner mostly between e11 and e18. On the other hand, neuronal migration and lamination continues until several weeks after birth. The changes that occur in neurodevelopment in mice from approximately e15 until 7 to 10 days after birth are considered equivalent to those that take place during the third trimester of gestation in human foetuses. This includes selective elimination of unneeded cells by programmed cell death (apoptosis). Apoptosis occurs mostly in neurons whose axons are not able to form proper connections with their targets and is crucial for the formation of correct circuits in the nervous system. Other important events are synaptogenesis, dendritic arborisation and myelinization.

2.2. Cortical neurogenesis

Before neurogenesis, the neural plate and the neural tube are composed of a single layer of neuroepithelial cells (NEC) organised into a pseudostratified neuroepithelia. Initially,

NEC expand their pool by undergoing successive symmetric cell divisions (**Figure 9a**). Later, these cells divide asymmetrically giving rise to radial glial cells that sit at the ventricular zone of the cortex[126,127]. Similarly to NEC, radial glial cells (RGC) have a bipolar structure with their centrosomes localizing at the surface of the apical process during most of the interphase[128]. At the apical surface, the centrosome serves as basal body for a short non-motile primary cilium that protrudes towards the lateral ventricle (**Figure 9b**). This primary cilium is disassembled and reassembled every cell cycle and is required for basal-apical polarity of RGCs and its localization at the VZ[129]. On top of that, activity of the primary cilia as a sensor for the Sonic Hedgehog pathway seems to be involved in neurogenesis by regulating the balance between symmetric vs asymmetric divisions of RGCs[130].

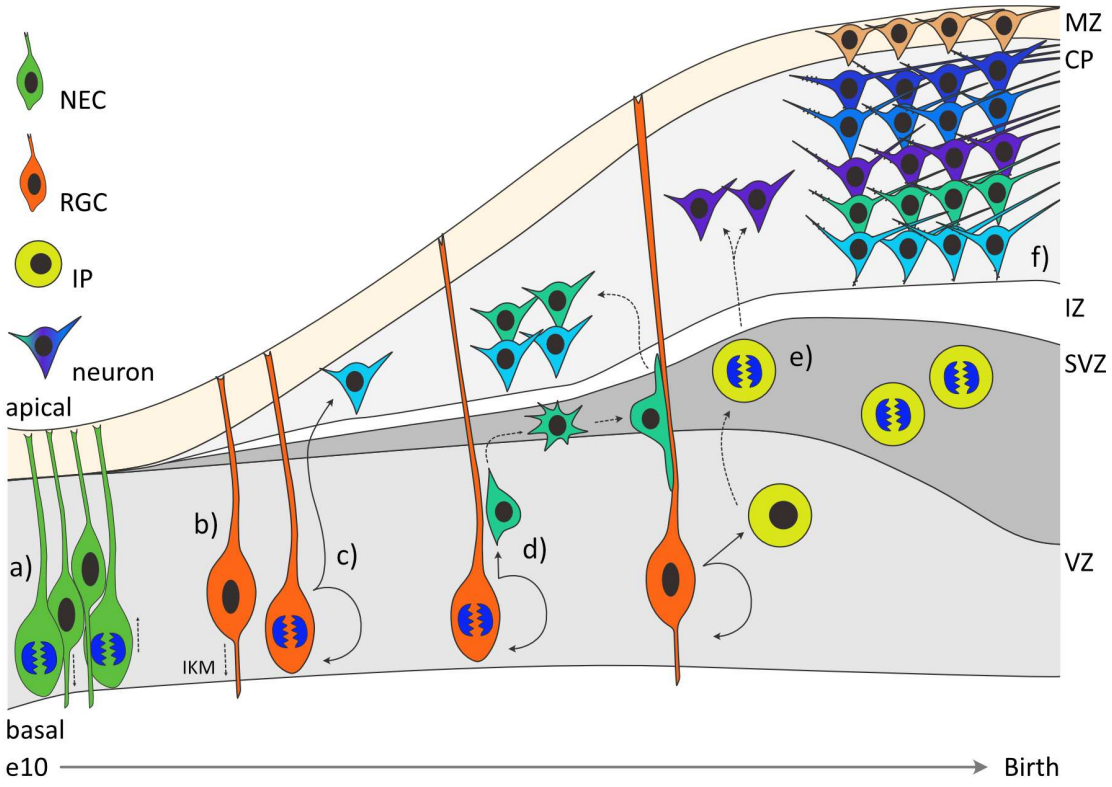

Figure 9 – Schematic representation of the main cellular events occurring embryonically during cortical neurogenesis. Details on the mechanisms described from (a) to (f) are given throughout the main text. Abbreviations: NEC (neuroepithelial cell); RGC (radial glial cell); IP (intermediate precursor); IKM (inter-kinetic nuclear movement); VZ (ventricular zone); SVZ (subventricular zone); IZ (intermediate zone); CP (cortical plate); MZ (marginal zone). Adapted from: [127].

During interphase, the nuclei of RGCs lie within the VZ (**Figure 9b**). In each cell cycle, the nuclei in RGCs undergo interkinetic nuclear migration so that mitosis occurs close to the ventricular surface. At the onset of corticogenesis, neurogenesis occurs mostly through asymmetric divisions of RGCs, producing one daughter RGC and one neuron (**Figure 9c**). Then, neurons migrate apically to outer layers of the cortical plate (**Figure 9d**) through mechanisms that will be described in the next section.

Later in neurogenesis, RGCs give rise to intermediate precursors (IPs) that detach from the apical surface and localize at the subventricular zone (SVZ). In contrast with RGCs, most IPs divide symmetrically giving rise to two identical neurons (**Figure 9e**).

It is important to consider that not only neurons are generated during cortical development. Apart from neurons, other cells types like glia (which can be classified as oligodendrocytes or astrocytes) play a critical role in neurological functions. Whereas during development of lower organisms like flies, neurons and glia are originated coincidentally, in vertebrates, neurogenesis and gliogenesis occur consequentially in time. As previously mentioned, neurogenesis from division of RGCs occurs interruptedly from e11 to e18. Around e18 neurogenesis is supressed and gliogenesis starts with RGCs dividing into astrocytes. Postnatally, gliogenesis proceeds with the formation of oligodendrocytes (revised in [131]).

2.3. Neuron migration

The cerebral cortex comprises two main types of neurons: (1) excitatory projection neurons that migrate radially to integrate the cortical plate; (2) inhibitory interneurons that migrate tangentially to reach the cortical plate[132].

Excitatory cortical neurons originated through division of RGCs migrate towards their final destinations at the cortical plate in a multi-step process[133]. In summary, early after neurogenesis, the newly born neuron adapts a bipolar shape and ascends rapidly towards the SVZ using radial glial fibres as a trail. There, it remains for some time (~24h in the rat brain) assuming a multipolar shape (**Figure 9d**). Neuron migration proceeds by

radial locomotion with the neuron acquiring again a bipolar shape that consists of a leading process towards the cortical plate and a trailing process towards the ventricular zone. In some neurons, axon-dendritic polarization starts already during the migration process. During cellular migration, and depending on the neuronal type, either the leading or the trailing will give rise to the axon[134].

The 6 layers of the cerebral cortex form in an "inside-out" manner with the earlier migrating neurons remaining in the more inner layers (close to the lumen) and the later migrating neurons forming successively outer layers of the cortex (**Figure 9f**).

Centrosomes are involved in both radial and tangential neuron migration. During radial migration, the centrosome localises at the base of the leading process, ahead of the nucleus. While the neuron moves towards the cortical plate, MTs generated at the centrosome extend towards the leading process, producing pulling forces that cause the centrosome to move into the leading process and the nucleus to follow. Nonetheless, some studies show that the nucleus and the centrosome can move independently[135,136].

2.4. Neuron differentiation *in vitro* and *in vivo*

Pyramidal neurons are the most abundant type of excitatory neurons in the cerebral cortex and hippocampus. In fact, pyramidal neurons comprise around two thirds of the neurons in the mammalian cerebral cortex, playing a key role in many cognitive functions[137]. Morphologically, they are multipolar with each neuron containing a central soma (where the nucleus and centrosome are found), one long and thin axon and several shorter but highly branched dendrites (**Figure 11**). The flow of signal in these neurons is mostly unidirectional: (1) dendrites receive chemical synaptic *inputs* coming from other neurons; (2) this chemical signal is translated into an electrical signal by triggering action potentials which are propagated, first to the soma, and then along the axon; (3) at pre-synaptic structures in the axon, action potentials are translated into a chemical signal which, through the release of neurotransmitters, pass on information to another post-synaptic neuron.

As already mentioned, *in vivo*, neuron polarization of cortical/hippocampal pyramidal cells starts during migration, as the leading and trailing edges become either the axon or the apical dendrite. Once neurons reach their final destinations, both elongation of the axonal and dendritic processes, branching of axons and dendrites and formation of dendritic spines proceed until post-natal stages.

Most of the *data* on the molecular mechanisms underlying the different steps of neuronal differentiation come from studies using *in vitro* cultured neurons. In this context, one of the most widely used models is the culture of hippocampal and neocortical neurons from mouse embryos. This was de model used in the *in vitro* work presented in this thesis. Despite being already polarised in the e17.5 embryo, once isolated and plated *in vitro*, these neurons resume their cell differentiation program that includes 5 well-characterised steps **(Figure 10)** [134,138]:

- Stage 1: Shortly after attachment to the surface, cells form motile lamellipodia around the soma from where neurites will preferentially arise.
- Stage 2: These neurites grow forming processes that resemble the ones present in multipolar migrating neurons.
- Stage 3: Some hours after neurite appearance one of the neurites starts growing ~10 times faster than the other neurites and forms branches. This growing neurite will give rise to the axon.
- Stage 4: The other neurites become the dendrites, form branches and grow (still, at a much lower rate than the axon). At this stage axonal growth proceeds and there is maturation of the axon initial segment.
- Stage 5: Around 7 DIV, a process termed maturation or final differentiation starts. This includes the formation of dendritic spines and functional synapses. At this stage, even though there is little growth of axonal and dendritic processes, cells actively make connection between them through the formation of synapses.

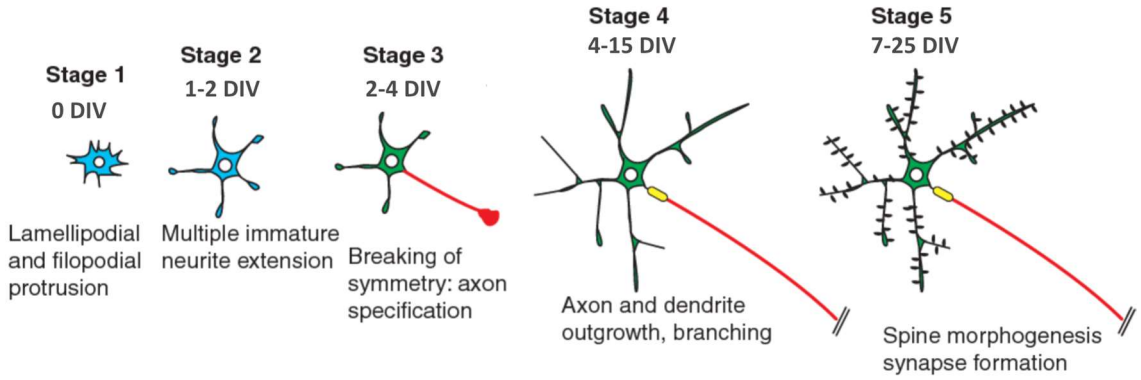

Figure 10 – Model of differentiation stages found in cultured pyramidal neurons. In dissociated cultures, postmitotic cortical neurons display specific transitions with their maturation state classified into five main stages. In stage 1 immature post-mitotic neurons display intense lamellipodia and filopodia around the soma where neurites will preferentially form during stage 2. During stage 3 neuronal symmetry breaks and a single neurite grows rapidly to become the axon (red) while the other neurites acquire dendritic identity (green). Stage 4 is characterized by rapid axon grown and dendritic outgrowth. During stage 4 there is the formation of the axon initial segment (yellow). During stage 5, neurons terminate its differentiation into pyramidal neurons forming dendritic spines and establishing synapses with other neurons. Image copied from:[134].

It is important to consider that there is no strict boundary between each of the stages and that within a neuron primary culture, at a specific timepoint, neurons at different stages develop and cohabitate.

2.5. Role of microtubules during neuron development in vitro

2.5.1. Neuritogenesis

During neuronal migration *in vivo*, or shortly after plating *in vitro*, neuritogenesis starts by the formation of small lamellipodia around the soma. In this process MTs directly invade or are transported by motor proteins into the lamellipodia, originating parallel arrays with their (+)-ends oriented towards the tip of the neurite[139]. At the lamellipodia, MTs become stabilised and push the actin tip, promoting neurite elongation.

2.5.2. Axon and dendritic specification

Neuronal symmetry breaks once one of these minor neurites undergoes rapid growth, becoming the axon, while the growth of the other neurites, which will later become the dendrites, is inhibited.

Cytoskeleton dynamics play a critical role during axonal specification with newly formed axonal shafts showing destabilisation of the actin network and stabilisation of MTs when compared to the other neurites. Indeed, MT stabilisation is a key inducer of axon specification as treatment of *in vitro* cultured rat hippocampal neurons with the MT stabilising drug Taxol leads to the formation of multiple axons. Moreover, local activation of a photoactivatable form of Taxol within an individual neurite can induce that neurite to become the axon. Indeed, newly formed axons are enriched in acetylated and de-tyrosinated MTs, two posttranslational modifications (PTMs) that are characteristic of stable MTs[140]. During the period of this thesis these data were confirmed in our laboratory in a small summer project performed by Mar Fillat (a high school student) which I tutored.

In vitro work suggested that the centrosome determines which neurite will give rise to the axon, by localizing in its proximity[141]. However, another study by the same group showed that upon axotomy, the centrosome is not reoriented towards the newly assigned axon suggesting that, in more mature neurons, centrosome localization is not required for axon re-specification[142]. Still, this is quite a controversial topic with several other studies showing examples of radially migrating neurons where the centrosome localizes close to the leading process that instead of becoming the axon, becomes the primary dendrite[143].

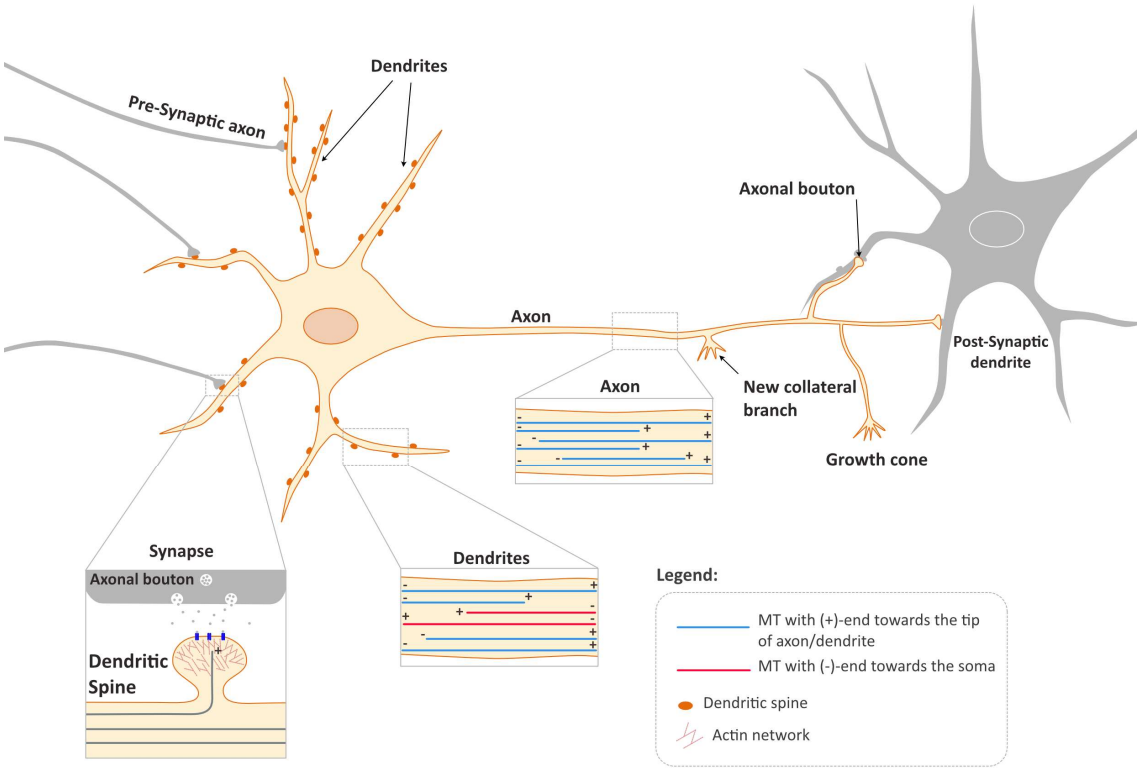

Figure 11 – Microtubule organisation in the different subcellular compartments of mammalian pyramidal neurons. Schematic representation highlighting: microtubule (MT) invasion of dendritic spines and its interaction with the actin cytoskeleton in this subcellular compartment; MT mixed polarity in the dendritic compartment; MT uniform polarity in the axon. Apart from dendrites, dendritic spines and the axon other subcellular structures of the neuron are represented in this scheme: Synapse, new axonal collateral branches, growth cone and axonal bouton.

Even though both axon and dendrites display a MT network with MTs organised into dense bundles, they differ in the orientation of these MTs. In the axon, there is a uniform MT polarity with almost all the MTs pointing with their (+)-ends towards the tip of the axon. In contrast, dendrites display mixed MT polarity with the (+)-end of MTs pointing both towards the soma and the tip of the dendrites (**Figure 11**)[144]. The mechanisms through which these distinct polarities are generated and maintained have been a puzzle and matter of debate for many years.

Another difference between axons and dendrites is their composition in terms of MAPs[145]. A clear example is the distinct distribution of MAP2 and tau, which belong to the same protein family[146]. In mature neurons, MAP2 localizes almost exclusively in the somatodendritic compartment inducing MT stability possibly through MT bundling. Tau,

is enriched in the axon where it may induce stabilisation of MTs both through induction of MT-crosslinking and protection of MTs from the activity of MT severing enzymes like katanin[147,148].

2.5.3. Axon growth and branching

As mentioned before, axons are characterised by the presence of MTs with uniform polarity with barely all MT (+)-end pointing towards the tip of the axon (**Figure 11**). One proposal for how uniform MT polarity is maintained in the axon is that motor proteins sort MTs in this cellular compartment depending on their polarity. This model is based on observations suggesting the existence of transport of short-MTs along MT tracks in the axon in a process mediated by motor proteins. According to this model, which is discussed in [149,150], MT motors transport (+)-end-out MTs anterogradely towards the tip of the axon while (-)-end-out MTs are cleared from the axon by retrograde transport towards the soma. Another speculation is that short (-)-end out MTs generated, for example, through MT nucleation or severing can undergo flipping events at the growth cone, reorienting these MTs to a correct polarity. In this thesis we will discuss another mechanism where the correct (+)-end out polarity of axonal MTs is determined already during MT nucleation events.

Axon specification is followed by fast axonal growth and branching. During both processes, the growth cone, a structure initially identified by Ramon y Cajal in 1890, plays a critical role.

The axon growth cone consists of a “hand-like” structure that is present at the tip of growing axonal branches and is responsible for directed axonal growth (**Figure 11**). Structurally, it is composed of 3 regions named peripheral zone (comprising both actin-rich filopodia and lamellipodia), transition zone and central zone.

At the level of the growth cone, axonal growth can be divided into three individual phases[151]: (1) protrusion, consisting of the extension of lamellipodia and filopodia at the

peripheral zone through actin filament polymerisation; (2) engorgement, where MTs advance and invade the previously formed lamellipodia, carrying membrane vesicles and organelles; (3) consolidation, where MTs are bundled and stabilised and the proximal part of the growth cone assumes a cylindrical structure becoming part of the pre-existing axon shaft. Microtubules at the growth cone are highly dynamic and suppression of MT dynamics slows down axonal growth and supresses growth cone turning in response to guidance cues[152,153].

Axon branching allows neurons to connect to several postsynaptic targets. There are two ways of generating new axonal branches: either through bifurcation of a growth cone, or through the formation of a collateral branches along the axon shaft (**Figure 11**). The second one involves local remodelling of the actin cytoskeleton and generation of a new growth cone through the process described in the previous paragraph. Curiously, in the branching zone, a large number of short MT fragments is observed[154]. At least part of these short MTs is generated by the activity of MT severing enzymes and might serve as seeds to produce new MTs. In fact, spastin depletion decreases axonal branching while its overexpression induces it[155]. Once a new branch is formed, MTs are stabilised (as denoted by an increase in acetylated-tubulin at the proximal part of the branch), whereas at the tip of the new growth cone MTs remain very dynamic[156]. Neurons also display mechanisms to control the generation of new axon collateral branches. For example, the MT depolymerase KIF2A has been proposed to act on newly formed branches, restraining their growth[157].

2.5.4. Dendrite formation, growth and branching

Dendritic development occurs after axonal specification, corresponding to the stage 4 of the development of hippocampal neurons *in vitro* (**Figure 10**). Contrarily to axonal development, dendritic development involves a break with the uniform (+)-end out MT polarity observed in primary neurites. In dendrites there is a mixed MT polarity with

both (+)-end-out and (-)-end-out MTs. This mixed MT polarity increases during dendritic development and is more prominent in proximal regions of the dendrite when compared to more distal regions[139,158].

How this mixed MT polarity is achieved is still not very clear. Recent studies suggest the existence of a difference in stability between MTs of opposite polarity with (-)-end-out MTs being more stable[159]. However, MT-based molecular motors also seem to play a role in this process.

Results from different groups show that inhibition of either KIF23 or kinesin-12 (also known as KIF15) prevents the formation of a mixed polarity MT network in dendrites with (-)-end-out MTs being moved towards the soma, leading to an enrichment in (+)-end-out MTs[160]. These results suggest that the mixed MT polarity in the dendrites must be constantly maintained through the transport of (-)-end-out MTs into the dendrites by molecular motors. Recent work from our laboratory showed that Eg5/KIF11 is able to counteract the dendritic functions of KIF23 and kinesin-12 in the regulation of the percentage of microtubules, suggesting that these motors have the opposite effect in sorting/transporting microtubules[30].

One question that arises from the fact that dendrites possess MTs of mixed polarity is how molecular motors can distinguish between different MT orientations, a requirement for directional cargo transport. Recent outstanding work performed by Roderick Tas and colleagues helps to unravel this puzzle[161]. The authors proposed that, in dendrites, MTs of opposite polarity are organised separately in bundles such that all MT within a bundle have the same polarity and differ in posttranslational modifications: whereas (-)-end-out MTs are more stable and display high levels of tubulin acetylation, (+)-end-out MTs are less stable and enriched in tyrosinated tubulin. Furthermore, two kinesins (kinesin-1 and kinesin-3) were found to interact preferentially with acetylated and tyrosinated MTs, respectively. This mechanism can explain how motor proteins can move in specific directions inside the dendritic shaft, despite the presence of a mixed polarity MT network.

Microtubule severing also has a relevant role during dendritic development. Similar to observations in the axon, activity of both katanin and spastin enzymes is involved in dendritic growth and arborisation[162,163].

2.5.5. Dendritic spine formation

Dendritic spines are small membranous protrusions enriched in post-synaptic components like neurotransmitter receptors, organelles and signalling systems essential for synaptic function and plasticity (**Figure 11**). For a long time, the presence of MTs at these neuronal structures was not clear. However, around 10 years ago it was shown that, indeed, dynamic MTs are able to invade dendritic spines and that an increase in MT invasion correlates with an increase in neuronal activity, spine formation, changes in spine morphology and synaptic plasticity[164,165]. Furthermore, the ability of these dynamic MTs to invade dendritic spines seems to be dependent on the presence of the (+)-TIP protein EB3 at the (+)-end [166].

Whereas MT-based transport of cargos into dendritic spines has not yet been visualised directly, there are several lines of evidence suggesting that MTs are important structures in mediating synaptic cargo delivery (discussed in[167]).

2.6. Sources of new microtubules and microtubule nucleation in developing neurons

In the previous section I have discussed the importance of MTs and of their proper organisation for neuronal development. However, little is known about how new MTs are generated in neurons and how this process is regulated.

For some time, it was believed that neuronal MTs were mostly nucleated at the centrosome. After being nucleated, these MTs would then be released or cleaved through the activity of severing enzymes (katanin, spastin or fidgetin) and transported through the activity of MT-based motor proteins to both axon and dendrites[168–172,160].

However, in 2010 this model was challenged by observations using *in vitro* cultured rat hippocampal neurons showing that, in mature 9 days *in vitro* cultured (DIV) neurons, most of the growing MTs found in the soma were not associated with the centrosome[173]. In contrast, in young neurons (2DIV) most of the MTs were centrosomal. This suggests that, during the process of neuronal differentiation, the centrosome loses its role as major MTOC. Furthermore, laser ablation of the centrosome in young neurons did not affect axonal growth, showing that axonal growth does not depend on MT nucleation from the centrosome. Similarly, it was also observed that centrosome ablation in *Drosophila* neurons did not affect MT polarity at dendrites and axons[174].

These data are in agreement with observations showing that γ-tubulin, γTuRC targeting factor GCPWD/NEDD1 and γTuRC activator CDK5RAP2 are lost from the centrosome during neuronal maturation[175,176]. Furthermore, mutant flies that lack centrosomes in the brain develop normally, questioning the need of centrosomes as a source of neuronal MTs[177].

Even though the centrosome loses its role as major neuronal MTOC, MT nucleation mediated by the γTuRC is still required for the generation of new MTs in the developing neuron. Indeed, data published by our laboratory and by the laboratory of Casper Hoogenraad show that γ-tubulin depletion in *in vitro* cultured mouse hippocampal neurons cultured reduce the amount of MTs in the soma and in the axon, leading to MT unbundling in the soma and impairment of axonal growth[175,178].

One could hypothesise that, during neuron development, another cellular structure may assume the role of the centrosome acting as a non-centrosomal MTOC. Indeed, it was proposed that non-centrosomal γTuRC can nucleate MTs from Golgi outposts localized at branching points in dendrites and that this mechanism is important for dendritic growth and branching[179]. However, these results are still controversial with data using a similar model showing that, indeed, γ-tubulin mediates MT nucleation at dendritic branch points but that Golgi outposts are not required for γ-tubulin to localise to these dendritic locations[180].

2.7. Microtubules in brain diseases

Brain development and homeostasis is particularly sensitive to defects in: (1) neuroprogenitor cell division; (2) neuronal migration and maturation; (3) intracellular trafficking in developing and mature neurons. Therefore, and considering the critical role of MTs in all these cellular processes, it is not surprising that deficiencies in the MT network and MT-based transport have been linked to different types of brain diseases, from neurodevelopmental defects to neurodegeneration.

Microcephaly is a brain malformation characterised by a reduction in the size of the brain and particularly of the cortex. Microcephaly has been linked to defects in the proliferation of neuroprogenitors and increased cell death, as well as the premature differentiation of these cells into neurons (all of which can deplete the neuroprogenitor pool in the developing brain)[181]. Lissencephaly-pachygyria spectrum syndromes are a spectrum of diseases generally caused by defects in neuron migration during brain development[182]. Intellectual disabilities associated with these diseases can range from mild to severe.

Several mutations in genes encoding for α and β-tubulins were shown to cause a wide range of brain malformations often referred to as tubulinopathies [183,184]. In most cases, like mutations in *TUBA1A*, *TUBB2B* and *TUBB3* genes, brain malformations are mostly characterised by lissencephaly or pachygyria which can be accompanied by microcephaly (reviewed in [185]). On the other hand, patients carrying mutations in the TUBB5 gene present microcephaly as the primary brain defect [186]. There are also cases of tubulinopathies whose phenotypes arise postnatally. For example, patients from different families and carrying mutations in the *TUBB4A* gene (poorly expressed during central nervous system development but highly expressed in the adult cerebellum, brainstem and striatum) develop motor dysfunction during infancy, but present normal cognitive and language development[185]. However, the cellular and molecular mechanisms underlying these phenotypes are still poorly understood.

The range of tubulin genes involved in the generation of tubulinopathies was broadened when mutations in the gene encoding γ-tubulin (*TUBG1*) and other γTuRC subunits

(GCP2, GCP4, GCP5, GCP6)[184,187–195] were identified in patients displaying congenital malformations of cortical development. Most patients carrying mutations in the TUBG1 gene develop both microcephaly and pachygyria, accompanied by mild to severe intellectual disabilities. In patients with mutations in *TUBGCP4*, *TUBGCP*5 and *TUBGCP6* microcephaly is also observed. These data confirm the role of the γTuRC in brain development during both division of neuroprogenitors (which is not surprising considering the role of the γTuRC in mitotic spindle assembly) and neuron migration. Indeed, depletion of γ-tubulin or expression of disease related γ-tubulin missense mutants in migrating neurons causes defects in neuronal migration during mouse cortical development[187,188].

But examples of mutations in cytoskeleton-related proteins linked to neurodevelopmental disorders are not restricted to tubulin and γTuRC subunit genes. Indeed, many other examples can be found in the literature where mutations in MAPs, motor proteins or genes required for proper MTOC function affect normal brain development in humans[185]. For example, mutations in the *CDK5RAP2* gene which, as previously mentioned, is involved in activation and targeting of the γTuRC to the centrosome, cause recessive primary microcephaly (MCPH). CDK5RAP2 is highly expressed in the neuronal progenitor pool and, probably, MCPH is caused by spindle and mitotic defects leading to premature neurogenesis and non-proliferative divisions in these cells [196–198]. Moreover, mutations in several genes involved in centriole duplication (namely, *CEP152*, *CEP63*, *CEP135*, *SAS6*, *STIL*, *CPAP*/*CENPJ*) have been linked to MCPH (reviewed in [199]).

Together these data show the importance of MT nucleation and, particularly, the importance of centrosomes for control of proper cell division in neuroprogenitors during human brain development. Furthermore, studies in mice reveal that centrosome loss in neuroprogenitors causes microcephaly by inducing mitotic delay and apoptosis in these cells[200]. On the other hand, little is known about the contribution of other spindle assembly pathways like the augmin or the chromatin-mediated pathways in ensuring mitotic progression and proliferation in neuroprogenitors during brain development.

Additionally, in post-mitotic neurons, reduction in MT mass from axons and dendrites is often associated with neurodegenerative diseases [201,202]. However, it is still unclear how neurons control the formation of new microtubules once MT nucleation at the centrosome is strongly reduced.

Before I started working on my PhD thesis Dr. Carlos Sanchez Huertas, a former Postdoc in our laboratory, observed that despite the requirement of γTuRC-mediated MT nucleation for neuronal development, staining with γ-tubulin specific antibodies did not reveal any cellular structure with γ-tubulin accumulation outside the centrosome. Therefore, he hypothesised that post-mitotic neurons, rather than using a specific MTOC, may nucleate MTs from the lattice of pre-existing MTs in a process mediated by the augmin complex.

When I started my PhD, I contributed to and completed ongoing work on the role of augmin in axonal development. These data were published in 2016 in Nature Communications in a study were I was co-author[175]. Following this study, I decided to study the role of augmin during dendritic development, a cellular compartment where, in contrast to the axon, MTs present a mixed polarity. These results will be presented in the first chapter of this thesis.

In vitro works performed at our and other laboratories implicate augmin in mitosis/cell proliferation and in neuronal morphogenesis in mammalian cells, raising the question of what the *in vivo* role of augmin-mediated MT nucleation is. In this context, studying brain development is a very good model as it allows us to evaluate the role of augmin in both proliferation of neural progenitors and neuron differentiation *in vivo*. With this purpose we generated three conditional *knockout* (cKO) mice where *Haus6* gene is deleted in specific cells during brain development (neuroepithelial cells, young immature neurons and mature hippocampal neurons). Data regarding the characterisation of these cKO mice will be presented in the second chapter of this thesis.

At last, targeting and activation of the γTuRC are important regulatory mechanisms for controlling MT nucleation in different cells. Therefore, I aimed to obtain the first γTuRC

interactome in neurons in order to identify possible targeting, activation and inhibition factors involved in MT nucleation during neural development. The obtained γTuRC interactome and characterisation of a selection of γTuRC interactor candidates during axonal growth will be presented in the third chapter of this thesis.

OBJECTIVES

The main aims of my thesis were the following:

1. Determine the role of augmin-dependent nucleation in the establishment of the neuronal axonal and dendritic microtubule network *in vitro.*

2. Study the *in vivo* role of the augmin complex in proliferation and differentiation during neural development.

3. Analyse how γTuRC-dependent microtubule nucleation is regulated in neurons.

MATERIAL AND METHODS

Mice generation and maintenance

In order to obtain embryonic brain tissue for the experiments with neuron primary cultures, pregnant 6-weeks-old female mice (*Mus musculus*; strain OF1) were purchased from Janvier Laboratories and maintained at the animal facilities of the Barcelona Science Park (PCB), in strict accordance with the Spanish and European Union regulations. At e17.5-e18.5 days of gestation, females were euthanized by cervical dislocation and embryos sacrificed by decapitation.

For the experiments using *Haus6* conditional knockout (cKO) mice, sperm from *Haus6* floxed mice (Assessing number: CDB1354K) was obtained from the laboratory of Dr. Gohta Goshima (Nagoya University, Japan). Originally, *Haus6* floxed mice were generated as described in[203]. Sperm from *Haus6* floxed mice was then used by IRB Mutant Mouse Facility to *in vitro* fertilize C57BL6/J females. The obtained *Haus6* floxed mice were maintained at the animal facilities of the PCB.

Nestin-Cre *Haus6* cKO, Baf53b-Cre *Haus6* cKO and CamKIIα-Cre *Haus6* cKO mouse strains were obtained by crossing *Haus6* floxed mice with B6.Cg-Tg(Nes-cre)1Kln/J, Tg(Actl6b-Cre)4092Jiwu/J and B6.Cg-Tg(Camk2a-cre)T29-1Stl/J mice, respectively.

Transgenic mice expressing Cre recombinase gene under a *Nestin* promotor (B6.Cg-Tg(Nes-cre)1Kln/J) were a gift from Maria Pia Cosma's Laboratory (CRG) and previously purchased by Jackson Laboratories . Transgenic mice expressing Cre-recombinase gene under a *Baf53b* or *CamKIIα* promotors (B6.Tg(Actl6b-Cre)4092Jiwu/J and B6.Cg-Tg(Camk2a-cre)T29-1Stl/J, respectively) were purchased from Jackson Laboratories.

All the mouse strains were generated and maintained on a C57BL/6 background.

Animals were maintained in strict accordance with the European Community (2010/63/UE) guidelines in the Specific-Pathogen Free (SPF) animal facilities in the Barcelona Science Park (PCB). Protocols were approved by the Animal Care and Use

Committee of the PCB (IACUC; CEEA-PCB) in accordance with applicable legislation (Real Decreto 53/2013). All efforts were made to minimize use and suffering.

In order to obtain embryonic tissue from Nestin-Cre *Haus6* cKO mice, pregnant females at e13 and e17 days of gestation were sacrificed by cervical dislocation and embryos sacrificed by decapitation. From these embryos brain tissue was collected for histopathology analysis and tissue from the tail collected for genotyping.

Mouse Genotyping

Genotyping was performed by PCR using genomic DNA extracted from tail biopsies taken at the time of sacrifice or ear biopsies taken at the time of weaning (3 weeks after birth). Both ear and tail biopsies were digested with Proteinase-K (0.4 mg/mL in 10 mM Tris-HCl, 20 mM NaCl, 0.2% SDS, 0.5 mM EDTA) overnight at 56ºC. DNA was recovered by isopropanol precipitation, washed in 70% ethanol, dried and resuspended in H_2O to use in PCR reactions.

To detect *Haus6* wt (800 bp), *Haus6* floxed (1080 bp) and *Haus6* KO (530 bp) alleles by PCR the following pair of primers was used: mAug6KO_FW (5'-CAACCCGAGCAACAGAAACC-3') and mAug6KO_Rev (5'- CCTCCCACCAACTACAGACC-3'). These PCR were run for 35 cycles with an annealing temperature of 64.5◦C.

To detect transgenic Cre-recombinase allele in Nestin-Cre cKO mice and CamKIIα-Cre cKO mice (100bp) the pair of primers olMR1084 (5'- GCGGTCTGGCAGTAAAAACTATC-3') and olMR1085 (5'-GTGAAACAGCATTGCTGTCACTT-3') was used. For this PCR, primers olMR7338 (5'- CTAGGCCACAGAATTGAAAGATCT-3') and olMR7339 (5'-GTAGGTGGAAATTCTAGCATCATCC-3') were used as internal PCR controls (324 bp). These PCRs were run for 35 cycles with an annealing temperature of 51.7◦C.

To detect Cre-recombinase in Baf53b-Cre cKO mice (650bp), the pair of primers 26994 (5'-GCTGGAAGATGGCGATTAGC-3') and 30672 (5'-TCAGCCTGGTTACAAGGAACA-3') was used. For this PCR, primers olMR7338 (5'- CTAGGCCACAGAATTGAAAGATCT-3') and

olMR7339 (5'-GTAGGTGGAAATTCTAGCATCATCC-3') were used as internal PCR controls (324bp). These PCRs were run in two steps of PCR cycles, starting with 10 cycles with a temperature of annealing that starts in 65°C and decreases 0.5°C in each consecutive cycle followed by 28 cycles with a temperature of annealing of 60°C.

All PCR reactions were performed with Taq polymerase (Biotools).

Histology and immunofluorescence of tissue sections

For histopathology analysis of e13 and e17 mouse embryos, animals were euthanized by decapitation and fixed in paraformaldehyde (PFA) 4% diluted in phosphate buffer saline (PBS) pH 7.4. Fixation was performed by incubating the tissue with fixative solution for 3 hours at room temperature followed by overnight incubation at 4°C. After fixation, samples were washed 3 times for 15 minutes with PBS, followed by cryoprotection by incubating the tissue overnight in 30% sucrose diluted in PBS. Tissue was then frozen in OCT (from Tissue-Tek) at -80°C.

For histopathology analysis of 9-10 months mice, animals were euthanized and perfused intracardially with 4% PFA diluted in PBS by using a Gilson peristaltic pump (flow rate: 2-3 mL/minute; perfusion duration: 15 minutes). After perfusion, different tissues were isolated (brain, pancreas, gastrocnemius muscle, kidney, cecum and spleen) and incubated overnight in 4% PBS diluted in PBS at 4ºC. After fixation, samples were washed 3 times for 15 minutes with PBS and embedded into paraffin using standard histological procedures.

From OCT frozen samples, cryosections were cut at 10 µm thickness and placed on glass slides. When a general overview of the tissue histology was required, cryosections were stained with Hematoxilin/Eosin using standard protocols. For immunofluorescence staining, cryosections were thawed at room temperature for 5 minutes and then washed in PBS 3 times for 15 minutes. In PFA fixed samples, this step was followed by heat-mediated antigen retrieval in citrate buffer (10 mM citric acid) at pH6. Tissue sections

were then permeabilized by incubation with PBS containing 0.05% of TX100 detergent (PBST-0.05%) 3 times for 15 minutes and blocked for 1 hour at room temperature with 5% milk powder diluted in PBS containing 0.1% of Triton TX100 detergent. After the blocking step, samples were incubated overnight at 4°C with the desired antibodies diluted in blocking solution. The day after, samples were washed with PBS-T 0.05% (3 times for 15 minutes) and incubated for 1 hour at room temperature with the desired secondary Alexa Fluor antibodies diluted in blocking solution. Incubation with secondary antibodies was followed by washing 3 times with PBS-T 0.05% (5 minutes each wash). When desired, nuclei were labelled by incubation with DAPI.

For paraffin embedded samples, 7 µm thick sections were performed and after paraffin removal using standard histological procedures, stained with either haematoxylin and eosin or with DAPI.

Quantitative real time PCR

Dissected tissue was collected on ice and frozen. Tissues were disrupted in 500 µL of Trizol (Invitrogen) using by passing it several times through a thin needle. After tissue disruption in Trizol, RNA was isolated by addition of 130 µL o Chloroform. The previous mix was incubated for 5 minutes at room temperature and then centrifuged for 15 minutes at 12000g. The transparent supernatant (where the RNA fraction relies) was isolated and incubated with isopropanol for 5 minutes in a 1:1 ratio. The previous mixed was centrifuged for 15 minutes at 12000g and the obtained pellet washed with 75% ethanol. After centrifugation (15 minutes, 12000g) the obtained pellet was dried and resuspended in 50 µL of RNase free water. An amount of 1.5 µg of RNA was used in a reverse transcriptase reaction using a high-capacity RNA-to-cDNA kit (Applied Biosystems) according to manufacturer's specifications. Amplification of the cDNA was done with TaqMan master mix and specific probes for *Haus6*. Probes for *Gapdh* were used as housekeeping controls. Reactions were run on a 7900HT thermocycler (Applied

Biosystems) and data were plotted using SDS2.3 software. The 2−ΔΔCT method was used for the analysis of the amplification products.

Cell cultures

Hippocampal and cortical cell cultures were prepared from brain tissue of e17.5-18.5 mouse embryos. Briefly, tissue was dissected on 10 cm dishes placed on ice and containing cold Hank's solution (0.14 M NaCl, 1 mM $CaCl_2$, 0.4 mM $MgSO_4 \bullet 7H_2O$, 0.5 mM $MgCl_2 \bullet 6H_2O$, 0.3 mM $Na_2HPO_4 \bullet 2H_2O$, 0.4 mM KH_2PO_4, 6 mM D-Glucose, 0.4 mM $NaHCO_3$, pH 7.4 – all reagents from Merck/Sigma). Isolated hippocampi / neocortexes were treated with 0.25% trypsin (Life Technologies) and DNAse (Roche) for 15 minutes at 37°C and dissociated into single cells by gentle pipetting. Neuron density in suspension was calculated by counting cells in a Neubauer chamber. Neurons were then seeded on glass coverslips or plastic plates pre-coated with 0.1 mg/ml Poly-D-lysine (Sigma) diluted in Borate Buffer pH 8.5. Neurons were plated at 6.6 x 10^4 cells per cm^2 for normal density cultures or 1 × 10^4 cells per cm^2 for low-density cultures in DMEM containing 10% fetal bovine serum (FBS) and penicillin/streptomycin (100 IU/ml and 100 µg/ml, respectively). Two hours later, this Plating medium was replaced by Maintenance Medium, consisting on Neurobasal medium supplemented with 2% B27, penicillin/streptomycin (100 IU/ml and 100 µg/ml, respectively), 0.6% Glucose and Glutamax (all reagents from Life Technologies). Neurons were maintained at 37◦C in a humidified atmosphere containing 5% CO2. Cytosine arabinoside (1 µM; Sigma) was added to cultures at 3DIV and 1/3 of the medium was refreshed every 4–5 days. Cultures of low density were supplemented at 2DIV with conditioned media from mature cultures.

HEK293T and Neuro-2a cells were cultured in DMEM containing 10% FBS and penicillin/streptomycin (100 IU/ml and 100 µg/ml, respectively) and kept at 37◦C in a humidified atmosphere containing 5% CO2.

Plasmids

The target sequence for depletion of mouse HAUS7 (sh HAUS7: CCAGATGACCAGGATCTTCTA) and HAUS1 (sh HAUS1: GCTGAACTTACCAAGAAAGTA) were cloned for expression as short-hairpin RNAs (shRNAs) into plKO.1 plasmids. A pLKO.1 plasmid expressing a scrambled sequence (CAACAAGATGAAGAGCACCAA) was used as control. All these pLKO.1 plasmids with shRNA constructs were obtained as bacteria clones from a library of the IRB Barcelona Functional Genomics facility (as a partnership with Sigma-Aldrich RNAi program). The target sequences for simultaneous depletion of mouse γ-tubulin isotype 1 and isotype 2 (CAAGGAGGACATCTTCAA) and mouse CEP170 (CEP170 shRNA #1:GGCGAACCATCTCTAGGAT) (CEP170 shRNA#2: GGATACCAGAGCAGACGTA) were cloned into a pLL3.7 shRNA expression plasmid (Addgene plasmid #11795) following a protocol described in[204]. A pLL3.7 plasmid expressing a shRNA against luciferase (CTTACGCTGAGTACTTCGA) was used as control.

The reporter plasmid EB3-Tomato was a generous gift of Anne Straube (University of Warwick, UK).

Full-length GCP8B was PCR amplified from a human liver cDNA library using the following primers: CCGCTCGAGCGATGGCGGCGCAGGGCGTAGG and CCGGAATTCCTAGGTGCTGCCCTGCGTAGGGCT. For expression in human cells amplified GCP8 sequences were inserted into pEGFP-C1 (Clontech, Palo Alto, CA) containing a modified multiple clone sites using FseI and AscI restriction sites. Green Fluorencence Protein (GFP)-GCP8 was sub-cloned into a pCS2+N-FLAG (Addgene) and pCS2+HA using FseI and AscI restriction sites. GFP-KIF2A plasmid was a gift from the Gohta Goshima laboratory. pEGFP-C1-CEP170 plasmid was a gift from the laboratory of Erich Nigg.

Other plasmids used in this thesis were GFP-GCP8 N-terminal region (amino acids 1-155) and GFP-GCP8 C-terminal region (amino acids 112-158)[205].

Cell culture treatments

Hippocampal neurons were transfected at 2DIV using Lipofectamine 2000 (Life Technologies) according to manufacturer's instructions. To perform transfections, the Maintenance medium was replaced by warmed 37°C Transfection medium (same as Maintenance medium but without penicillin/streptamicin) 20 minutes before the moment of transfection. DNA and Lipofectamine 2000 mixes were made in Neurobasal medium and then added to the neuron plates/well. For the experiments of time-lapse microscopy of EB3-comets, neurons were co-transfected with EB3-tomato and plkO.1 plasmids containing shRNA against HAUS1 or HAUS7 on a ratio 1:3.

HEK293T cells were transfected with Lipofectamine 2000 (Life technologies) according to manufacturer's instructions.

Lentivirus production and transduction

Lentivirus was generated using the LentiLox3.7 system[206]. Briefly, HEK293T cells were co-transfected with a pLL3.7 or pLKO.1 plasmids containing the desired shRNA, and the viral package and envelope plasmids, by using calcium phosphate. 72 hours later, lentivirus particles in the medium were concentrated by ultracentrifugation at 27000 rpm during 2 hours at 4◦C. Virus particles were resuspended in ice-cold PBS and aliquoted and stored at −80°C. Infectivity was assayed for GFP-carrying virus by infecting HEK293T cells with serial dilutions of the concentrated lentivirus, and sorting of GFP-positive cells by FACS 72 hours after infection. Neurons were infected at 1DIV at multiplicity of infection 3. In the case of low-density cultures we used multiplicity of infection 6. The complete medium was replaced with fresh Maintenance medium 16–18 hours after infection.

Antibodies

Table 1 – List of antibodies used in this thesis and respective references and dilutions used for immunofluorescence (IF), Western Blot (WB) and Immunoprecipitation (IP) experiments. Other abbreviations: IgG (Immmunoglobulin G).

Antibody:	Reference:	Raised in:	Dilution:
α -tubulin	Sigma, clone DM1A	Mouse (IgG1)	1:2000 (IF) 1:500 (IF in tissue sections)
Acetylated-α-tubulin	Sigma #T6793	Mouse (IgG2b)	1:50000 (IF)
Actin	MP Biomedicals #691001	Mouse (IgG1)	1:10000 (WB)
β3-tubulin (TuJ1)	AbCam #ab18207	Rabbit	1:1000 (IF)
β3-tubulin (TuJ1)	Biolegend #801201	Mouse (IgG2a)	1:1000 (IF)
CEP170	Bionova #A301-024A	Rabbit	1:2000 (WB); 1:250 (IF)
Cleaved caspase-3	Novus Biologicals #MAB835	Rabbit	1:500 (IF)
Faloidin (polymerised actin)	Alexa 488-phalloidin: Life Technologies #A12379	-	1:500 (IF)
γ-tubulin	ExBio Clone TU-30	Mouse (IgG1)	1:500 (IF)
γ-tubulin	Sigma Clone GTU-88	Mouse (IgG1)	1:5000 (WB)
GCP3	Custom-made antibody produced in our laboratory as described in[207,208]	Rabbit	1:2000 (WB); 1:500 (IP)
GCP4	Custom-made antibody produced in our laboratory as described in[207,208]	Rabbit	1:2000 (WB)
GCP8	Custom-made antibody produced in our laboratory as described in[207,208]	Rabbit	1:2000 (WB), 1:500 (IP)
GFP	Life Technologies #A11120	Mouse (IgG2a)	1:500 (IP)
GFP	Torres Pines Biolabs #TP401	Rabbit	1:2000 (WB)
GFP	Aves Labs #GFP-1020	Chicken	1:1000 (IF)
KIF2A	Novis Biologicals #NB500-180	Rabbit	1:10000 (WB) 1:500 (IF)

Antibody:	Reference:	Raised in:	Dilution:
p53	Cell signaling # CST2524S	Mouse (IgG1)	1:500 (IF)
PAX6	Biolegend #901301	Rabbit	1:300 (IF)
Phospho-Histone3	Millipore #06-570	Rabbit	1:1000 (IF)
Alexa Fluor 488 goat anti-mouse IgG (H+L)	Life Technologies #A11029	Goat	1:500 (IF)
Alexa Fluor 568 goat anti-mouse IgG (H+L)	Life Technologies #A11031	Goat	1:500 (IF)
Alexa Fluor 488 goat anti-mouse IgG1	Life Technologies #A21121	Goat	1:500 (IF)
Alexa Fluor 568 goat anti-mouse IgG1	Life Technologies #A21124	Goat	1:500 (IF)
Alexa Fluor 488 goat anti-mouse IgG2a	Life Technologies #A21131	Goat	1:500 (IF)
Alexa Fluor 633 goat anti-mouse IgG	Life Technologies #A21050	Goat	1:500 (IF)
Alexa Fluor 488 goat anti-mouse IgG2b	Life Technologies #A21141	Goat	1:500 (IF)
Alexa Fluor 568 goat anti-rabbit IgG (H+L)	Life Technologies #A11036	Goat	1:500 (IF)
Alexa fluor 488 goat anti rabbit IgG (H+L)	Life Technologies #A11034	Goat	1:500 (IF)
Alexa chicken 488	Life Technologies #A11039	Goat	1:500 (IF)
Anti mouse IgG-HRP	Jackson Immuno Research Lab. #115-035-003	Goat	1:10000 (WB)
Anti rabbit IgG-HRP	Jackson Immuno Research Lab. #111-035-003	Goat	1:10000 (WB)

Lysates, Immunoprecipitation, Western blot and mass spectrometry

For experiments using *in vitro* cultured primary neurons, cells were lysed at 1DIV, 3DIV, 5DIV or 7DIV with lysis buffer containing (50 mM HEPES pH 8.0, 100 mM KCl, 2 mM EDTA, 0,1% NP40, 10% glycerol) in the presence of protease inhibitors (Complete, Roche) and phosphatase inhibitors (PhosSTOP EASYpack, Roche). Primary neurons infected with virus expressing shRNAs against CEP170 were lysed at 4DIV using the same buffer. For the immunoprecipitation experiments using HEK293T cells, cells expressing either GFP, GFP-GCP8 full length, GCP-GCP8 N-terminal region (aa 1-111), GFP-GCP8 C-terminal region (aa 112-158), GFP-KIF2A or GFP-CEP170 were lysed 24 hours after transfection using the same lysis buffer.

For immunoprecipitation experiments, lysates were clarified by centrifugation (16000 rpm, 15 minutes at 4^{o}C) and cleared lysates incubated for 2 hours at 4^{o}C with 1 µg of purified rabbit IgG or with specific antibodies against either GCP3 or GCP8 (for the experiments with *in vitro* cultured primary neurons) or with a specific antibody against GFP (for the experiments with HEK cells). Then, dynabeads Protein G (Sigma, 10003D) were added to the mixture and incubated for 1 more hour at 4^{o}C. Beads were pelleted and washed with the described lysis buffer 3 times. Beads were then incubated with 1x sample buffer (83 mM Bis-Tris, 50 mM HCl, 3.3% glycerol, 1.3% SDS, 0.3 mM EDTA, 0.01% bromophenol blue, 0.83% β-mercaptoethanol) containing 0.1 M dithiothreitol (DTT). Beads were pelleted and the supernatant was prepared for SDS-PAGE by incubation for 5 minutes at 95^{o}C.

Samples from immunoprecipitation experiments performed with *in vitro* cultured neurons were loaded on a Bis-Tris acrylamide gels (4% for stacking and 12% for running gels) and run at 120 mV in 1x Laemmli buffer (25 mM Tris, 192 mM glycine, 0.1% SDS). The rest of the samples were loaded into Bis-Tris acrylamide gels (4% for stacking and 10% for separation) and run at 120 mV in 1x MOPS buffer (50 mM MOPS, 50 mM Tris-base, 0.1 %SDS, 1 mM EDTA). Proteins were transferred to Nitrocellulose membranes (Milipore) for 90 minutes at 60V in 1x transfer buffer (25 mM Tris, 192 mM Glycine, 20% methanol, 0.1% SDS). Membranes were blocked in 1x TBS-T (25 mM Tris, 150 mM NaCl,

2 mM KCl and 0.1 % Tween20) + milk (5%) and probed with antibodies diluted in 1x TBS-T + milk (5%). Membranes were washed with TBS-T between each incubation step.

For the immunoprecipitation experiments used for identifying candidate GCP3 interactors by MS, 36 wells of 6 multi-well plates containing 7DIV primary cortical neurons cultured at a cell density of ~80000 cells/cm^2 were lysed in lysis buffer containing (50 mM HEPES pH 8.0, 100 mM KCl, 2 mM EDTA, 0,1% NP40, 10% glycerol) in the presence of protease inhibitors (Complete, Roche) and phosphatase inhibitors (PhosSTOP EASYpack, Roche). Lysates where clarified by centrifugation 16000rpm, 15 minutes at 4^{o}C). Cleared lysates were incubated for 2 hours at 4^{o}C with 50 µL of Protein G Sepharose beads (GE Healthcare) previously cross-linked to either control IgGs or to a specific antibody rose in rabbit against GCP3 human protein.

To cross-link the antibodies to beads, Protein G Sepharose beads were washed 3 times with PBS and then incubated with either IgG control or GCP3 antibody (in a proportion of 0.5 µg of antibody per µL of beads) for 1 hour at 4^{o}C. Beads were then washed 3 times with 0.2 M sodium borate pH 9.0 at room temperature. After these washing steps, cross-linking of antibodies to the beads was performed by incubation for 30 minutes at room temperature with 0.02 M dimethyl suberimidate (DMS) diluted in 0.2 M sodium borate pH 9.0. The cross-linking reaction was stopped by incubating the beads with 0.1 M ethanolamine pH 8.0 diluted in sodium borate buffer for 2 hours at room temperature. Beads were then washed with lysis buffer before using them for immunoprecipitation experiments.

After incubation of neuronal extracts with antibody-crosslinked beads for 2 hours, beads were washed 5 times with 1 mL of lysis buffer containing protease inhibitors. Beads were then washed twice with rinsing buffer containing 50 mM ammonium bicarbonate and 75 mM KCl (pH 8-8.5). For elution, beads were incubated with 100 µL of elution buffer (0.125 M ammonium hydroxide pH >11) for 10 minutes. Two consecutive elution steps were performed. Eluates were then lyophilised, resuspended in 200 µL of HPLC-graded water and lyophilized again.

For the preliminary studies using Neuro2a cell lines, lyophilised eluates were resuspended in sample buffer and prepared for SDS-PAGE by incubation at 95^{o}C for 5 minutes. Samples were loaded on a Bis-Tris acrylamide gels (4% for stacking and 10% for separation) and run at 120 mV in 1x MOPS buffer (50 mM MOPS, 50 mM Tris-base, 0.1 %SDS, 1 mM EDTA). Acrylamide gels were then stained with silver nitrate solution using standard protocols.

In order to identify candidate GCP3 interactors from neuronal extracts by MS, lyophilised eluates were resuspended in 100 µL of 50 mM ammonium bicarbonate (pH 8 – 8.5). Trypsin digestion was performed adding 1 µL of trypsin (0.5 µg/µL Promega sequencing grade) to the previous solution. Eluates were trypsinised overnight at 37 ^{o}C and, the next morning, an additional trypsinization step was performed by incubating eluates with additional 1 µL of trypsin for 2 more hours at 37 ^{o}C. Trypsinised eluates were lyophilized in speedvac to evaporate ammonium bicarbonate.

High performance liquid chromatography was conducted using a 2cm pre-column (Acclaim PepMap 50 mm x 100 um inner diameter (ID)), and 50 cm analytical column (Acclaim PepMap, 500 mm x 75 um diameter; C18; 2 um; 100 Å, Thermo Fisher Scientific, Waltham, MA), running a 120 min reversed-phase buffer gradient at 225 nl/min on a Proxeon EASY-nLC 1000 pump in-line with a Thermo Q-Exactive HF quadrupole-Orbitrap mass spectrometer. A parent ion scan was performed using a resolving power of 60,000, then up to the twenty most intense peaks were selected for MS/MS (minimum ion count of 1,000 for activation), using higher energy collision induced dissociation (HCD) fragmentation. Dynamic exclusion was activated such that MS/MS of the same *m/z* (within a range of 10 ppm; exclusion list size = 500) detected twice within 5 sec were excluded from analysis for 15 sec. For protein identification, Thermo .RAW files were converted to the .mzXML format using Proteowizard [18606607], then searched using X!Tandem [14976030] and Comet [23148064] against the human Human RefSeq Version 45 database (containing 36113 entries). Search parameters specified a parent ion mass tolerance of 10 ppm, and an MS/MS fragment ion tolerance of 0.4 Da, with up

to 2 missed cleavages allowed for trypsin. Variable modifications of +16@M and W, +32@M and W, +42@N-terminus, and +1@N and Q were allowed. Proteins identified with an iProphet cut-off of 0.9 (corresponding to ≤1% FDR) and at least two unique peptides were analyzed with SAINT Express v.3.3. Two control runs of anti-IgG control (raised in rabbit) IP were compared to the two technical replicates of anti-GCP3 IP. High confidence interactors were defined as those with a BFDR<1%.

Immunofluorescence staining of cultured neurons

For experiments with *in vitro* cultured primary neurons, cells were fixed with 4% PFA containing 4% sucrose (diluted in PBS) for 15 minutes. For staining with α-tubulin/Acetylated-α-tubulin, cells were fixed using 4% PFA diluted in PHEM buffer (60 mM Pipes, 25 mM Hepes pH 7.4, 5 mM EGTA, 1 mM $MgCl_2$) supplemented with 4% sucrose, 0.25% glutaraldehyde and 0.1% Triton X-100, all from Sigma-Aldrich. All fixed cells were washed with PBS and permeabilised with 0.25% Triton X-100 in PBS for 5 minutes, blocked for 1 hour with 4% bovine serum albumin (BSA, Sigma) diluted in PBS and incubated overnight at 4°C with primary antibodies diluted in blocking solution in a wet chamber. Alexa350, Alexa488, Alexa568 or Alexa633 secondary fluorescent antibodies were used (Invitrogen) and DNA was stained with DAPI. Coverslips were washed with PBS between incubations.

Microscopy

Histology sections stained with hematoxilin/eosin were imaged with the digital slide scanner Nanozoomer 2.0 HT from Hamamatsu.

Immunofluorescently labelled histology sections were imaged with a confocal microscope TCS-SP5 (Leica Microsystem, GmbH).

To analyse α-tubulin / acetylated-α-tubulin levels, and dendritic and axonal length in HAUS1 and HAUS7 depleted neurons and to analyse axonal length in CEP170 depleted

neurons, single-plane images were acquired with an Orca AG camera (Hamamatsu) coupled to Leica DMI6000B microscope. For analysis of α-tubulin / acetylated-α-tubulin levels, a 40x objective was used. To assemble mosaics of complete axons/dendritic arbours 20x and 10x objectives were used and complete mosaics were reconstructed using Las X software from Leica. To analyse CEP170 and KIF2A localisation at the axonal tip a confocal microscope TCS-SP5 (Leica Microsystem, GmbH) equipped with a 63x/1.40 OIL objective was used.

Time-lapse microscopy

Hippocampal cultures were plated in 0.1mg/ml Poly-D-lysine coated glass-bottom dishes (MatTek) and transduced with virus expressing shRNA and/or co-transfected with EB3-Tomato reporter and plKO.1 shRNA expressing plasmids. For double depletion experiments of γ-tubulin and HAUS7, hippocampal cultures were firstly nfected at 1DIV with virus expressing a pLL3.7 plasmid containing shRNA plasmids. For analysis after expression of CDK5RAP2 construct, 3DIV neurons were cotransfected with EB3-tomato and either GFP or GFP-CDK5RAP2 plasmids and imaged 24 hours later.

Live-imaging of EB3-comets was performed in the proximal axonal (~60-80 µm away from the soma) and distal dendritic regions (~20 µm close to the tip of the dendrite) of random transfected neurons using an Olympus IX81 microscope equipped with Yokogawa CSU-X1 spinning disc and a temperature-controlled CO_2 incubation chamber. Image stacks were acquired with 100x/1.4 OIL immersion objective and an iXon EMCCD Andor DU-897 camera, using iQ2 software. Fluorescent images with pixel size of 0.14 µm were taken at intervals of 1 second for 150 seconds. Multiple planes were imaged with a step size of 0.2 µm. Z-stacks were performed by using ImageJ software (NIH).

Image analysis

Histology sections scanned with Nanozoomer 2.0 HT were analysed with NDP.view 2 from Hamamatsu.

The rest of images were processed and quantified using the ImageJ software (NIH).

For all fluorescence intensity measurements, background signal was measured in an adjacent area and subtracted. For each experiment, intensities were measured in images acquired with constant exposure settings and background-subtracted intensities were normalised to the average intensity of the control.

Whole axon and dendritic lengths were measured using NeuronJ macro (ImageJ software). Sholl analysis was performed using Sholl analysis plugin as described before[209] using binary versions of the dendrite tracings generated with the NeuronJ plugin.

Axonal and dendritic EB3-comet analysis was performed using the kymograph macro (ImageJ software), with lines drawn on the trajectories of comets.

Statistical analysis

Statistical analysis was done using the Prism 6 software. Two-tailed unpaired t-tests were performed to compare the experimental groups. The details are reported in the figures and figure legends. For **Figures 12a** group mean differences were assessed using a linear model including the experiment run as a covariate. As a deviation from the normal distribution was observed in the data, a transformation was applied to the data in order to meet the assumptions of the model. This transformation was chosen from the Box–Cox family as it showed to be optimal according to the Maximum Likelihood criteria[210]. For interpretation purposes, results are expressed as adjusted means and standard errors in their original scale after undoing this transformation. For doing so, standard errors were computed from 1,000 simulations generated by the corresponding

model using the R package arm (http://CRAN.R-project.org/package=arm)[211]. A 5% level was chosen for significance of group differences after multiple contrasts adjustment[212].

RESULTS

CHAPTER 1:

IN VITRO ANALYSIS OF THE ROLE OF THE AUGMIN COMPLEX IN ESTABLISHING NEURONAL MICROTUBULE NETWORK

The establishment of a proper microtubule (MT) network is essential for neuronal development and homeostasis. However, little is known about how the generation of new MTs is controlled and regulated during neuronal development. Different studies show that the γTuRC is essential for establishing the neuronal MT network but where these MTs are nucleated is still unclear[175,178]. As discussed in the introduction of this thesis, during neuron maturation the centrosome loses its role as major MTOC. Furthermore, in mouse hippocampal neurons cultured *in vitro*, staining with γ-tubulin specific antibodies does not reveal any structure with γ-tubulin accumulation outside the centrosome. Therefore, Dr. Carlos Sanchez hypothesised that post-mitotic neurons may nucleate MTs from the lattice of pre-existing MTs in a process mediated by the augmin complex.

In the first part of this chapter I will present the results with which I contributed to understand the role of augmin-dependent MT nucleation in the axon and that were published in 2016 in Nature Communications[175].

Augmin controls γTuRC-dependent nucleation and microtubule polarity in the axon

In the axon, MTs display a uniform polarity forming tight bundles of MTs with their (+)-ends growing towards the tip of the axon. The augmin complex is known to promote MT branching with the new nucleated MT having the same polarity as the template MT. Therefore, we hypothesised that augmin could be important for the establishment of the uniform MT polarity observed in the axon.

In order to test this hypothesis, we cultured hippocampal neurons derived from embryonic mouse brain and depleted the γTuRC using a shRNA against γ-tubulin and the

augmin complex using a shRNA against HAUS7 **(Figure 12a,b)**. As a read-out for nucleation events we used the (+)TIP protein EB3 fused to tdTomato fluorescent protein and performed live imaging of EB3 comets in the axon of γ-tubulin and augmin-depleted neurons.

At 1 *day in vitro* (DIV), neurons were infected with lentivirus expressing shRNAs against either luciferase or γ-tubulin. At 3DIV, neurons were co-transfected with a plasmid expressing the (+)-tip reporter EB3-tomato and a plKO.1 plasmid expressing either a control shRNA or a shRNA against HAUS7. EB3 comets were analysed 24 hours after transfection by time-lapse microscopy.

We observed that γ-tubulin depletion causes a reduction in the density of growing (+)-tips in the axon when compared to control. HAUS7 depletion had no significant effect on the density of growing (+)-tips in the axon **(Figure 12c,d)**. On the other hand, whereas control axons only had few MTs with their (+)-tips towards the soma (~2.8% of retrograde microtubules), HAUS7 depleted neurons displayed an increase in MTs with this configuration (~8%) **(Figure 12c,e)**. In this thesis I only present the results that I obtained using one shRNA against γ-tubulin and one shRNA against HAUS7. However, results presented by us in [175] show a comparable reduction in comet density using another shRNA against γ-tubulin and an increase in retrograde MTs using a shRNA against another subunit of the augmin complex, HAUS1.

These results suggest that γTuRC dependent MT nucleation is required to generate MTs in the axon and that augmin properly targets γTuRC to the lattice of pre-existing MTs ensuring that MTs are nucleated with the correct polarity. We suggest that, in the absence of the augmin complex, MT nucleation occurs ectopically and with a random orientation. Indeed, we observed that co-depletion of γ-tubulin and HAUS7 was able to rescue the MT orientation phenotypes observed with HAUS7 depletion alone **(Figure 12c,e)**, supporting our hypothesis.

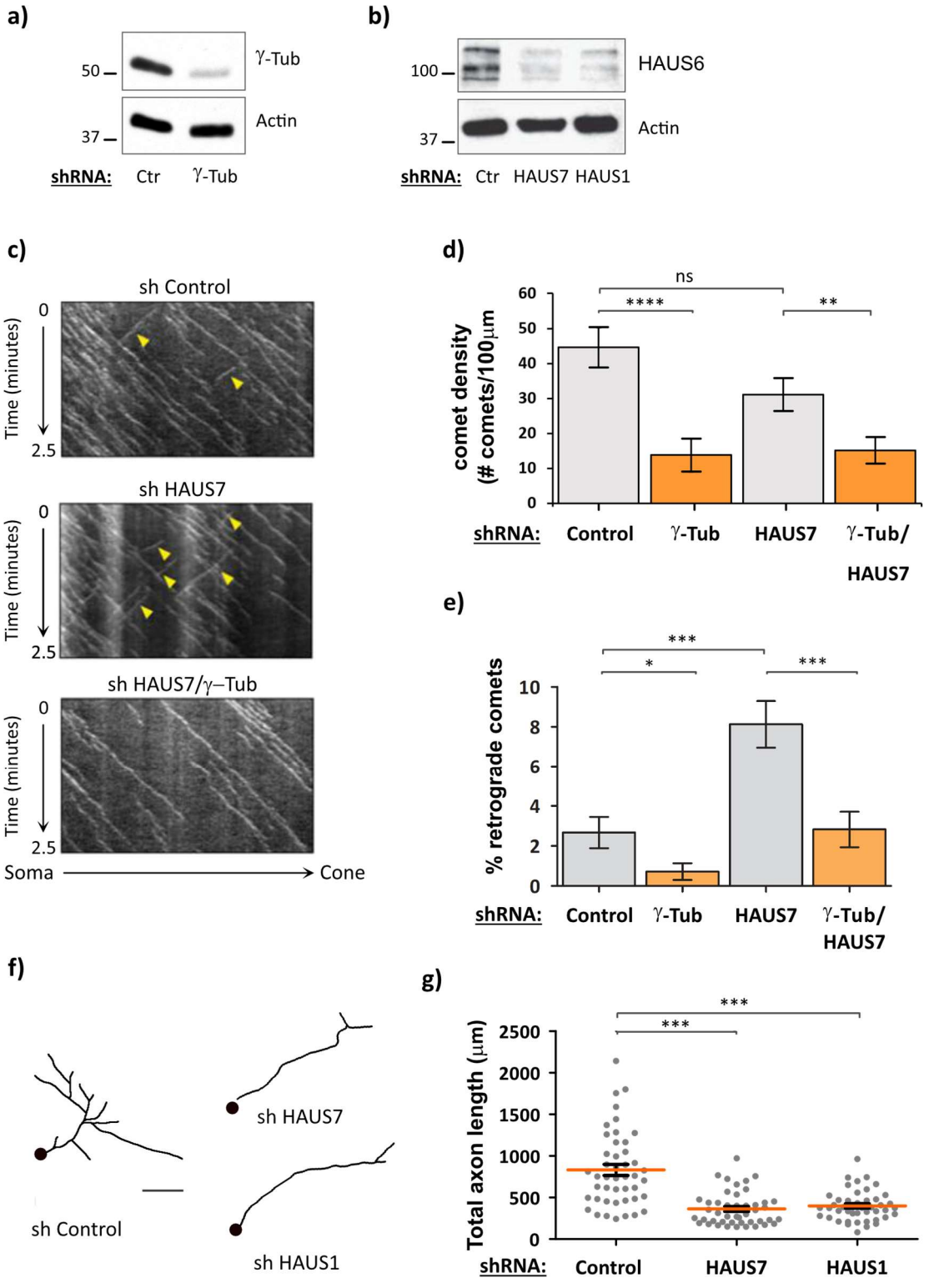

Figure 12: Augmin-dependent nucleation is required for ensuring axonal microtubule uniform polarity and axonal growth. (a) Immunoblot of 4DIV neurons expressing either a shRNA control (Ctr) or a shRNA against γ-tubulin (γ-Tub) using a γ-tubulin specific antibody and a specific antibody against actin as a loading control. **(b)** Immunoblot of 4DIV neurons expressing either a shRNA control (Ctr) or shRNAs against augmin complex subunits HAUS7 and HAUS1. HAUS6 immunoblot is used as read-

out for augmin depletion and actin as loading control. **(c)** Representative kymographs of EB3-comets from control, HAUS7 and HAUS7 + γ-tubulin depleted 4DIV axons. Yellow arrowheads mark retrograde comets (growing towards the soma). **(d,e)** Quantification of EB3-comet density and % of retrograde comets from kymographs like in **(d).** 30-48 axons from 3 individual experiments. *P<0.05, **P<0.01, ****P<0.0001 in the Wald t-tests derived from a linear model. Graph bars show averages normalised using a linear model +/- SEM **(e)** 30-48 axons from 3 individual experiments. *P<0.05, ***P<0.0001 in t-tests. Graph bars show averages +/- SEM **(f)** Representative images of control and HAUS7 and HAUS1 depleted 4DIV neurons. Scale bar 100 µm. **(g)** Quantification of the total axon length from neurons like in d. n=45 axons from 3 individual experiments. ***P<0.001 in two-tailed t-test.

To evaluate the role of augmin-dependent MT nucleation for the development of the axon we measured the axon length in young 4DIV cultured HAUS7 or HAUS1 depleted neurons. We observed that depletion of either augmin subunits caused a strong decrease in the axon length, showing the relevance of this mechanism in axonal growth **(Figure 12f,g)**.

CDK5RAP2 is a human microcephaly protein that, amongst other motifs, contains (1) a centrosomal targeting domain, (2) a Golgi targeting domain and (3) a small γTuRC binding motif which acts as γTuRC-mediated nucleation activator (known as γ-TuNA)[65,213]. In U2OS cells overexpression of the small CDK5RAP2 γ-TuNA domain (aa 51-100) induces ectopic MT nucleation in the cutoplasm.

According to our model we thought that induction of ectopic MT nucleation, by other means rather than removal of the augmin complex, would also cause a disruption in the uniform MT polarity in the axon. To test this hypothesis, we analysed the polarity of EB3-labeled MT (+)-ends in axons of neurons overexpressing the small CDK5RAP2 fragment that harbours the γ-TuNA domain (amino acids 51-100). Indeed, overexpression of this small domain led to an increase, not only in the density of EB3-labelled comets in the axon **(Figure 13b,d)**, but also in the percentage of retrograde MTs (growing towards the soma) **(Figure 13b,c)**. This result clearly shows that induction of ectopic MT nucleation causes defects in MT polarity in the axon.

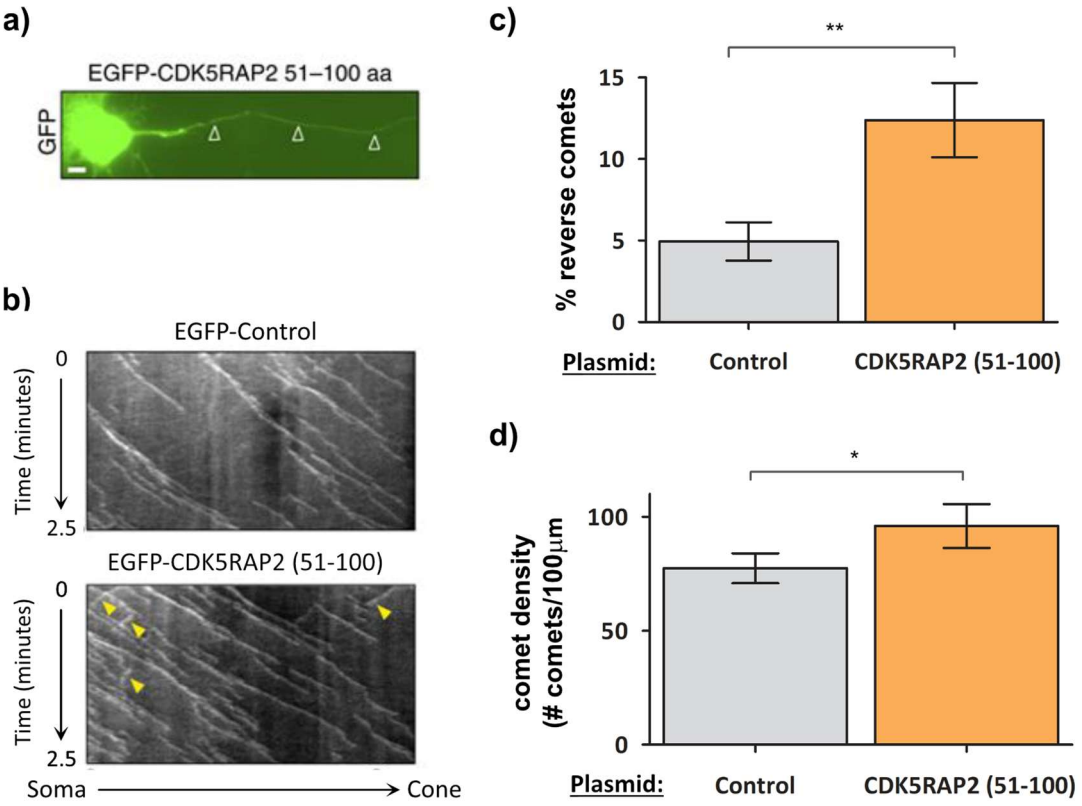

Figure 13 - Induction of ectopic microtubule nucleation impairs uniform microtubule polarity in the axon. (a) Immunofluorescence image of EGFP-tagged CDK5RAP2 51–100 aa in the axon. Scale bar, 5 µm. **(b)** Representative kymographs of EB3-comets in EGFP-Control or EGFP-CDK5RAP2 51–100 transfected axons. Yellow arrowheads mark reverse comets. **(c,d)** Quantification of **(c)** % of retrograde comets and **(d)** comet density in axons of EGFP (Control) and EGFP-CDK5RAP2 51–100 (51–100) transfected neurons from kymographs like the ones in **(b)**. **(c,d)** n=27 (control) and n=28 (CDK5RAP2 51–100) axons analysed from three independent experiments. **(c)** *P<0.05, ***P<0.001 by two-tailed t-test. Graph bars show averages +/- SEM **(d)** Graph bars show averages normalised by a linear model +/- SEM *P<0.05 in the Wald t-tests derived from a linear model.

Augmin-dependent microtubule nucleation is involved in the generation of dendritic microtubule network

In contrast to the uniform MT polarity found in the axon, dendrites have a distinct MT configuration with a mixed polarity containing MTs with (+)-ends growing both towards the soma and towards the tip of the dendrites. We aimed to understand how this mixed MT polarity is controlled and whether augmin could have a role in controlling the amount of anterograde *versus* retrograde MTs or in the generation of both.

We started by analysing how augmin depletion affects the overall MT density in dendrites. For that, 4DIV HAUS7 and HAUS1 depleted neurons were fixed and stained with antibodies under conditions that extracted most of the soluble tubulin but preserve MTs **(Figure 14a)**. Staining with an antibody against α-tubulin revealed that in dendrites from HAUS7 or HAUS1 depleted neurons the density of dendritic MTs was decreased by ~22% and ~47%, respectively **(Figure 14b)**. Since neuronal MTs are highly stable, we evaluated if augmin depletion could also influence dendritic long-lived MTs. A hallmark of long-lived MTs is the abundance of post-translational modifications like acetylation. Therefore, we stained augmin depleted neurons with a specific antibody against acetylated α-tubulin (Acetyl-α-Tub). We observed, that HAUS7 or HAUS1 depletion led to a reduction of ~18% and ~32%, respectively, in the amount of stable MTs **(Figure 14c)**.

To assess the role of augmin-dependent nucleation in establishing the mixed dendritic MT polarity we co-transfected 2DIV neurons with the (+)-tip reporter EB3-tomato and a plKO.1 plasmid expressing shRNAs against either HAUS7 or HAUS1 subunits. 48 hours later, EB3 comets at the distal region of dendrites were imaged by time-lapse microscopy. Both comet density and comet orientation (here shown as % of reverse comets) were measured. Our results show that depletion of either HAUS7 or HAUS1 both cause a significant reduction (~28% and ~25%, respectively) in the EB3-comet density when compared to the control **(Figure 14e)**. On the other hand, no significant difference was found for the orientation of these comets with both control and HAUS7 or HAUS1 depleted dendrites showing ~11-14% of comets growing towards the soma **(Figure 14f)**. These results suggest that augmin is required in dendrites for the generation of MTs with both orientations.

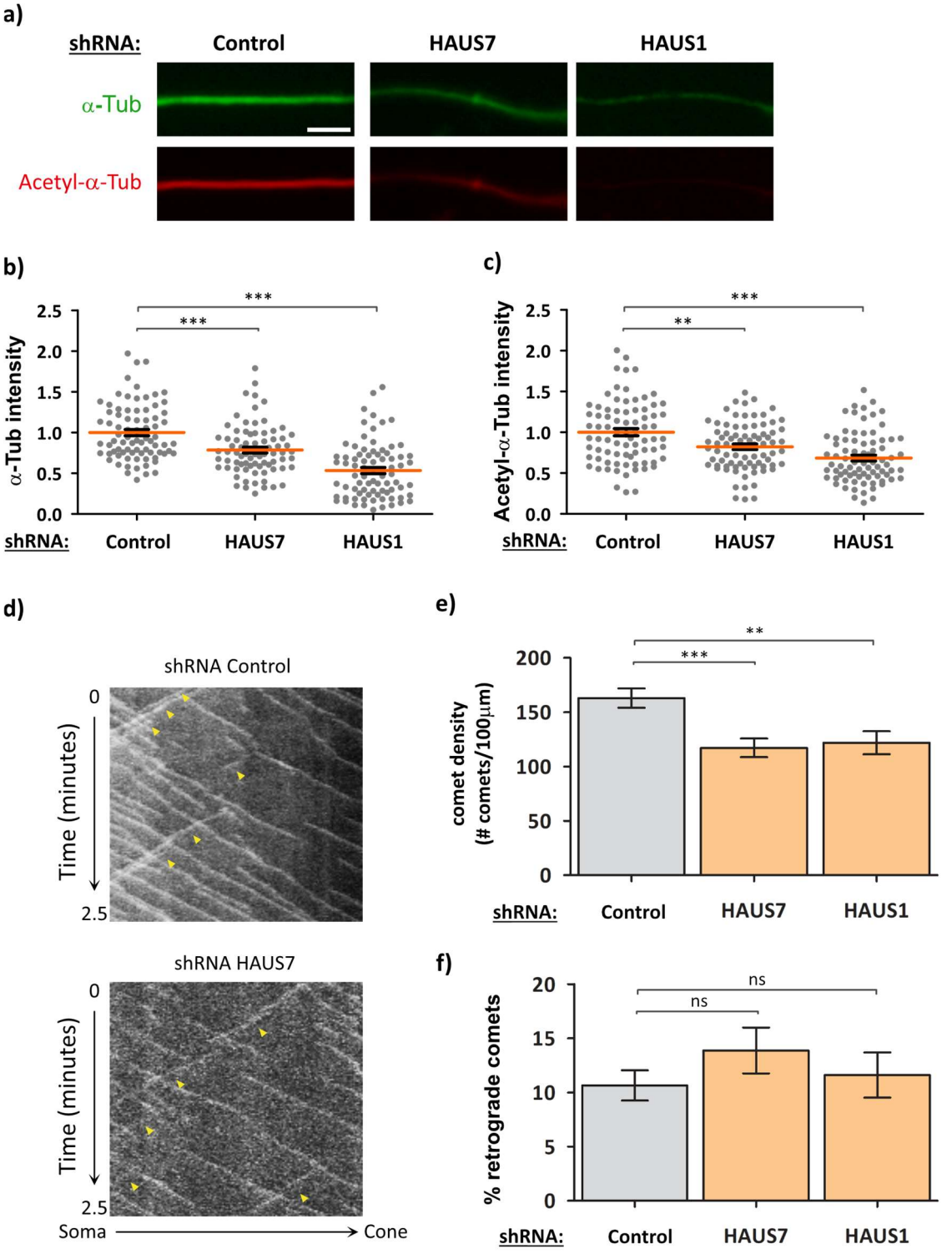

Figure 14 - **Augmin is required to ensure proper microtubule density, but not polarity in dendrites** **(a)** Examples of α-tubulin and acetylated-α-tubulin (acetyl- α-tubulin) co-stainings in dendrites of control, HAUS7 or HAUS1-depleted neurons. Scale bar: 10 µm **(b,c)** Quantification of the mean intensity of α-tubulin and acetyl-α-tubulin staining normalized to the average intensity in control neurons. Dotblots show average +/- SEM n=78-80 cells from 3 individual experiments. (**d)** Representative kymographs of EB3-comets from control, HAUS7 or HAUS1 4DIV depleted neurons. Yellow arrowheads mark retrograde comets. **(e,f)** Quantification of the EB3-comet density and % of

retrograde comets from kymographs like in **(d)**. n=23-33 axons from 3 individual experiments. Graph bars show average +/- SEM **(b,c,e,f)** *P<0.05, **P<0.01, ***P<0.001 by two-tailed t-test.

This reduction in the amount of dendritic MTs causes a delay in dendritic development in young neurons with 4DIV HAUS7 or HAUS1 depleted neurons showing shorter dendrites (~35% and ~22% shorter, respectively, when compared to control) **(Figure 15a)** and a reduction in the dendritic arbour (Sholl analysis shows significant drop in the number of intersections between 10 to 30 µm of distance from the soma) **(Figure 15b)**.

Therefore, we suggest that, even though augmin is not involved in generating the mixed MT polarity characteristic of dendrites, it is required to reinforce the dendritic MT network and consequently, assure their capacity to properly develop and grow.

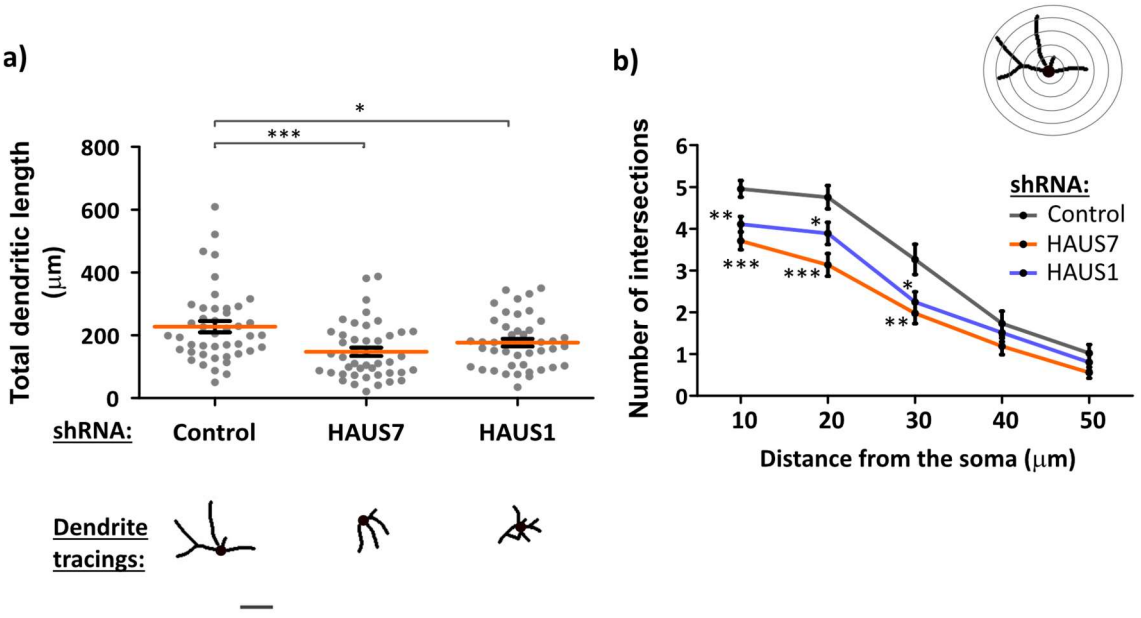

Figure 15 - Augmin depletion impairs dendritic growth in young cultured neurons. **(a)** Dendrite tracings and quantification of total dendritic length of control and HAUS7 and HAUS1 depleted 4DIV neurons. Dotplots show average +/- SEM n=44-45 from 3 individual experiments. Scale bar 30 µm. **(b)** Dendritic sholl analysis of the neurons analysed in a. Graph show average +/- SEM **(a,b)** *P<0.05, **P<0.01, ***P<0.001 in two-tailed t-test.

CHAPTER 2A:

STUDY OF THE MITOTIC ROLES OF THE AUGMIN COMPLEX DURING MOUSE BRAIN DEVELOPMENT

Our data clearly show that augmin-dependent MT nucleation is required for establishing a correct and robust MT network in both axons and dendrites during early neuronal development *in vitro*.

My next goal was to test the relevance of this mechanism in an organism context during brain development. Brain development is very complex and relies on the effectiveness of processes like division of neuroprogenitors and neuronal specification, migration, maturation and survival. At a cellular level all these processes require the establishment and maintenance of a robust MT network. Therefore, we consider that unravelling the role of augmin-dependent MT nucleation during each one of these processes is very pertinent.

With this purpose we took advantage of the C57BL/6-*Haus6* flox mice generated by Dr. Sadanori Watanabe in the laboratory of Dr. Gohta Goshima (Nagoya University).

Haus6 flox mice were obtained from *Haus6* flox Neo mice (Accession No. CDB1218K) previously described in [99]. In these mice, exon 1 of the *Haus6* gene (a key augmin complex subunit) was flanked by LoxP sites but also contained an adjacent PGK-neo cassette. In order to remove the PGK-neo cassette, *Haus6* flox Neo mice were crossed with C57BL/6-Tg(CAG-flpe)36Ito/ItoRbrc (RBRC01834)mice expressing a FLP recombinase (CAG-FLPe). The resultant *Haus6* flox mice without the PGK-neo cassette were maintained by heterozygous crossing in a C57BL/6N background. A scheme showing the genetics strategy used to generate these mice is presented in **Figure 16a**.

It is important to point out that, as described in [99], homozygous *Haus6* KO mice are not viable and die in pre-implantation stages during early embryogenesis. Therefore, studying the role of augmin during brain development requires obtaining tissue specific *Haus6* gene deletion. This can be carried out by crossing *Haus6* flox mice with commercially available transgenic mice expressing Cre-recombinase under control of tissue-specific gene promotors. Therefore, by selectively expressing the recombinase it is possible to induce cellular and tissue specific *Haus6* KO. **Figure 16b** shows that only in mice carrying both the floxed-*Haus6* allele and the Cre-recombinase transgene there is induction of *Haus6* deletion, seen by the appearance of a smaller PCR product that corresponds to the KO allele.

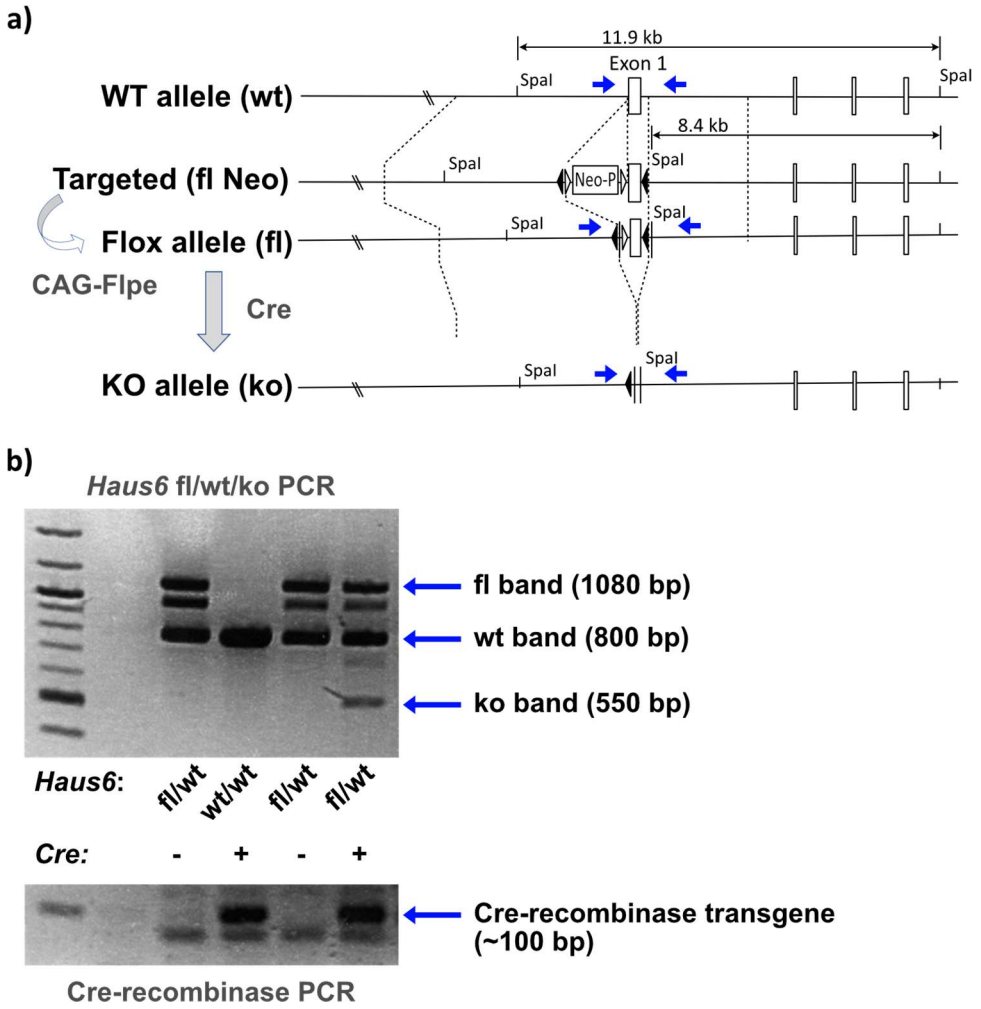

Figure 16 – Strategy to generate floxed-Haus6 mice and Haus6 conditional KO mice. (a) Schematic representation of the wildtype (wt) *Haus6* allele, the targeted allele and the floxed *Haus6* allele.

Positions of exons 1–4, loxP sequences (black triangles), FRT sequences (white triangles), neomycin resistance cassette (neo) and the SpeI site are shown. Positions of PCR primers are indicated by blue arrows (wildtype, floxed and knockout (KO) *Haus6* alleles). **(b)** PCR product using genomic DNA isolated from the tail of 3 weeks-old mice from *Haus6* Nestin-Cre line. For these PCRs, the primers identified as blue arrows in (a) were used resulting in a 1080 basepair (bp) band for the floxed *Haus6* allele, 800bp for the wt *Haus6* alleles and 550bp for the recombined KO *Haus6* allele.

At the beginning of this project we obtained sperm of *Haus6*$^{fl/wt}$ (*Haus6* flox heterozygous) mice fom Gotah Goshima's laboratory (Nagoya University) in a collaboration with Dr. Sadanori Watanabe. This sperm was then used by the IRB mouse mutant facility to perform *in vitro* fertilization (IVF) in order to rederive these mice and obtain living *Haus6*$^{fl/wt}$ mice at the PCB mouse facility.

Microtubules play a critical role during brain development to establish the mitotic spindle of neuroprogenitors and to support neuron migration, maturation and survival. Therefore we wanted to study the role of augmin-mediated MT nucleation in three different steps of brain development: (1) division of neuroprogenitors; (2) in new-born neurons to study neuronal migration and axonal and dendritic formation; (3) in mature neurons in order to study the requirement of augmin for neuron survival and homeostasis.

In order to induce *Haus6* gene deletion during specific stages of mouse brain development, *Haus6*$^{fl/fl}$ (*Haus6* flox homozygous) mice were crossed with mice from 3 different transgenic lines, which express Cre-recombinase under control of promotors for the following genes: *Nestin*, *Actl6b*, *CamKIIα*. Therefore, for each one of the mouse lines generated, KO of augmin occurs only in cells expressing either NESTIN, ACTL6B or CAMKIIα. These mice that have tissue-specific gene deletion are commonly known as conditional knock-out (cKO). Known tissue-specific Cre expression for each of the transgenic lines is summarized in **Table 2**.

Table 2 – Summary of Cre-recombinase expression data found in the literature for the selected transgenic mouse strains used to generate tissue-specific Haus6 conditional knock-out (cKO) mice

Cre-line	Mouse line full name	Tissue expression	Ref.s:
Nestin	Tg(Nes-Cre)1Kln	Progenitor cell types present in the neuroectoderm. At e15.5 recombination might occur in virtually all cells of the brain. Recombination might also occur in the mesonephros and in the somites during development and in the germline.	[214], [215], [216]
Baf53b	Tg(Actl6b-Cre) 4092Jiwu	Neuronal specific. Cre-recombinase is widely expressed at e15.5 in the central nervous system (fore, mid and hind brains and in the spinal cord). At P8 it is also expressed in peripheric and sensory neurons. Recombination also occurs in pancreatic islets.	[217]
CamKIIα	Tg(CamK2α-Cre) T29-1Stl	Forebrain specific recombination occurs postnatally, starting in the hippocampus ≈2 weeks after birth. In 2-month-old mice recombination is uniform in the hippocampus and neocortex.	[218]

Nestin-Cre Haus6 cKO mice are not viable

By crossing *Haus6*$^{fl/fl}$ or *Haus6*$^{fl/wt}$ with *Haus6*$^{fl/wt}$ *Nestin-Cre*$^{+}$ mice, as predicted by Mendel's rule of inheritance, the expected ratio of Nestin-Cre *Haus6* cKO offspring (*Haus6*$^{fl/fl}$ Nestin-Cre^{+}) would be 25% and 12,5%, respectively. After performing numerous crosses, we could never identify any *Nestin-Cre Haus6 cKO* mice at the time of weaning (3-4 weeks after birth) (**Table 3**). This suggested that most likely these *Haus6* conditional KOs were not viable and would die either embryonically or during the first weeks of life. Indeed, when we analysed the new-born offspring from these crosses at P0 we were able to identify some Nestin-Cre *Haus6* cKO mice. However, these mice were not alive.

Table 3 – Genotype analysis of the 3 weeks-old offspring obtained from intercrossing of *Haus6*$^{fl/wt}$ Nestin-Cre^{+} with *Haus6*$^{fl/wt}$ Nestin-Cre^{-} mice. A total of 83 mice genotyped at 3-4 weeks of age were included in these quantifications.

Genotype		Total number of animals	Experimental % of animals	Theoretical (Mendelian) % of animals
Haus6	Nestin-Cre			
fl/fl	**+**	0	0.0%	12.5%
fl/fl	**-**	11	13.3%	12.5%
fl/wt	**+**	17	20.5%	25.0%
fl/wt	**-**	37	44.6%	25.0%
wt/wt	**+**	8	9.6%	12.5%
wt/wt	**-**	6	7.2%	12.5%
Other Genotypes		4	4.8%	0.0%

Another observation from analysis of the offspring obtained from these crosses revealed that, in few cases, mice that do not carry the Cre-recombinase transgene would surprisingly show full recombination of one of its *Haus6* flox alleles, (represented as *Haus6*$^{ko/fl}$ or *Haus6*$^{ko/wt}$). This only occurred when one of the parents carried the Nestin-Cre transgene. As expected, these *Haus6* heterozygous mice were viable. These results are in agreement with the literature where it has been shown that, in some cases, Nestin-Cre transgenic mouse strains express Cre-recombinase transgene in the germline of both males and females[219].

It is relevant to mention that when carrying out these crosses only one of the parents (either the male or the female) carries the Nestin-Cre allele. Since by PCR it is not possible to distinguish from mice carrying one or two alleles of Cre-recombinase, this strategy ensures that the progeny of these crosses will carry at most one copy of the transgene. This avoids ambiguities when characterizing our mouse model due to expression of different levels of Cre-recombinase protein.

Nestin-Cre *Haus6* cKO mice abort brain cortical development during embryogenesis

Nestin-Cre *Haus6* cKO are not viable and the few newborn cKO identified were not alive. Therefore, we decided to analyse these animals at late embryonic stages to get more insight into the reasons leading to this lack in viability.

For that, pregnant females at 17 days of gestation were sacrificed and its embryos genotyped and fixed in paraformaldehyde 4% (diluted in PBS) for brain histopathology analysis. As shown in **Figure 17a,b**, macroscopically there were signs of head and brain development defects in the Nestin-Cre *Haus6* cKO embryos. However, there was no apparent reduction in body size and embryos were still alive. This led us to conclude that cKO embryos die either at the last days of gestation or at birth.

Histopathology analysis revealed a clear disruption in brain development and, particularly, in forebrain development as shown in **Figure 17c,d**. Surprisingly, we observed complete agenesis of the cortex, thalamus and hypothalamus. Different structures of the midbrain and hindbrain (Pons and Medulla oblongata) were present but histologically defective. In addition, Nestin-Cre *Haus6* cKO embryos, also showed agenesis of the cerebellum. Choroid plexus, responsible for cerebrospinal fluid production and movement, was also present in both controls and *Haus6 cKO* embryos.

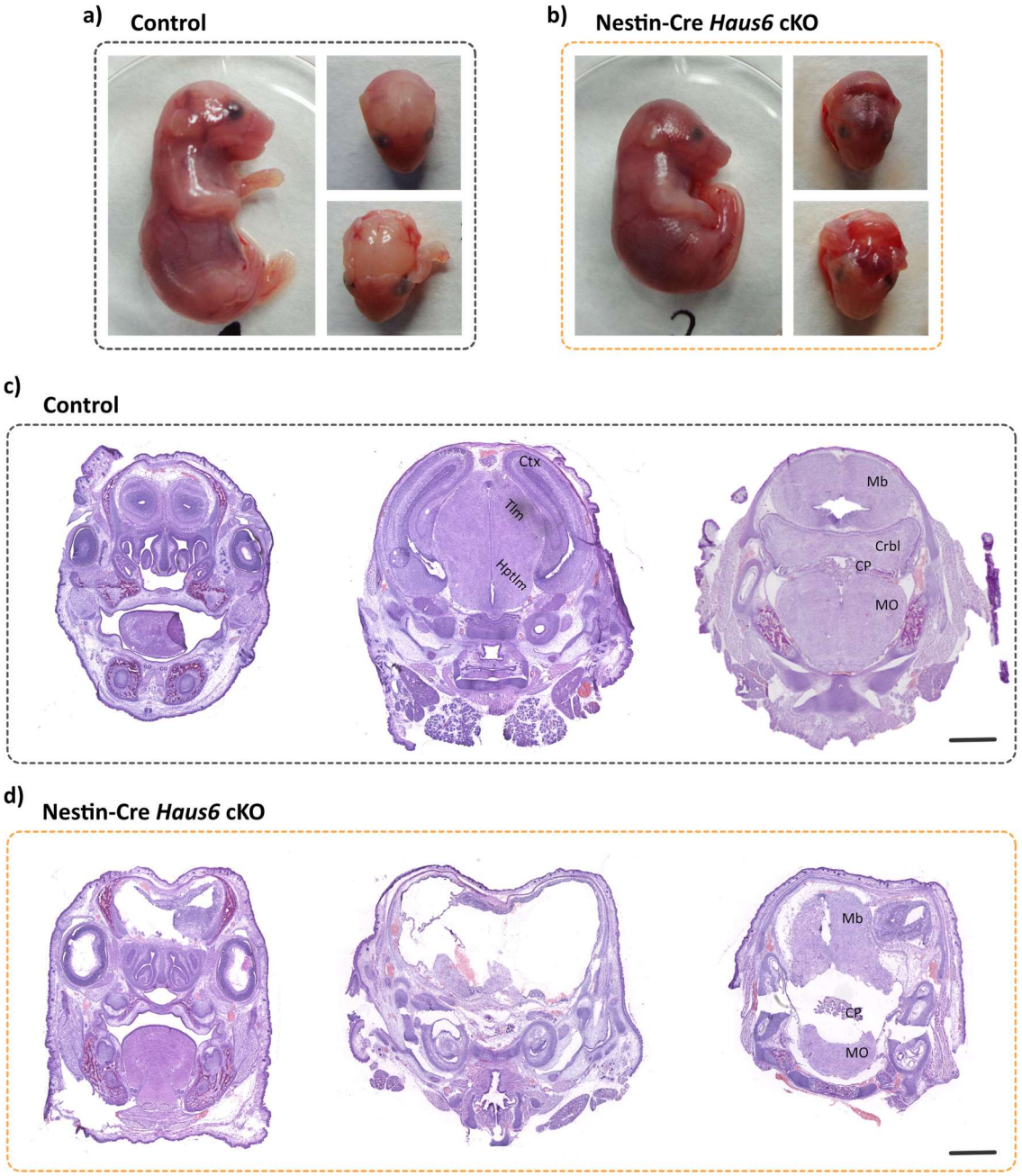

Figure 17 – *Haus6* Nestin-Cre conditional KO mice present drastic brain defects with agenesis of the cerebellum, cortex and other forebrain structures. (a,b) Pictures taken from e17 **(a)** Control (*Haus6*$^{fl/fl}$ Nestin-Cre^{-}) and **(b)** Nestin-Cre *Haus6* cKO (*Haus6*$^{fl/fl}$ Nestin-Cre^{+}) embryos. **(c,d)** Coronal histological sections taken from embryos shown in **(a)** for **(c)** Control and in **(b)** from **(d)** Nestin-Cre *Haus6* cKO and stained with hematoxilin and eosin. Scale bar: 1 mm. Different brain structures are highlighted in these images: **ctx** (cortex), **tlm** (thalamus), **hptlm** (hypothalamus), **mb** (midbrain), **crbl** (cerebellum), **mo** (medulla oblongata) and **cp** (choroid plexus).

Considering that at 17 days of gestation brain defects in these cKO mice were very severe (with absence of many forebrain structures) it was not possible to use these samples to study the mechanisms triggering the observed defects. We decided to analyse Nestin-Cre *Haus6* cKO mice earlier during embryogenesis. Since, forebrain structures were strongly defective in cKO mice we focused our study in this brain region. Neuroprogenitor division during cortical development is a well characterized process with a high rate of neuroprogenitor proliferation around 13 to 15 days of embryogenesis.

Analysis of e13 embryos revealed that, at this embryonic stage, brain development was already impaired in cKOs (**Figure 18a,b**). Surprisingly, at this point there was an almost complete absence of the lateral cortexes in cKO mice. Still, it was possible to identify the structures that will give rise to the thalamus and hypothalamus which surround the third ventricle of the brain. Therefore, we decided to focus our study in this embryonic brain area in order to try to understand the mechanisms leading to impairment in brain development.

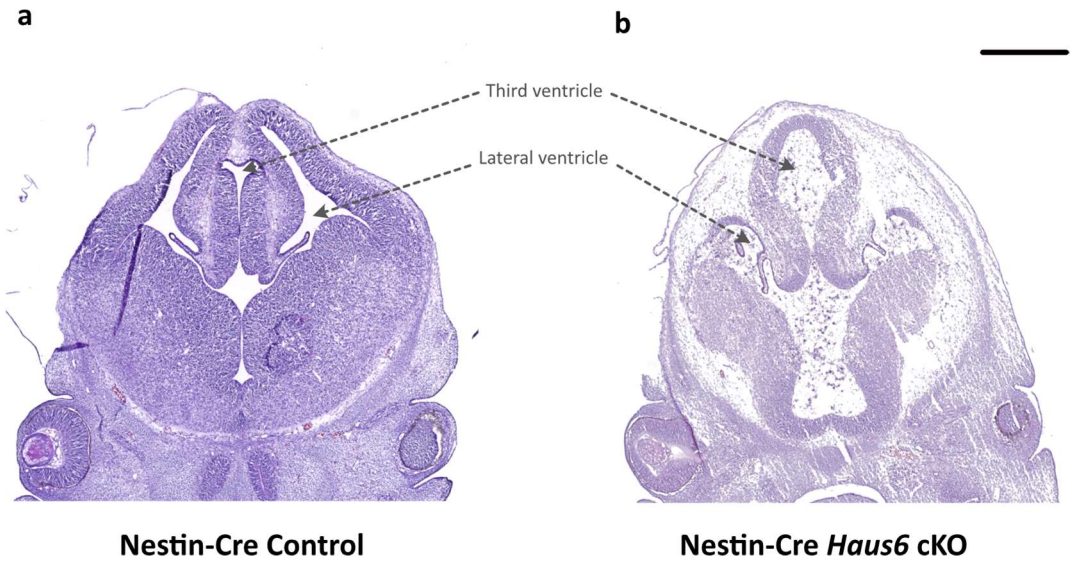

Figure 18 – Forebrain development is impaired in e13 Nestin-Cre Haus6 cKO embryos. (a,b) Pictures taken from e13 **(a)** Nestin-Cre Control (*Haus6*$^{fl/wt}$ Nestin-Cre^{+}) and **(b)** Nestin-Cre *Haus6* cKO (*Haus6*$^{fl/wt}$ Nestin-Cre^{+}) coronal sections stained with hematoxilin and eosin. Scale bar: 0.5 mm.

Since no phenotypic differences were visible between *Haus6*$^{fl/fl}$ Nestin-Cre^{-}, *Haus6*$^{wt/wt}$ Nestin-Cre^{+} and *Haus6*$^{fl/wt}$ Nestin-Cre^{+} (conditional *Haus6* heterozygous) mice, from this point on Nestin-Cre conditional *Haus6* heterozygous mice were be used as controls for this mouse strain.

Haus6 KO in neuroprogenitors leads to accumulation of cells in mitosis

Neuroprogenitor division and the robustness of the mitotic spindle in these cells are essential for neurogenesis during embryonic brain development. Taking this premise into account we evaluated whether mitosis could be affected in *Haus6* deficient neuroprogenitors in Nestin-Cre *Haus6* cKO embryos.

To quantify the amount of neuroprogenitors undergoing mitosis in Nestin-Cre *Haus6* cKOs, coronal sections of e13 embryos were stained by immunofluorescence with an antibody against the phosphorylated form of Histone 3 (pH3), a widely used mitotic marker (**Figure 19a**). Then, the density of mitotic cells was quantified at different distances from the ventricular surface (VS) of the third ventricle (**Figure 19b**). As mentioned in the introduction of this thesis, to divide, neuroprogenitors undergo interkinetic nuclear migration and mitosis occurs mostly closer to the ventricular surface (VS) in the lateral and third ventricles. We observed an almost 3-fold increase in the density of neuroprogenitors undergoing mitosis in the ventricular zone (0 to 30 µm away from VS) in Nestin-Cre *Haus6* cKO when compared to controls. Furthermore, in cKO there was also an increase in ectopic mitoses, with a high increase (>50x) in the density of mitotic cells dividing further than 60µm from the ventricular surface.

An increase in the amount of neuroprogenitors undergoing mitosis at a certain timepoint could have two possible explanations: either there are more cells entering mitosis or there is a mitotic delay during cell division. Considering that spindle and centrosomal defects generally cause an increase in mitotic duration we hypothesised that the existence of a mitotic delay in *Haus6* cKO neuroprogenitors might be the underlying cause for the increase in the mitotic index in the tissue.

To test this hypothesis, we analysed the mitotic phase of neurogenitors dividing close to the third ventricle surface (0 to 30 µm) (**Figure 19c**). For this analysis, classification of the mitotic phase of dividing neuroprogenitors was performed considering the DNA appearance in tissue sections stained with haematoxylin and eosin. When compared to controls, Nestin-Cre *Haus6* cKO displayed a significant 1.7-fold increase in the percentage of cells in prometaphase, accompanied by 0.58, 0.24 and 0.21-fold decrease in the percentage of cells in metaphase, anaphase and telophase, respectively. These data suggested the existence of a mitotic delay in neuroprogenitors from *Haus6* cKO. Still, we also considered relevant to compare which percentage of cells were found in pre-anaphase and post-metaphase stages of mitosis. This analysis showed that in *Haus6* cKO mice 96±2% of the mitotic cells are in prophase, prometaphase and metaphase, whereas in control mice this value was significatively smaller (82±3%) (**Figure 18d**). Together, these data clearly suggest the existence of a large mitotic delay in *Haus6* deleted neuroprogenitors.

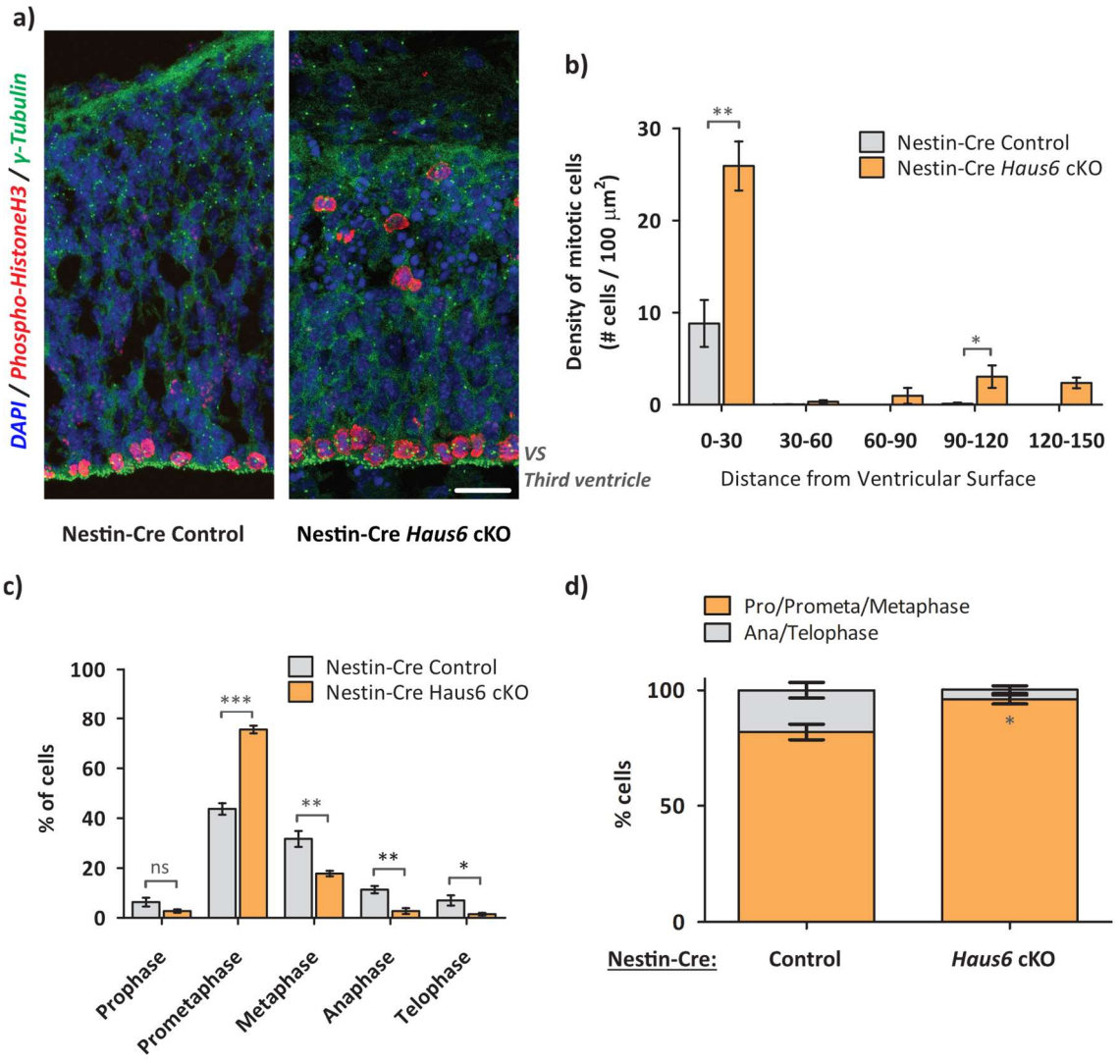

Figure 19 – *Haus6* deletion causes mitotic delay in neuroprogenitors. (a) Representative image of thalamic structures surrounding the third ventricle obtained from coronal sections of e13 Nestin-Cre control (*Haus6*$^{fl/wt}$ Nestin-Cre^{+}) and Nestin-Cre *Haus6* cKO (*Haus6*$^{fl/fl}$ Nestin-Cre^{+}) embryos. IF staining against phospho-Histone3 (magenta-mitotic marker), γ-tubulin (green) and DAPI (blue) Scale bar: 25 μm. **(b)** Quantification of the density of neuroprogenitors undergoing mitosis (# mitotic cells/100 μm) at different distances from the ventricle surface (VS) of the third ventricle. N=4 (Nestin-Cre control) and n=3 (Nestin-Cre *Haus6* cKO) different embryos. **(c)** Relative distribution of mitotic neuroprogenitors along the different cell cycle stages. **(d)** Percentage of dividing neuroprogenitors found in pre-anaphasic and post-metaphasic stages of mitosis. **(c,d)** For this analysis only cells dividing close to the ventricle surface were counted. N=3 (Nestin-Cre Control) and n=4 (Nestin-Cre *Haus6* cKO) different embryos. (b,c,d) Column bars show average±SEM. *P<0.05, **P<0.01, ***P<0.001 by two-tailed t-test.

Haus6 cKO causes centrosome fragmentation in mitotic neuroprogenitors

The augmin complex is known to target the γTuRC to the mitotic spindle, promoting MT nucleation from the lattice of pre-existing spindle MTs. Depletion of several augmin complex subunits causes removal of the γTuRC from spindle MTs, shown by disappearance of the spindle-associated, but not the centrosomal γ-tubulin staining[103,105].

We observed that, in dividing neuroprogenitors from e13 *Haus6* cKO embryos the spindle staining of γ-tubulin was lost. We realised that, whereas in control embryos almost 80% of the dividing neuroprogenitors displayed two circular γ-tubulin dots (which correspond to the two centrosomes), in cKO embryos ~29% of the mitotic cells displayed more than two γ-tubulin dots (a ~6-fold increase when compared to control) (**Figure 20b**). Most of these "extra" γ-tubulin dots are smaller, less roundish and do not display the typical shape of a γ-tubulin centrosomal staining (**Figure 20a**). On top of that, in *cKO* mice, even in mitotic neuroprogenitors presenting two γ-tubulin dots, in most of the cases the γ-tubulin staining presents an aberrant shape characteristic of a fragmented centrosome. While in control embryos only ~13% of dividing neuroprogenitors showed fragmented centrosomes, in cKO embryos this percentage was 7-fold increased to ~56% (**Figure 20c**).

Furthermore, we observed a ~2.5 fold increase in the presence of abnormal/multipolar spindles in neuroprogenitors dividing close to the VS of the third ventricle in *Haus6* cKO embryos when compared to controls (where ~82% of the mitotic cells present proper bipolar spindles) (**Figure 20d,e**).

These results are in agreement with previous data showing that depletion of augmin subunits in HeLa cells cause mitotic spindle defects and centrosome fragmentation during mitosis[104].

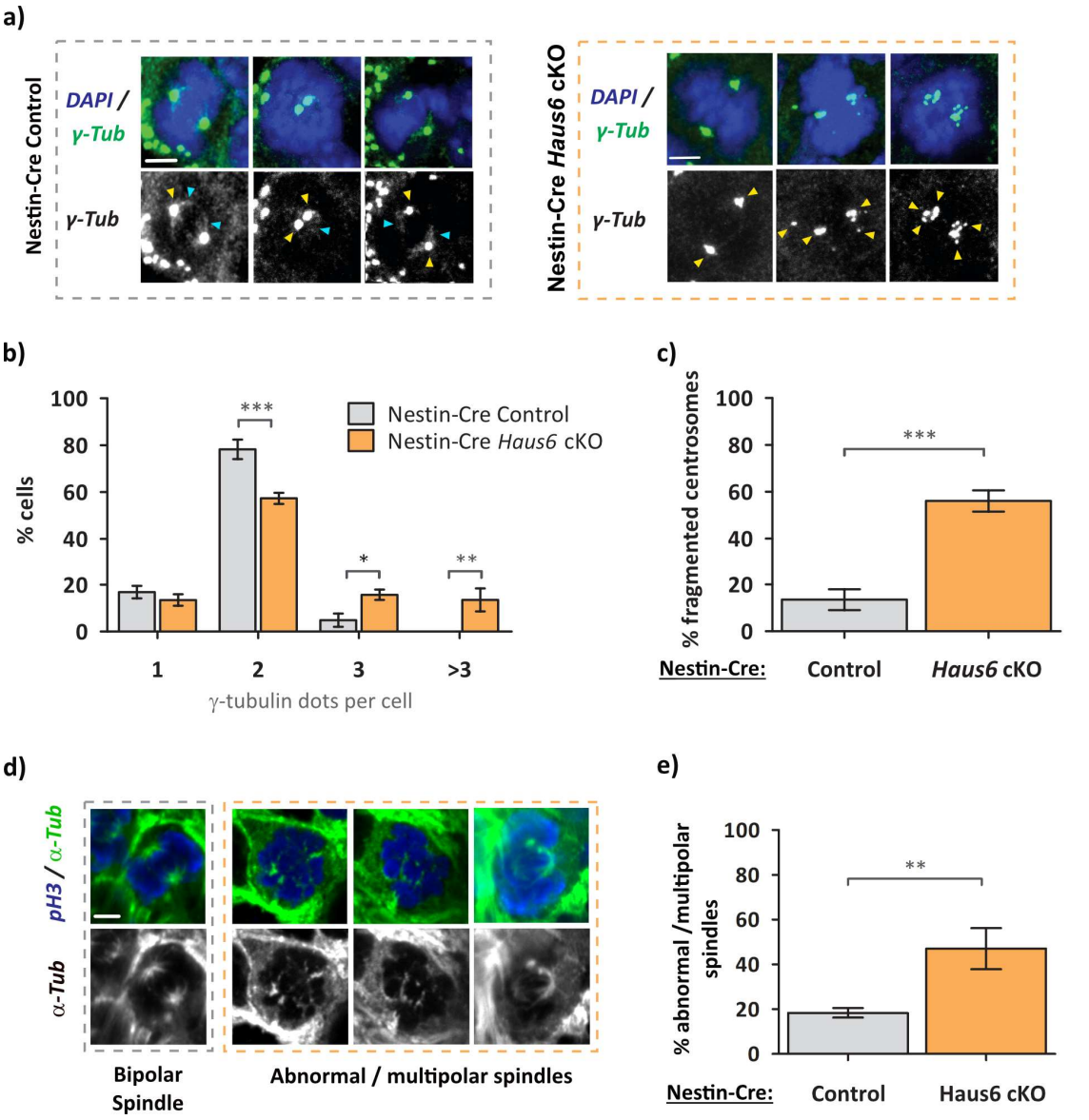

Figure 20 – *Haus6* deletion causes centrosome fragmentation and mitotic spindle defects in dividing neuroprogenitors. (a) Representative images of Nestin-Cre Control (*Haus6*$^{fl/wt}$ Nestin-Cre^{+}) and Nestin-Cre *Haus6* cKO (*Haus6*$^{fl/fl}$ Nestin-Cre^{+}) neuroprogenitors dividing close to the ventricular surface (VS) of the third ventricle. Histologic e13 coronal sections were stained with an antibody against γ-tubulin (green in the upper panel and white in the lower panel) and DNA (DAPI, blue in the upper panel). Scale bar: 3 µm. Yellow arrowheads point to pole-associated γ-tubulin staining. Light blue arrowheads point to spindle-associated γ-tubulin staining **(b,c)** Quantification of the number of γ-tubulin dots per cell and % of cells with fragmented centrosomes in dividing neuroprogenitors like the ones shown in **(a). (d)** Representative images of different mitotic spindle morphologies found in neuroprogenitors dividing close to the VS of the third ventricle. Histologic e134 coronal sections were stained with an antibody against α-tubulin (green) and antibody against phosphorylated Histone-3 (blue), which labels mitotic DNA. **(e)** Quantification of the percentage of mitotic neuroprogenitors from Nestin-Cre Contol and *Haus6* cKO e13 embryos displaying abnormal/multipolar spindles to the **(b,c,e)** Column bars show average±SEM. *P<0.05, **P<0.01, ***P<0.001 by two-tailed t-test.

Haus6 KO leads to massive apoptosis and p53 upregulation in neuroprogenitors

Hematoxilin eosin staining of e13 embryos already showed a high amount of cell debris in the lateral and third ventricles (**Figure 18b**) and an increase in the amount of pyknotic nuclei (characteristic of apoptotic cells) in the tissues that surround them (**Figure 19a**).

In order to confirm the existence of apoptotic cells in these tissues we performed staining with an antibody against cleaved caspase-3, a marker of cells undergoing apoptosis (**Figure 21a**). Whereas in control embryos only a few cleaved caspase-3 positive cells could be identified, in cKO embryos there was a massive concentration of cells expressing the apoptotic marker in the tissue surrounding the third ventricle (**Figure 21b**). Most of the cells expressing cleaved caspase-3 were found in layers closer to the ventricular surface and did not express the neuronal marker β3-tubulin (**Figure 21a**). This data confirms that there is massive cell death in Nestin-Cre *Haus6* cKO forebrain, explaining why these brain structures fail to develop.

One of the most well characterized intracellular signalling pathways that lead to cell cycle exit and apoptosis after delayed mitosis is the pathway dependent on the p53 protein[220–222]. Therefore, we decided to test whether this could be the pathway involved in triggering apoptosis in the brains of Nestin-Cre *Haus6* cKO embryos. As observed with the cleaved caspase-3 staining, barely any p53 positive cells were found in the tissue surrounding the third ventricle in control embryos. On the other hand, a high density of cells expressing increased levels of p53 was found in this tissue in cKO brains (**Figure 21a,c**). Once again, most of the cells overexpressing pP53 were found in more apical regions of the tissue, in the region where neuroprogenitors rely.

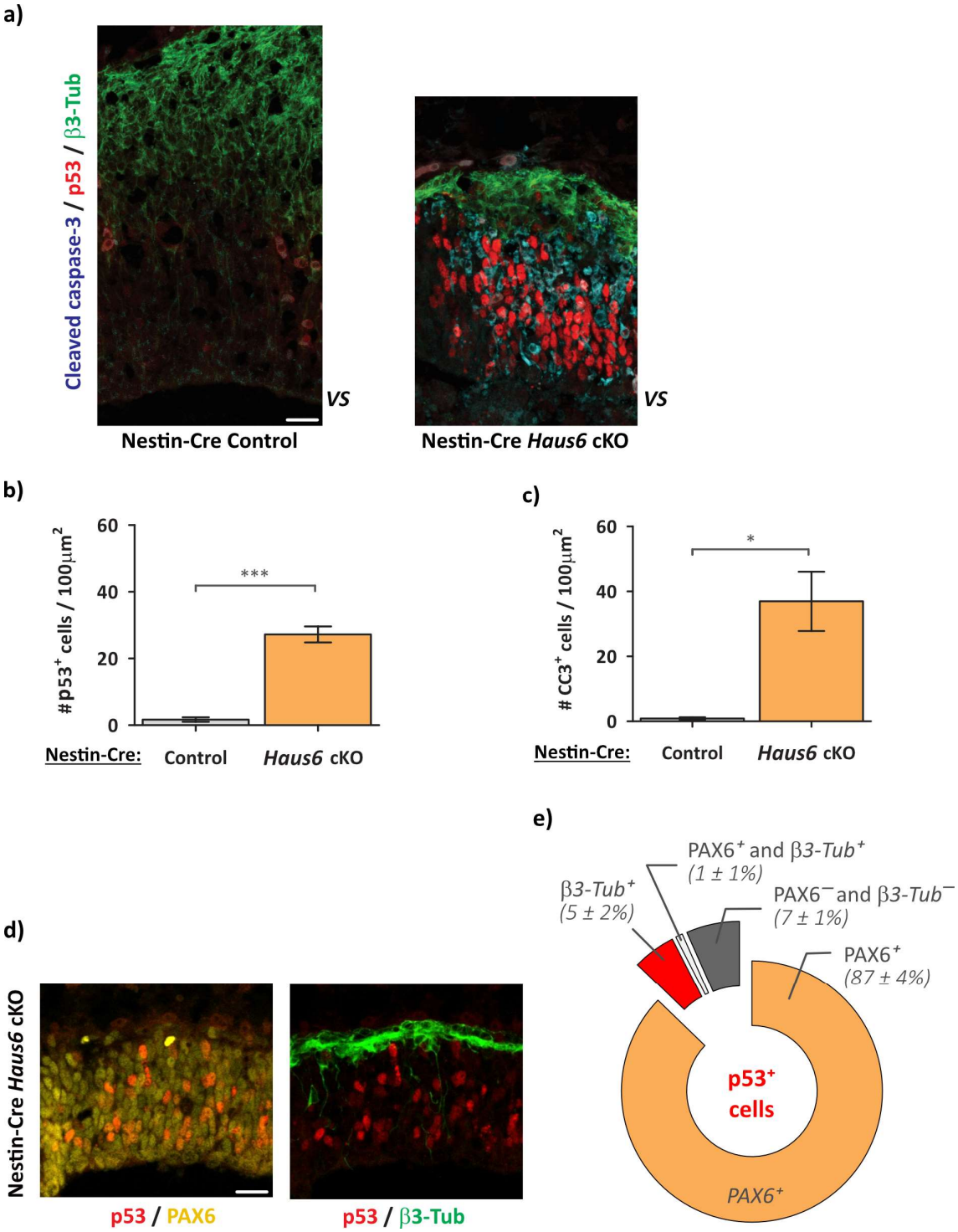

Figure 21 – *Haus6* gene deletion causes massive apoptosis and activation of the P53 pathway in neuroprogenitors. (a) Representative image of thalamic structures surrounding the third ventricle obtained from coronal sections of e13 Nestin-Cre control (*Haus6*$^{fl/wt}$ Nestin-Cre^{+}) and Nestin-Cre *Haus6* cKO (*Haus6*$^{fl/fl}$ Nestin-Cre^{+}) embryos. IF staining against p53 (red), cleaved caspase-3 (light blue) and β3-tubulin (green). Scale bar: 20 µm. **(b,c)** Quantification of the density of cells overexpressing **(b)** p53 and **(c)** Cleaved Caspase 3 from images like the ones shown in **(a)**. Column

bars show average ± SEM. N=3 quantification from 3 individual Nestin-Cre Control and Nestin-Cre *Haus6* cKO. *P<0.05, ***P<0.001 by two-tailed t-test. **(d)** Representative image of thalamic structures surrounding the third ventricle obtained from coronal sections of e13 Nestin-Cre control (*Haus6*$^{fl/wt}$ Nestin-Cre^{+}) and Nestin-Cre *Haus6* cKO (*Haus6*$^{fl/fl}$ Nestin-Cre^{+}) embryos. IF staining against P53 (red), neuroprogenitor marker PAX6 (yellow) and β3-tubulin (green). Scale bar: 20 µm. **(e)** Circular graphic showing quantifications of the percentage of p53-overexpressing cells with co-express either only PAX6 (orange), β3-tubulin (red), both PAX6 and β3-tubulin (white) or none of these markers (grey). Graph bars show averages ± SEM. N=3 quantifications from three individual Nestin-Cre *Haus6* cKO e13 embryos.

In order to evaluate which cells were overexpressing p53 we performed a triple staining with antibodies against p53, the neuronal marker β3-tubulin and the neuroprogenitor marker PAX6 (**Figure 21d**). Since in brain sections from control embryos the amount of cells overexpressing p53 was almost negligible this staining was only performed in histology sections from brains of Nestin-Cre *Haus6* cKO embryos. This experiment revealed that ~87% of the cells positive for p53 co-expressed the neuroprogenitor marker PAX6 and only a small fraction (5%) of p53-posive cells were in fact neurons (β3-tubulin-positive) (**Figure 21e**). It is also important to mention that p53 was not detected in the mitotic cells found in the tissue (data not shown), suggesting that neuroprogenitors undergoing delayed mitosis are able to complete mitosis and only afterwards induce the p53-dependent signalling pathway.

In the first part of this chapter I have discussed the role of the augmin complex in ensuring proper mitotic progression and cell survival of neuroprogenitors during mouse brain development through the analysis of Nestin-Cre *Haus6* cKO mice. In the next part of this chapter I will briefly present some of the results which we obtained with the analysis of Baf53b-Cre *Haus6* cKO mice, where *Haus6* deletion is supposed to occur in young post-mitotic neurons of the central and peripheric nervous system.

CHAPTER 2B:

POST-MITOTIC ROLES OF THE AUGMIN COMPLEX DURING MOUSE DEVELOPMENT

Baf53b-Cre Haus6 cKO are viable but present developmental defects postnatally and develop type-1 diabetes

By crossing *Haus6*$^{fl/wt}$Baf53b-Cre$^{+/-}$ mice with *Haus6*$^{fl/fl}$ mice we observed that Baf53b-Cre *Haus6* cKO (*Haus6*$^{fl/fl}$Baf53b-Cre$^{+/-}$) are viable. Furthermore, at the time of weaning (3-4 weeks after birth), no clear differences in development were observed between cKO mice and control mice (*Haus6*$^{fl/fl}$Baf53b-Cre-/- and *Haus6*$^{fl/wt}$Baf53b-Cre$^{+/-}$) of the same litters. However, and in clear contrast with control mice, which developed normally, Baf53b-Cre *Haus6* cKO mice failed to gain weight **(Figure 22a,b)**.

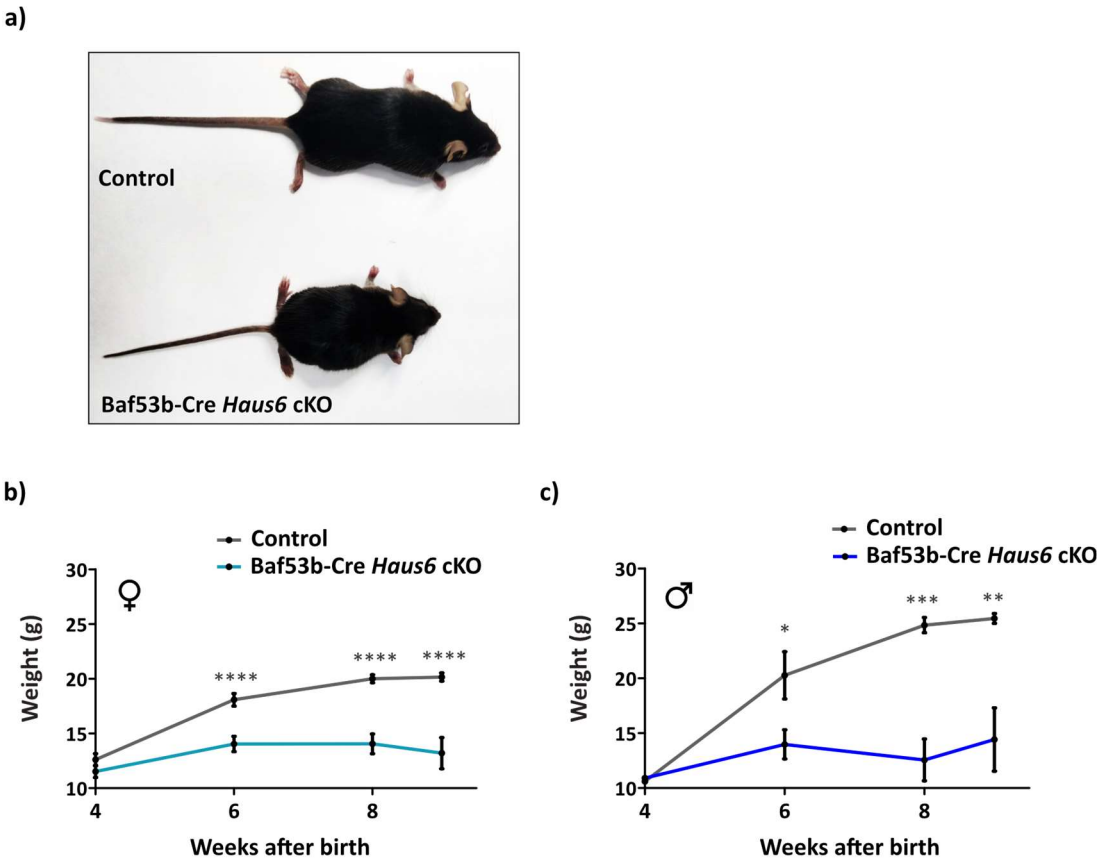

Figure 22 – Mice with Haus6 deletion under control of the Baf53b gene promotor are viable but present developmental defects. (a) Photographs of 9 weeks-old Control (*Haus6*$^{fl/fl}$ Baf53b-Cre$^{-/-}$) and Baf53b-Cre *Haus6* cKO (*Haus6*$^{fl/fl}$ Baf53b-Cre$^{+/-}$). (b,c) Graphical representation of the evolution in

weight of (b) female and male Control and Baf53b-Cre *Haus6* cKO mice between 4 and 9 weeks after birth. Graph shows average ± SEM from (b) 3-8 and (c) 2-5 mice. *P<0.05, **<0.01, ***P<0.001, ****P>0.0001 by two-tailed t-test.

Additionally, around 8 weeks after birth, cKO mice started to present clear welfare problems which included a curved posture, enlarged abdomen difficulties in locomotion and clear signs of pain. Therefore, and for ethical reasons, the endpoint criterium of the experiment was applied around 9-10 weeks after birth. Both Control and cKO mice were euthanised and their different organs fixed and analysed by histology (**Figures 23, 24, 25**).

One of my first observations was that, in cages where Baf53b-Cre *Haus6* cKO mice were housed, water consumption was strongly increased, and mice seemed to produce higher amounts of urine. Since increase in urination and water consumption are two hallmarks in the development of diabetes[223], and considering that Cre-recombinase expression in pancreatic islets have been reported for Baf53b-Cre mice[217] we decided to evaluate the existence of developmental defects in the pancreas of cKO mice.

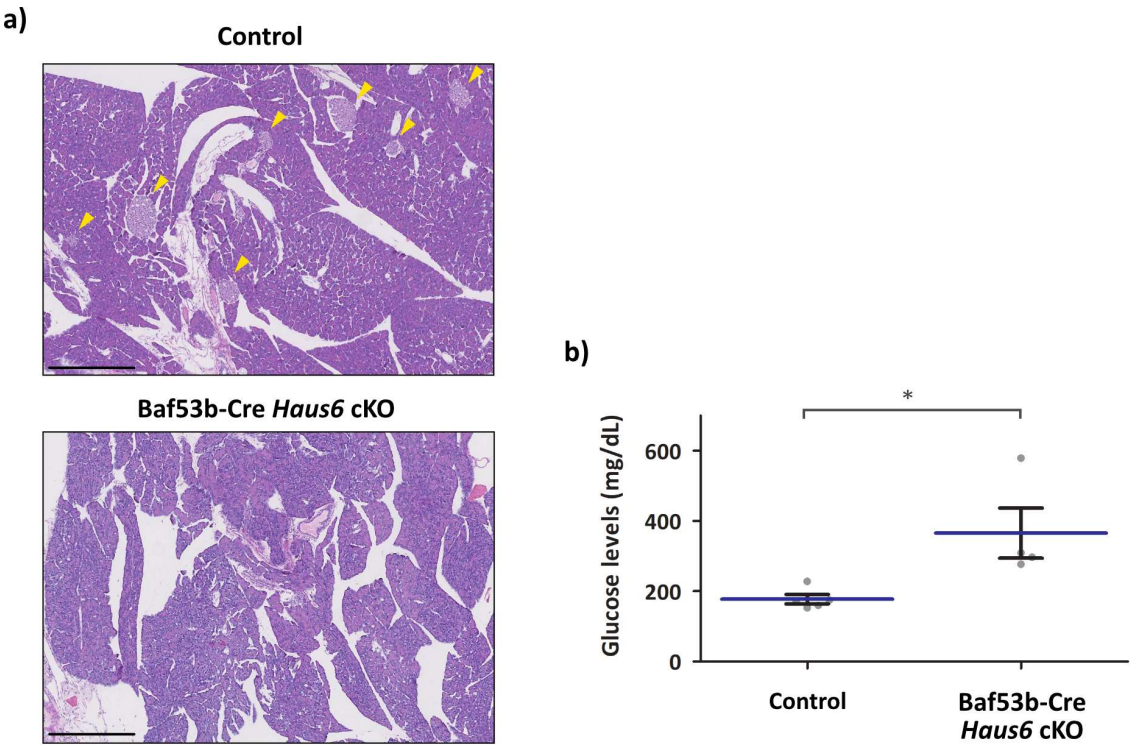

Figure 23 – Baf53b-Cre *Haus6* cKO mice present pancreatic islet atrophy presenting symptoms that suggest the development of type-1 diabetes. (a) Histological cuts stained with Haematoxylin and eosin from Control (*Haus6*$^{fl/fl}$Baf53b-Cre$^{-/-}$) and Baf53b-Cre *Haus6* cKO (*Haus6*$^{fl/fl}$ Baf53b-Cre$^{+/-}$) mice. Pancreatic islets are highlighted by yellow arrowheads. (b) Graphical representation of the glucose

concentration (mg/mL) in the blood of 9-10 weeks old non-fasted Control and Baf53b-Cre *Haus6* cKO mice measured between 8:30am and 10:00am. Graph show average (blue lines) ± SEM. *P<0.05 by two tailed t-test.

Cells of the endocrine pancreas responsible for hormone production cluster into numerous cellular clusters known as pancreatic islets or Langerhans islets. In rodents, 60-80% of the cells that constitute the pancreatic islets are β-cells which are responsible for insulin production. In pancreatic islets β-cells are surrounded by other types of endocrine cells, like α-cells which constitute 15-20% of the cells of the islets and are responsible from glucagon production[224]. Histologic analysis of the pancreas (performed in collaboration with Neus Prats, head of the Histopathology Facility of our institute) revealed a severe reduction in the number of pancreatic islets in Baf53b-Cre *Haus6* cKO mice, when compared to controls (**Figure 23a**). Whereas the controls presented an average of 8-12 of different sized pancreatic islets, only 0-3 small-sized islets were presented in the KO.

Considering the critical requirement of pancreatic islets for insulin production and the role of this hormone for glucose uptake from different tissues we analysed the levels of glucose in the circulating blood in Baf53b-Cre *Haus6* cKO mice. Not surprisingly, the blood of Baf53b-Cre *Haus6* cKO mice revealed a significantly higher glucose concentration in the blood when compared to control mice (**Figure 23b**). It is important to point out that in the graphics shown in **Figure 23b**, three cKO mice were excluded from the analysis as they presented blood glucose levels above the detection limit of the glucometer used (detection limit 600 mg glucose *per* dL of blood), confirming the severity of the phenotypes observed. Furthermore, the phenotypes suggest the development of *diabetes myelitis type 1* in Baf53b-Cre *Haus6* cKO mice.

Our main goal with the development of Baf53b-Cre *Haus6* cKO mice was to study the role of augmin in neuronal migration and axonal and dendritic formation during brain development. Since cortical development is one of the most well-established models to study these processes, we validated *Haus6* deletion in the cortex of cKO mice. With that

purpose we performed mRNA extraction from tissue cortical samples of 9-10 weeks old control (*Haus6*$^{fl/fl}$Baf53b-Cre$^{+/-}$) and Baf53b-Cre *Haus6* cKO mice followed by quantitative real-time PCR (qRT-PCR). These experiments revealed that, Baf53b-Cre *Haus6* cKO display a clear reduction (~75%) in the levels of *Haus6* mRNA (**Figure 24a**).

Interestingly, even though the overall brain morphology was not affected (**Figure 24b**), cKO mice reveal a small but significative reduction in the total brain weight (**Figure 24c**) and in the thickness of the sensory cortex (**Figure 24d**).

Neurons generated by asymmetric and neurogenic symmetric divisions of radial glial cells (in the ventricular zone) and intermediate progenitors (in the subventricular zone) migrate radially to form the different layers of the cortical plate. Neuron migration defects are generally characterised by deficiencies in the formation of these neuron cortical layers. Therefore, we decided to evaluate if the formation neuronal cortical layers was affected in Baf53b-Cre *Haus6* cKO mice. However, whereas there is a tendency in the reduction of the thickness of layers 2/3, 4 and 5/6/7 in cKO mice (which could justify the overall reduction in the thickness of the sensory cortex) no significative difference was observed between the formation of cortical layers between controls and Baf53b-Cre *Haus6* cKO mice (**Figure 24e**).

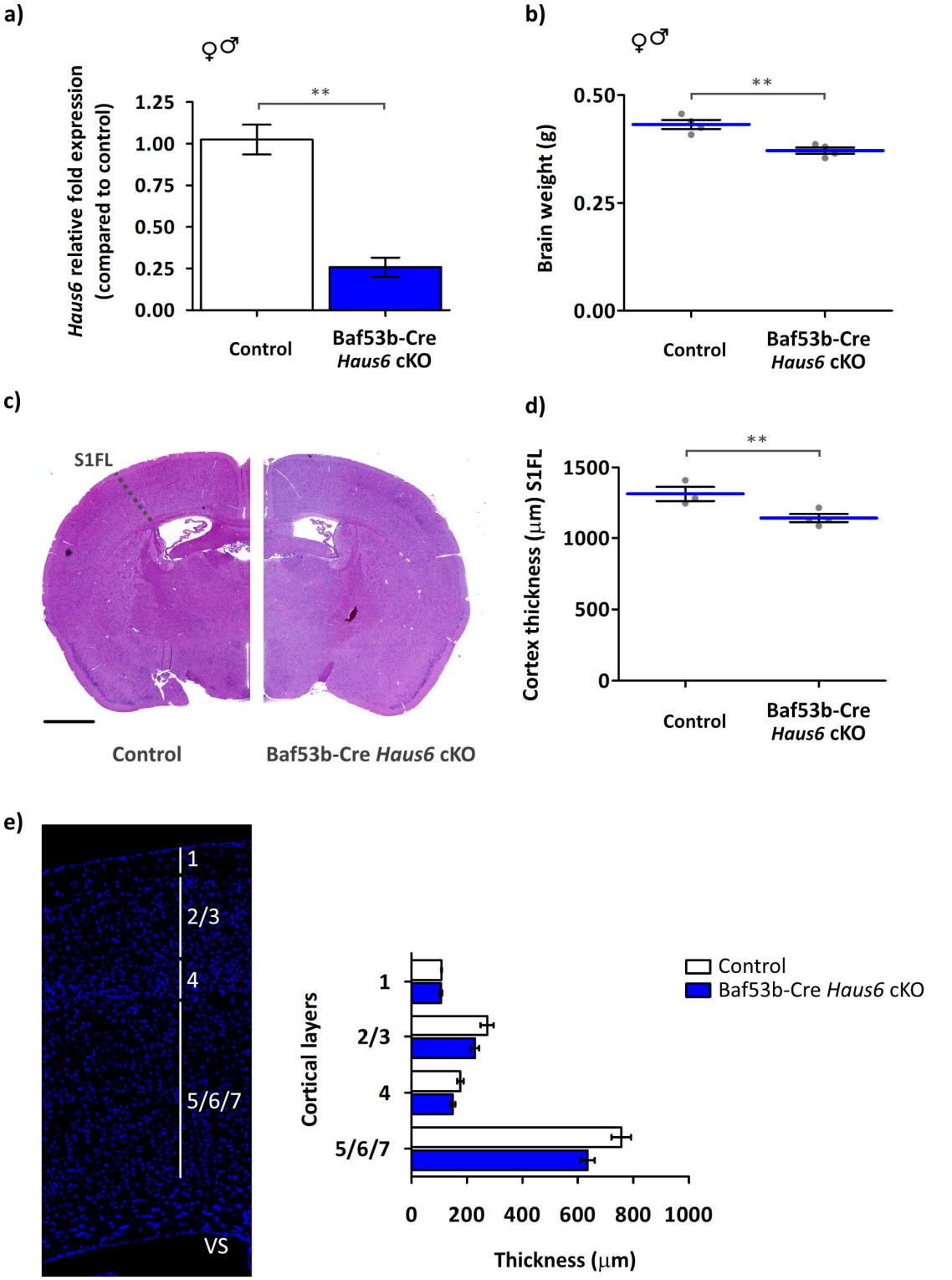

Figure 24 – Baf53b-Cre *Haus6* cKO display a mild reduction in brain size and cortical thickness with no major defects in the formation of cortical layers. (a) Analysis of the *Haus6* mRNA levels by quantitative real time PCR in cortical samples dissected from 9-10 months old Control (*Haus6*$^{fl/fl}$Baf53b-Cre$^{-/-}$) and Baf53b-Cre *Haus6* cKO (*Haus6*$^{fl/fl}$Baf53b-Cre$^{+/-}$) mice. N=3 mice per genotype **(b)** Analysis of the total brain weight of 9-10 weeks old Control and Baf53b-Cre *Haus6* cKO mice. For this analysis non fixed brains were used. N=4 mice per genotype. **(c)** Representative images of brain coronal sections from 9-10 months old Control and Baf53b-Cre *Haus6* cKO mice stained with

haematoxylin eosin. The region of the sensory cortex S1FL is highlighted. Scale bar: 1mm. **(d)** Quantification of the total cortical thickness of the sensory cortex region S1FL highlighted in **(c)** from Control and Baf53b-Cre *Haus6* cKO mice. N=3 control and n=4 Baf53b-Cre *Haus6* cKO mice. **(e)** *(left)* Representative DAPI staining from 9-month-old coronal sections showing the S1FL region of the sensory cortex and highlighting the different layers of the cortical plate. *(right)* Quantification of the thickness of the different layers of the sensory cortex region S1FL highlighted in **(c)** from Control and Baf53b-Cre *Haus6* cKO mice. N=3 control and n=4 Baf53b-Cre *Haus6* cKO mice. **(a,e)** Column bars show averages ± SEM. **(b,d)** Graph shows averages (blue lines) ± SEM. **P<0.01 in two tailed t-tests.

Apart from pancreatic defects and mild brain defects Baf53b-Cre Haus6 cKO mice also presented: (1) locomotive difficulties; (2) increase in the production of urine; (3) large enlargement of the cecum; (4) Strong reduction in spleen size. Therefore, in collaboration with Neus Prats we performed a histopathology study in control and Baf53b-Cre Haus6 cKO mice, which included analysis of the following organs: muscle (gastrocnemius), kidney, cecum and spleen. A summary of the results obtained from this histopathology analysis is presented in **Figure 25**.

The gastrocnemius is an important muscle that relies in the back part of the hind limbs. Histological analysis of the gastrocnemius revealed an atrophy of the muscle fibres with a severe decrease in its size in Baf53b-Cre *Haus6* cKO mice when compared to control mice (**Figure 25a**).

Furthermore, every cKO analysed presented a bilateral dilatation of the renal medula. These defects in the kidney were confirmed histologically by the presence of a pelvis renal dilatation and papillary atrophy (**Figure 25b**). The renal pelvis has a funnel-like structure and corresponds to a dilated part of the ureter in the kidney. Dilation of the renal pelvis is a characteristic of several types of hydronephrosis, a condition caused by an increase in urine pressure in this region of the kidney and often caused by a downstream obstruction of inability to expel sufficient amounts of urine into the bladder.

Another clear feature of Baf53b-Cre *Haus6* cKO was a severe increase in the size of the cecum. The cecum is the most proximal region of the large intestine. In opposition to humans where the cecum and the colon form contiguous regions of the large intestine, in rodents the cecum presents itself as an individualised organ, localised between the

small intestine and the colon. In rodents, the cecum is an important site for fermentation of plant materials as well as for the production of vitamin K and B. Histological analysis revealed that in the enlarged cecum of these mice the different layers presented a severe atrophy.

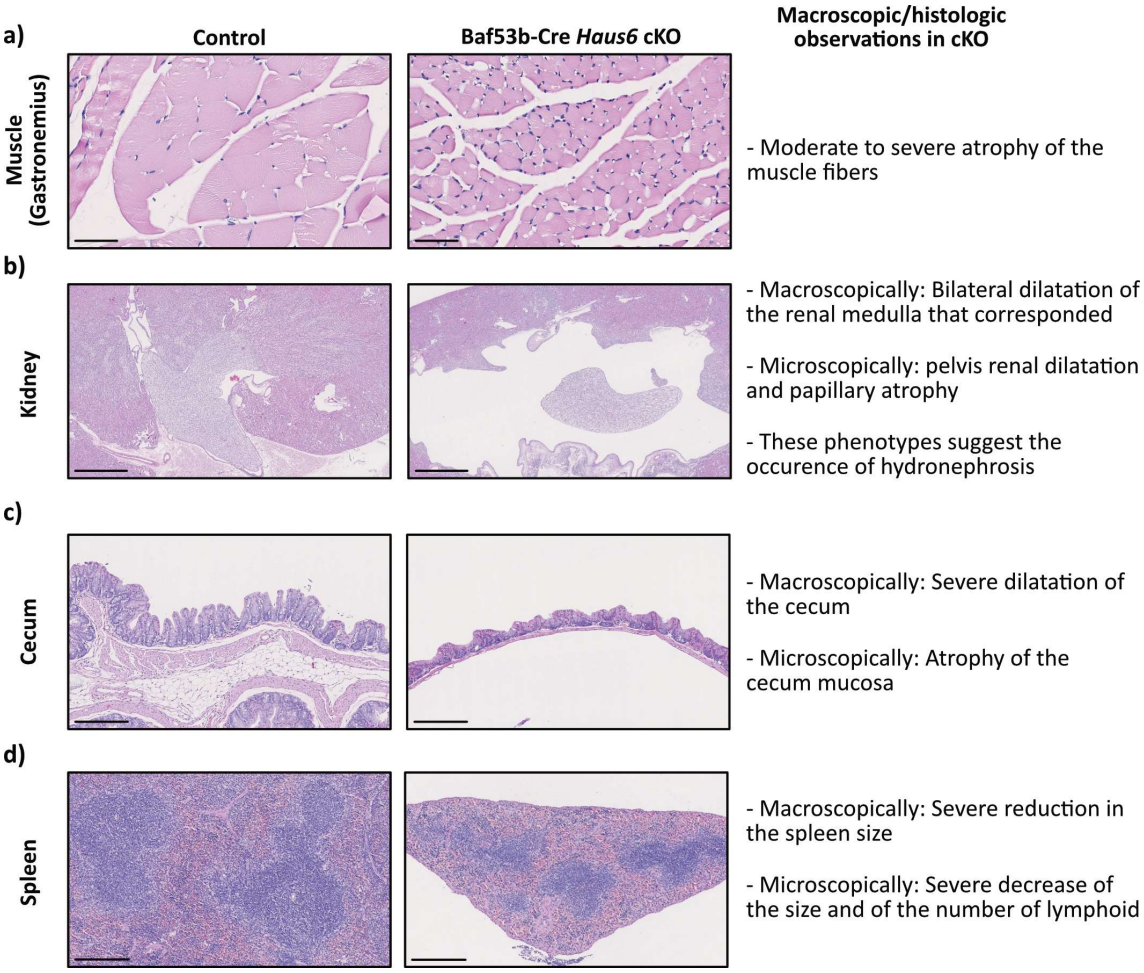

Figure 25 – Baf53b-Cre *Haus6* cKO display histological abnormalities in the muscle, kidney, cecum and spleen. Histological sections of the (a) Gastrocnemius muscle, (b) Kidney, (c) cecum and (d) spleen from control (*Haus6*$^{fl/fl}$ Baf53b-Cre$^{-/-}$) (left panel) and Baf53-Cre *Haus6* cKO (*Haus6*$^{fl/fl}$ Baf53b-Cre$^{-/-}$) (right panel) 9-10 weeks old mice. (a-d) Histological sections were stained with haematoxylin and eosin. Scale bar: (a) 50 µm, (b) 1 mm, (c-d) 250 µm.

As mentioned at the beginning of the Chapter 2a, I also generated Haus6 cKO mice where deletion of this augmin subunit is induced under control of the CamKIIα gene promotor. In these mice *Haus6* deletion occurs, specifically, in more mature neurons (~2 weeks after birth) of the forebrain. CamKIIα-Cre transgenic mice are widely used to induce specific gene deletion in brain structures of the forebrain and, more specifically, to study the role of specific genes in mature hippocampal neurons. I have observed that CamkIIα-Cre *Haus6* cKO mice are viable and develop normally. Furthermore, preliminary data did not show any signs of increased neuronal cell death in 3 months-old cKO mice. We are currently analysing dendritic morphology and dendritic spine morphology in hippocampal neurons *in vivo* using fixed brain sections from these cKO mice. However, further experiments are necessary to determine if augmin-dependent MT nucleation has any role in maintaining MT mass and ensuring neuronal homeostasis in mature post-mitotic neurons *in vivo*.

CHAPTER 3:

UNDERSTANDING THE γTURC INTERACTOME DURING AXON DEVELOPMENT

The importance of γTuRC-mediated MT nucleation during neuron development, and particularly, axonal development has been shown by studies from our and other groups[175,178–180,225,226]. Furthermore, unpublished data from our laboratory surprisingly suggest that overexpression of γ-tubulin can stimulate nucleation and promote axonal growth in mouse hippocampal neurons cultured *in vitro*. In the first chapter of this thesis I discussed the role of the augmin complex in targeting MT nucleation to the lattice of pre-existing MTs and ensuring the establishment of an organised MT network in neurons. Yet, it is still unclear how γTuRC activity is regulated and which other molecular players may be involved in modulating MT nucleation in neurons.

Development of a γTuRC pulldown experiment

We aimed to identify γTuRC interactors that may help us understand the mechanisms involved in the regulation of MT nucleation during axonal growth.

A good strategy to study the interaction network of a protein complex is to perform immunoprecipitation (IP) experiments. Briefly, in these experiments a cell lysate is incubated with a specific antibody against one of the subunits of the complex under study. Then, the obtained imunoprecipitate is analysed by mass spectrometry (MS).

We had a costum-made antibody in our laboratory that was raised against the γTuRC subunit GCP3 and that worked for IP. Therefore, our strategy was to use this antibody to immunoprecipitate endogenous GCP3 and associated proteins from mouse neuron lysates and identify proteins in purified imunoprecipitates by MS.

In order to avoid a high protein background in the imunoprecipitates analysed by MS due to the presence of large amounts IgGs, GCP3 antibody was cross-linked to Protein G sepharose beads prior to incubation with the neuronal extract.

As a first test we used cellular lysates obtained from the mouse neuroblastoma cell line Neuro2A. In this experiment, cellular extracts were incubated with Protein-G sepharose beads cross-linked to either a specific antibody against GCP3 or control IgGs. After washing the beads with lysis buffer, imunoprecipitates were eluted twice with ammonium hydroxide at pH 11. After that, and to analyse the non-eluted fraction, beads were incubated with Sample Buffer 1x at 95°C for 5 minutes. The resulting eluates were then run in an acrylamide gel and analysed by performing a Silver staining of these gels (**Figure 26**).

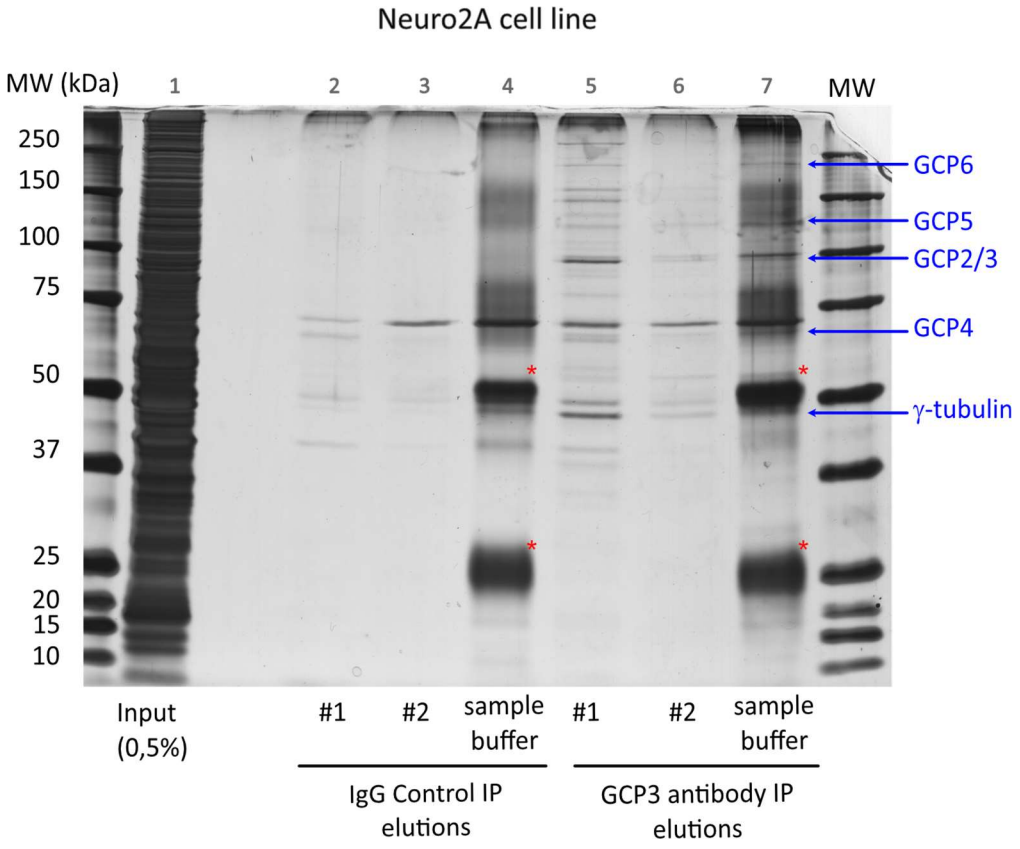

Figure 26 – Optimization of the GCP3 immunoprecipitation protocol using lysates from Neuro2A cells. Neuro2A cell lysates (Input 0.5%) were incubated with Protein G Sepharose beads previously crosslinked to either control IgGs (laines 2-4) or a GCP3 antibody (laines 5-7). For eluting the imunoprecipitates two consecutive elutions with ammonium hydrochloride were performed (laines 2-3 and 5-6) followed by elution with sample buffer 1x (laines 4 and 7). Red * identify the heavy and light chains of the IgGs. Proteins with a molecular weight matching the one of γTuRC subunits are shown are highlighted with blue arrows.

As shown in **Figure 26**, this first experiment showed that by eluting the immunoprecipitates with ammonium hydroxide: (1) IgGs are not eluted, (2) there is a large amount of proteins specifically immunoprecipitated with the GCP3 antibody, (3) some of the eluted proteins match the molecular weight of known γTuRC subunits (γ-tubulin and GCP2-6). Still, a significant amount of protein remained bound to the beads after high pH elution. According to the size of these bands they seem to match the molecular weight of γTuRC subunits, meaning that most likely a portion of proteins strongly bound to the beads (like γTuRC subunits) are not completely eluted with ammonium hydroxide at pH 11.

Still, we considered that these were good results and we proceeded with repeating this IP using lysates from cultured mouse cortical neurons. For this experiment, neocortical neurons were cultured *in vitro* and 7 days later cellular extracts were prepared. We chose to lyse neurons after 7DIV since, at this time point, axonal growth is abundant allowing us to study the γTuRC interaction network during this process. A similar protocol to the one used for the IPs with Neuro2A cellular lysates was followed.

Immunoprecipitates eluated with ammonium hydroxide at pH 11 were sent to our collaborators in Canada (Etienne Coyaud in the group of Brian Raught, Toronto University) who analysed them in order to identify possible GCP3 interactors by MS.

List of the identified GCP3 interactors

From our collaborators we received a list of proteins which were found in IgG control and GCP3 IPs and the respective peptide count (number of times that a specific peptide, corresponding to each indicated protein was identified by MS in the analysed samples). Significance Analysis of INTeractome (SAINT) was used to identify which of these proteins were enriched in the GCP3 over the control IP, determining which of the identified proteins could represent putative GCP3 interactors (hits). Only proteins with

a SAINT value >0.8 were considered as high confidence hits (generally corresponding to a ~1% false discovery rate).

A total of 53 proteins were identified as hits of GCP3 interactors. The full list of these hit together with a summary of the known biological functions for each one is presented in **Table 4**.

Table 4 – List of GCP3 candidate interactors identified from 7DIV neocortical culture lysates by MS. In this table the official gene name is presented followed by a brief summary of the known protein function and the respective SAINT value for the MS analysis**.**

Gene name:	Known information found in the literature:	Control #1	Control #2	GCP3 IP #1	GCP3 IP #2	GCP3 IP Total	SAINT value:
Tubgcp3	Structural component of the γTuSC and γTuRC complexes.			58	53	**111**	**1,00**
Pacs1	Coat protein that is involved in the localization of trans-Golgi network (TGN) membrane proteins that contain acidic cluster sorting motifs. Involved in ciliary traffic in olfactory sensory neurons. Mutations are involved in intellectual disability and craniofacial development defects. [227–230]			535	570	**1105**	**1,00**
Tubb4a	β-tubulin isotype 4a. Mutations in these gene have been implicated in neurodevelopmental defects.[231]	146		497	500	**997**	**1,00**
Cep170	Maker of mature centrosomes in interphase. During mitosis it localizes to the mitotic spindle targeting kinesin-13 protein KIF2B to this structure.[232,233]			335	315	**650**	**1,00**
Wdr37	Member of the WD40 repeat protein family. WD repeats heterotrimeric or multiprotein complexes. Mutations in flies and humans are involved in neurodevelopmental defects.[234]			308	312	**620**	**1,00**
Gphn	MAP involved in membrane protein-cytoskeleton interactions. Involved in anchoring glycine receptor (GLYR) to subsynaptic MTs. Protein dysfunction has implications in AD and epilepsy.[235]			239	239	**478**	**1,00**

Gene name:	Known information found in the literature:	Control #1	Control #2	GCP3 IP #1	GCP3 IP #2	GCP3 IP Total	SAINT value:
Homer1	Scaffold protein at postsynaptic compartments. Plays a central role in calcium signalling in the central nervous system. Homer1 knockdown has protective effects against neuronal injury in *in vitro* PD model.[236]			226	213	**439**	**1,00**
Tfg	Plays a role in the normal dynamic function of the endoplasmic reticulum (ER) and its associated MTs. Inhibition of TFG function causes axon degeneration by impairing ER structure.[237]	41	28	176	178	**354**	**1,00**
Sec16a	Defines endoplasmic reticulum exit sites (ERES) and is required for secretory cargo traffic from the endoplasmic reticulum to the Golgi apparatus.[238]	7		153	134	**287**	**1,00**
Tubgcp2	Structural component of the γTuSC and γTuRC complexes			119	133	**252**	**1,00**
Ywhaz	Member of 14-3-3 protein family. Binds tau in neurofibrilary tangles in AD.[10]	30	36	101	110	**211**	**1,00**
Ywhag	Member of 14-3-3 protein family. Mutations in this gene are involved in the early onset of epylepsy.[239]	31	35	100	105	**205**	**1,00**
Tubg1	Structural component of the γTuSC and γTuRC complexes. Mutations in this gene are involved in neurodevelopmental disorders.[188]			95	108	**203**	**1,00**
Pacs2	Multifunctional sorting protein that controls the endoplasmic reticulum (ER)-mitochondria communication, including the apposition of mitochondria with the ER and ER homeostasis.[240]			91	106	**197**	**1,00**
Iqsec2	Guanine nucleotide exchange factor for the ADP-ribosylation factor family of small GTPases. Mutations in these gene have been implicated in intellectual disability and disruption of dendritic spine morphogenesis.[241,242]			94	94	**188**	**1,00**
Ywhae	Member of the 14-3-3 protein family. Overexpression is correlated with the appearance of autism spectrum disorders, epilepsy and mental retardation and disrupts neuritogenesis by impeding MT entry into new neurites	21	23	83	96	**179**	**1,00**

Gene name:	Known information found in the literature:	Control #1	Control #2	GCP3 IP #1	GCP3 IP #2	GCP3 IP Total	SAINT value:
	in a process mediated by doublecortin.[243]						
Cttn	Contributes to the organisation of the actin cytoskeleton and cell shape. Involved in regulation of neuron morphology, axon growth, formation of neuronal growth cones and spine density.[17,18]			89	88	**177**	**1,00**
Ctbp1	Involved in controlling the equilibrium between tubular and stacked structures in the Golgi complex. Confers protection to Ad in rat models.[244,245]			81	78	**159**	**1,00**
Ywhaq	Member of the 14-3-3 protein family.	11	17	59	69	**128**	**1,00**
Ywhah	Member of the 14-3-3 protein family. Associated with familiar forms of psychotic bipolar disorders.[246]			57	69	**126**	**1,00**
Otud4	Deubiquitinase enzyme. [247]			68	57	**125**	**1,00**
Ywhab	Member of the 14-3-3 protein family.			56	65	**121**	**1,00**
Mycbp	Member of the Myc protein family.[248]			52	49	**101**	**1,00**
Kif2a	Member of the kinesin-13 family of MT depolymerases. Its activity is involved proper mitotic progression and during neuron development it promotes axonal pruning, inhibits growth of axonal colateral branches and is involved in proper hippocampal wiring. Mutations in Kif2a gene were implicated neurodevelopmental disorders. [249–253]			52	44	**96**	**1,00**
Hnrnpa3	Plays a role in cytoplasmic trafficking of RNA.[254]			40	48	**88**	**1,00**
Paip1	Stimulator of translation initiator.[255]			39	48	**87**	**1,00**

Gene name:	Known information found in the literature:	Control #1	Control #2	GCP3 IP #1	GCP3 IP #2	GCP3 IP Total	SAINT value:
Amph	Protein associated with the cytoplasmic surface of synaptic vesicles. Endocytic regulator involved in synaptic plasticity.[256]			42	34	**76**	**1,00**
Ctnna2	Function as a linker between cadherin adhesion receptors and the cytoskeleton, regulating cell-cell adhesion and differentiation in the nervous system. Regulates synaptic plasticity and cerebellar and hippocampal lamination during development.[257]			39	33	**72**	**1,00**
Elavl3	Member of the nElavl protein family, RNA-binding proteins that regulate RNA stability and alternative splicing. Elavl3 is involved in control of glutamate levels and neuron excitability.[258,259]			35	34	**69**	**1,00**
Dpysl3	Member of the CRMP family of proteins. Found to mediate growth cone behaviour *in vitro and axonal guidance in zebra fish.* A mutation in this gene has been implicated in amyotrophic lateral sclerosis. Localizes to spindle MTs in mitosis.[260–262]			30	36	**66**	**1,00**
Tkt	Enzyme involved in the pentose phosphate glucose metabolism pathway. Found in dopaminergic neurons.[263]			29	26	**55**	**1,00**
Mycbp2	E3 ubiquitin-protein ligase. In the nucleus of DRG neurons MYCBP2 co-localized with Ran and facilitated through its RCC1-like domain the GDP/GTP exchange of Ran.[264]			31	23	**54**	**1,00**
Cdh10	Member of the calcium-dependent cell adhesion protein family Cadherin. Important for maintaining correct inhibitory and excitatory strength in cortical neurons.[265]			25	24	**49**	**1,00**
Iqsec1	Guanine nucleotide exchange factor for the ADP-ribosylation factor family of small GTPases. Critical for development of mature glutamatergic synapses.[266]			19	26	**45**	**1,00**
Bin1	Also known as amphiphysin 2 it is involved in membrane curvature, endocytosis and calcium homeostasis. It has been described as the second most significant susceptibility locus for late-			18	15	**33**	**1,00**

Gene name:	Known information found in the literature:	Control #1	Control #2	GCP3 IP #1	GCP3 IP #2	GCP3 IP Total	SAINT value:
	onset AD. Suggested to link the MT cytoskeleton with the cellular membrane via CLIP170. [267,268]						
Ppp2r1a	Gene encoding a constant regulatory subunit of protein phosphatase 2, implicated in the negative control of cell growth and division. Associated with Ad and mental retardation.[269]	4	5	17	16	**33**	**0,99**
Hspd1	Member of the chaperonin family it is essential for the folding and assembly of newly imported proteins in the mitochondria and plays a role in neuronal survival. Mutations associated with Hspd1 cause autosomal recessive spastic paraplegia 13.[270]			13	17	**30**	**1,00**
Tjp1	Protein essential for tight junction assembly.[271]			12	14	**26**	**1,00**
Matr3	Nuclear matrix protein, proposed to stabilise certain messenger RNA species. Mutations in Matr3 are related to amyotrophic lateral sclerosis. Deregulation of Matr3 levels cause neurotoxicity.[272]			13	12	**25**	**1,00**
Ubr4	E3 ubiquitin-protein ligase. Together with clathrin, forms meshwork structures involved in membrane morphogenesis and cytoskeletal organisation.[273]			12	13	**25**	**1,00**
Hsdl1	Uncharacterized member of short-chain dehydrogenase/reductase (SDR) protein family.			11	12	**23**	**1,00**
Map1lc3a	Involved in the autophagy-lysosome pathway. MT binding protein. Stabilises MT networks by decreasing MT dynamicity and promoting growth over shortening events.[274]			12	11	**23**	**1,00**
Mzt2	Member of the γTuRC. [52]			12	11	**23**	**1,00**
Prdx2	Peroxiredoxin present at the cytoplasm. Inactivation peroxiredoxin-2 by phosphorilation induced by Cdk5 sensitizes neurons to the deleterious effects of parkinsonian toxins.[275]			11	12	**23**	**1,00**

Gene name:	Known information found in the literature:	Control #1	Control #2	GCP3 IP #1	GCP3 IP #2	GCP3 IP Total	SAINT value:
Dhx9	Also known as RNA helicase A. In the cytoplasm it is preferentially associated with actively translating polyribosomes and is necessary for efficient translation of RNAs that contain a highly structured 5'UTR.[276]			11	11	**22**	**1,00**
Set	Multitasking protein, involved in apoptosis, transcription, nucleosome assembly and histone chaperoning.			13	9	**22**	**1,00**
Basp1	Membrane bound protein, may function by regulating organisation and morphology of the plasma membrane. BASP1 overexpression stimulated neurite outgrowth.[277]	2		11	9	**20**	**1,00**
Sec13	Constituent of the endoplasmic reticulum and the nuclear pore complex. It has similarity to the yeast SEC13 protein, which is required for membrane-bending and vesicle biogenesis from endoplasmic reticulum during the transport of proteins.[278]			11	8	**19**	**1,00**
Tubgcp4	Structural component of the γTuRC complex. Mutations in GCP4 have been identified in microcephaly patients.[191]			9	9	**18**	**1,00**
Pabpc1	Poly(A) RNA-binding protein its depletion prevents protein synthesis and induces cell death in Hela cells. Also relevant in compensatory mechanisms in Purkinje neurons.[279]			9	7	**16**	**1,00**
Slc25a4	ADP/ATP translocator. Embedded in the inner mitochondrial membrane, it determines the rate of ADP/ATP flux between the mitochondrion and the cytosol.[280]			5	9	**14**	**1,00**
Birc6	Also known as BRUCe or APPOLON it contained a ubiquitin-conjugating enzyme E2, catalytic domain. Inhibits apoptosis by facilitating the degradation of apoptotic proteins by ubiquitination. Involved in neurodegeneration caused by kainic acid and its downregulation promotes neuronal death.[281]			4	7	**11**	**1,00**
Klhl22	E3 ubiquitin ligase. Involved in mono-ubiquitination of Plk1 and consequent removal from the kinetochores upon			7	4	**11**	**1,00**

Gene name:	Known information found in the literature:	Control #1	Control #2	GCP3 IP #1	GCP3 IP #2	GCP3 IP Total	SAINT value:
	chromosome biorientation. Also involved in regulation of mTOR pathway activity.[282,283]						
Hnrnpl	Splicing factor binding to exonic or intronic sites and acting as either an activator or repressor of exon inclusion.			4	2	**6**	**0,99**
Pkm2	Pyruvate kinase protein. Plays a significant role in tumour growth, angiogenesis, apoptosis and metastasis. In rat hippocampal neurons it is involved in neurodegeneration after hypoxia and in neuropathic pain.[284,285]			3	2	**5**	**0,99**

With the exception of GCP5 and GCP6 and apart from the bait GCP3, I identified the γTuRC subunits γ-tubulin, GCP2, GCP4 and MZT2/GCP8 (from here on I will name it GCP8) as high confidence interactors, which validated my approach. Surprisingly, and even though we have previously identified HAUS6 as a γTuRC interactor by Western blot in IP experiments from neuronal extracts[175] we were not able to identify any augmin subunit in our candidate list obtained by MS.

In order to have a better understanding of the types of other proteins that I identified I performed a Gene Ontology (GO) analysis using the Panther Classification System[286]. This analysis evaluates, for a given list of proteins, any significant enrichment in a specific GO category when compared to the overall proteome of a specific species. GO analysis of the "cellular component" (**Table 5**) and "biological process" (**Table 6**) was performed for our list of GCP3 interactor candidates.

Table 5 – Gene Ontology analysis of cellular components of identified candidate interactors using PANTHER classification system. GO terms, number of hits identified for each category and fold enrichment when compared to the mouse (Mus Musculus) proteome are represented in this table. Only significantly enriched (P value <0.5) and >5-fold enriched categories are presented.

GO cellular component term:	# proteins identified	Fold enrichment
γ-tubulin complex	5	> 100
Microtubule organising centre	11	6.68
Microtubule cytoskeleton	16	5.72
Polar microtubule	3	> 100
Spindle	9	13.36
Centrosome	10	7.98
Centriole	4	14.10
Centriolar subdistal appendage	2	90.08
Axon	9	5.23
Cell leading edge	6	6.45
Synapse	20	5.86
Extrinsic component of synaptic vesicle membrane	2	81.08
Presynapse	8	5.81
Photoreceptor ribbon synapse	2	67.56
Presynaptic active zone cytoplasmic component	3	57.91
Presynaptic active zone	4	17.63
Postsynaptic specialization	8	7.61
Postsynaptic specialization, intracellular component	4	43.83
Glutamatergic synapse	12	9.59
ER to Golgi transport vesicle membrane	2	36.85
Myelin sheath	6	11.42
Ribonucleoprotein granule	4	7.80

Table 6 - Gene Ontology analysis of biological process of identified candidate interactors using PANTHER classification system. GO terms, number of hits identified for each category and fold enrichment when compared to the mouse (Mus Musculus) proteome are represented in this table. Only significatively enriched (P value <0.5) and >5-fold enriched categories are presented.

GO biological process term:	# proteins	Fold enrichment
Microtubule nucleation	4	90.08
Spindle organisation	6	18.71
Protein targeting	6	11.69
Intracellular protein transport	10	5.39
Mitotic cell cycle	8	6.37

Both GO analysis presented in **Table 5** and **Table 6** show that in our GCP3 IP there is a clear enrichment in proteins related to MT nucleation, MT cytoskeleton, the centrosome and the mitotic spindle. These results are not surprising considering the known functions of GCP3 and the γTuRC and its subcellular localizations and the fact that several microtubule cytoskeleton associated genes that play a role in mitotic spindle assembly are also expressed during neuronal development[30]. Still, these results show that our IP worked well and may give us reliable results on GCP3 interactor candidates. From the "cellular component" GO analysis I would like to point out the enrichment in presynaptic components and, most clearly in postsynaptic components which could suggest a function of the γTuRC in synaptogenesis and synaptic function.

Furthermore, by performing a bibliographic research on the identified candidate interactors I observed that 33% have previously been linked to cytoskeleton function, 61% have a described function in neurons and 47% have been implicated in neurodevelopmental or neurodegeneration disorders (**Figure 27b**).

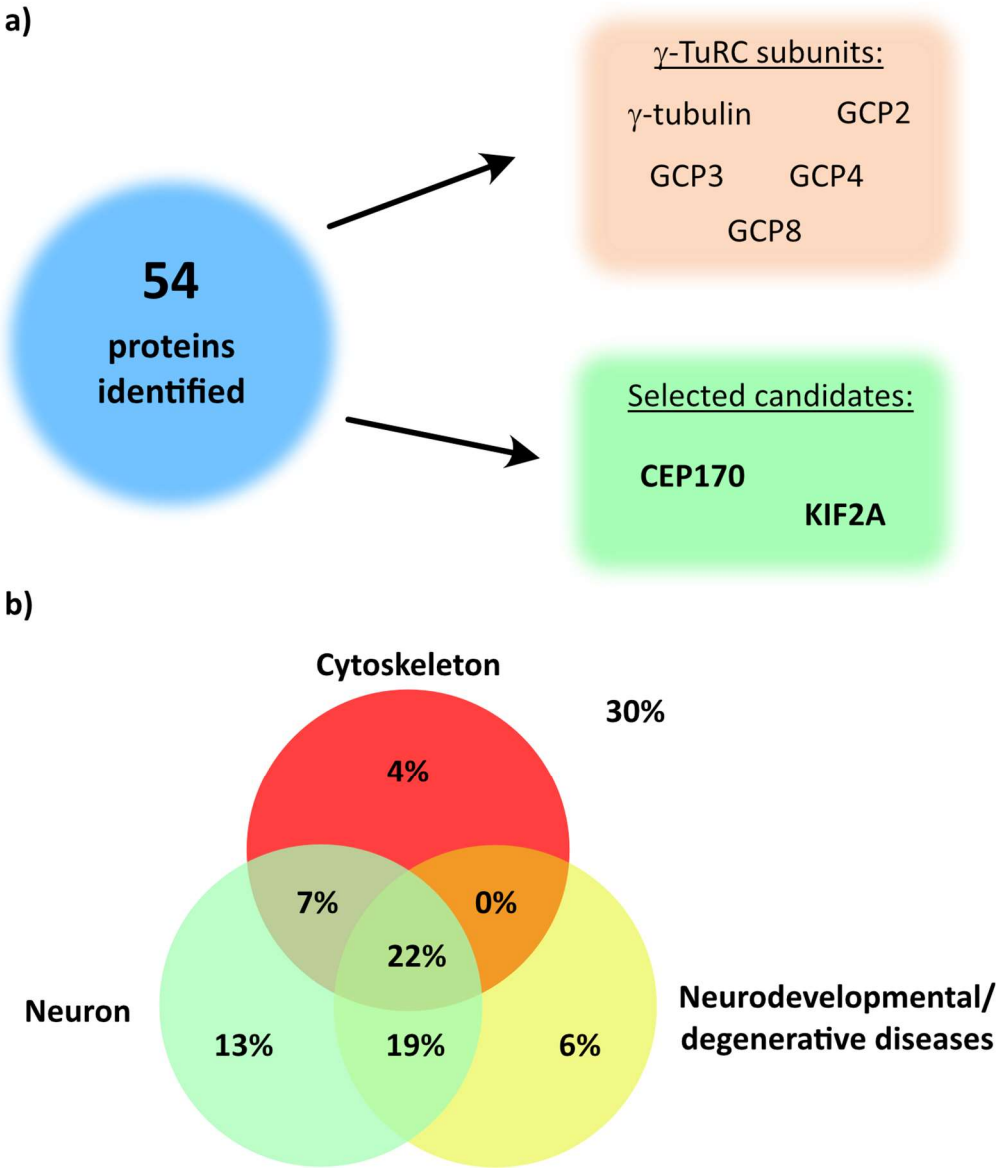

Figure 27 – Summary of the identified candidates and their known roles in cytoskeleton regulation, neuronal functions and brain-related disorders. (a) Summary of the number of found candidate interactors, highlighting the γTuRC subunits identified and selected proteins for further analysis. **(b)** Scheme showing the percentage of candidate interactors which have described functions in cytoskeleton, in neurons or have been related to neurodevelopmental or neurodegenerative diseases.

Amongst the identified γTuRC interactor candidates, two proteins stood out:

- **KIF2A** – Member of the kinesin-13 protein superfamily which is characterized by the absence of motor activity but the ability to promote MT depolymerisation at MT ends[287]. It is required during mitosis to ensure proper bipolar spindle formation and, when overexpressed, it correlates with bad prognosis in different types of cancer[250]. In neurons it has been shown to localise to newly formed axonal collateral branches inhibiting their growth[251] and it promotes axonal pruning[252]. *Kif2a* knockout mice present defects in neuronal wiring the hippocampus due to overgrowth of dendrites and the gain of axonal properties[253]. Different *KIF2A* mutations have been implicated in neurodevelopmental disorders and, more recently, KIF2A has been implicated in cilia disassembly at the entry of neuroprogenitors into the cell cycle[288,289]. Furthermore, by the time these results were obtained, former PhD student Artur Ezquerra identified KIF2A as a putative interactor of the γTuRC subunit GCP8 in cycling HeLa cells in immunoprecipitation experiments analysed by MS. Therefore, we were interested in understanding whether interaction of a MT depolymerase like KIF2A with the γTuRC could affect MT nucleation activity during axonal development.

- **CEP170** – CEP170 was one of the γTuRC interactor candidates that presented the highest spectral count in the MS analysis (**Table 4**). CEP170 is a centriolar protein which is widely used as a marker for mature centrosomes[232]. It contains a MT binding domain and upon infection with *Chlamidya trachomatis* it induces reorganisation of the MT network in host cells[290]. It targets the kinesin-13 protein KIF2B to the mitotic spindle and, more recently, it has been implicated in regulation of the ciliary cycle in neuroprogenitors together with KIF2A[233,289]. Therefore, we were interested in understanding whether CEP170 is involved in regulation/targeting of MT nucleation by the γTuRC and influence the functions of KIF2A during axonal development.

Validation of KIF2A and CEP170 as γTuRC interactors

In order to confirm the interaction between KIF2A and CEP170 with the γTuRC we performed further IPs using the same GCP3-specific antibody and analysed the resulting immunoprecipitates by westernblot (**Figure 23a**). Since at the time when I obtained these results Artur Ezquerra also identified KIF2A as a GCP8 interactor in Hela cell extracts, we also performed an IP with a GCP8-specific antibody (**Figure 28a**).

As shown in **Figure 28a**, both GCP3 and GCP8 antibodies can specifically pulldown the γTuRC (detected by GCP3, GCP4 and GCP8) and both KIF2A and CEP170. This result confirms that both KIF2A and CEP170 interact with the γTuRC.

Since CEP170 has never been described in neurons, we also showed that CEP170 (as KIF2A) is expressed from 1 to 7DIV during development of mouse hippocampal neurons *in vitro* (**Figure 28b**).

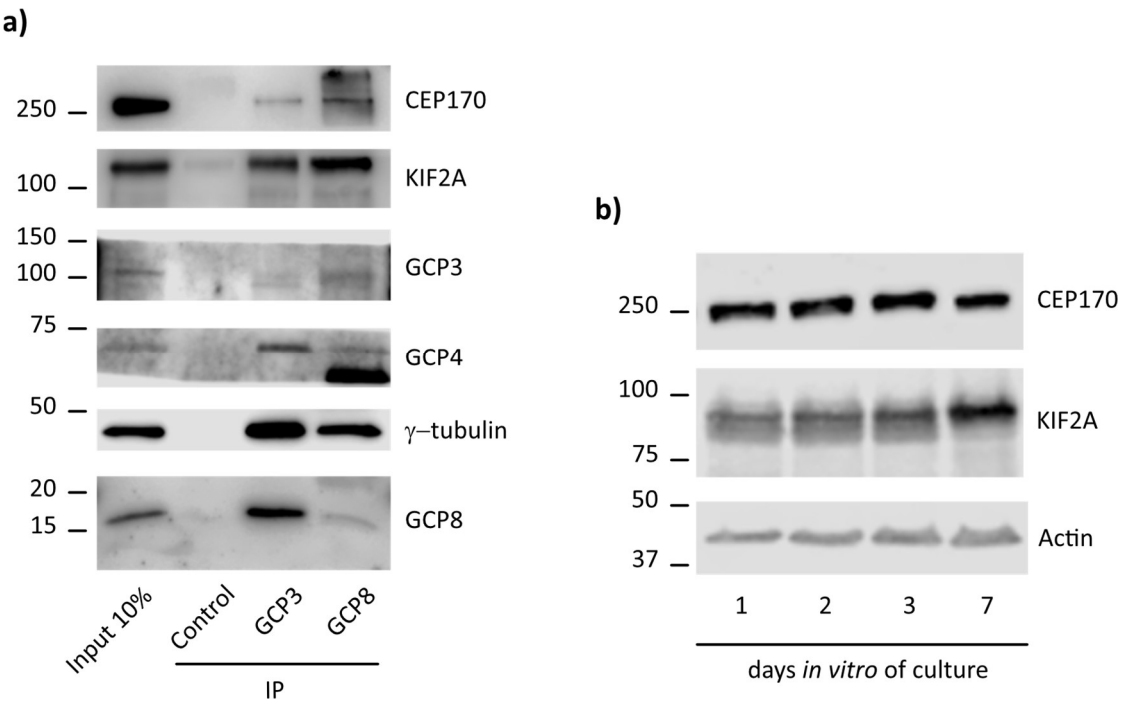

Figure 28 – Validation of GCP3 interactor candidates. (a) Immunoblot for CEP170, KIF2A and several γTuRC subunits of samples immunprecipitated with control IgG and GCP3 and GCP8 antibodies. **(b)** Immunoblot for CEP170, KIF2A and Actin of samples from primary mouse hippocampal neurons cultured during different days *in vitro***.**

KIF2A interacts with the C-terminal region of GCP8 and with CEP170

Considering that KIF2A was also identified as a GCP8 interactor in HeLa cells and that CEP170 had previously been identified as an interactor of another kinesin-13 protein family member KIF2C we wanted to address: (1) if it would be likely that GCP8 is the binding partner of KIF2A in the γTuRC; (2) in case KIF2A is a direct GCP8 interactor to which region of GCP8 it would bind; (3) if CEP170 is a KIF2A interactor. With that purpose we transfected human HEK cells with constructs expressing GFP-tagged KIF2A, CEP170, full length GCP8, an N-terminal fragment (aa 1 to 111) of GCP8 or a C-terminal fragment (aa 112 to 158) of GCP8 (**Figure 29**). Unpublished data from our laboratory (performed by Sabine Klischies) show that GCP8 interacts with the γTuRC through its N-terminal region (aa 1 to 111) and that its C-terminal region (aa 112 to 158) is not able to bind the complex. 24 hours after transfection, cells were lysed and cellular extracts used to perform IP experiments using a specific antibody against GFP.

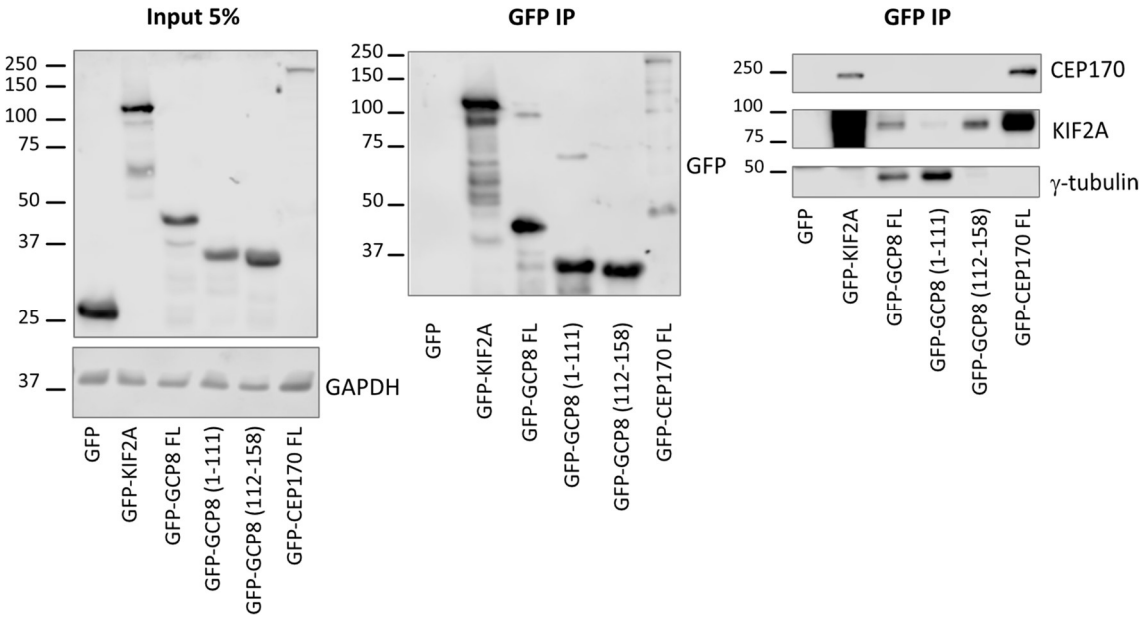

Figure 29 – KIF2A interacts with CEP170 and with the C-terminal region of GCP8 (a,b) Immunoblot against GFP showing (left) 5% of the extract amount (input) used for the immunoprecipitation experiments from HEK cells overexpressing GFP-tagged versions of KIF2A, GCP8 full length (FL), GCP8 N-terminal region (amino acids 1 to 111), GCP8 C-terminal region (amino acids 112 to 158) and CEP170 for 24 hours. **(centre)** Immunoblot against GFP from the samples shown in the inputs and immunoprecipitated with GFP specific antibody. **(right)** Immunoblot against CEP170, KIF2A and γ-tubulin from the samples shown in the inputs and immunoprecipitated with GFP specific antibody.

Our results show that overexpressed GCP8 can pulldown KIF2A and that KIF2A binds more strongly to the C-terminal region of GCP8, this is, the region which has a low ability to bind the γTuRC. This data suggests that KIF2A most likely interacts with the γTuRC directly through the C-terminal region of GCP8. We have also observed that overexpressed GFP-KIF2A is able to pulldown CEP170 and *vice versa* (**Figure 29**). At the time when these experiments were performed this interaction between KIF2A and CEP170 had not been described.

KIF2A and CEP170 localization at growth cones of developing neurons

Deletion of the *Kif2a* gene has been shown to induce overgrowth of axonal collateral branches in neurons. On the other hand, CEP170 function has never been described in neurons.

In order to get more insight into the cellular roles of these two proteins we fixed 2DIV cultured neurons with PFA 4% diluted in PBS and performed immunofluorescence stainings with antibodies against KIF2A and CEP170 (**Figure 30**).

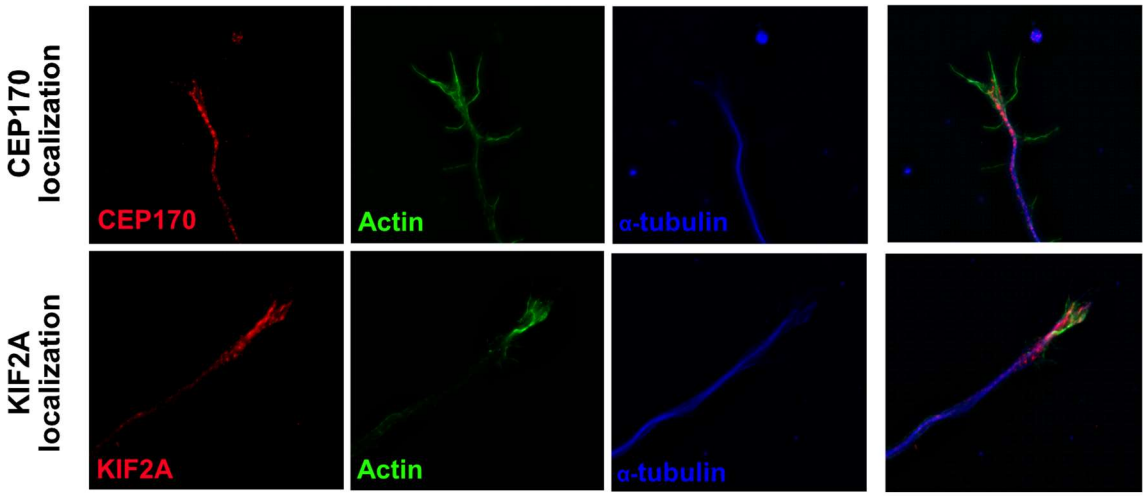

Figure 30 – CEP170 and KIF2A localize to the tip of a subset of axonal collateral branches. 2DIV neurons were fixed with paraformaldehyde 4% (diluted in PBS) and immunofluorescence labelled with antibodies against either CEP170 (first row) or KIF2A (second row) (red) and with Faloidin (in green with labels polymerised actin) and α-tubulin (in blue). Axonal tips are shown. 63x magnification was used.

We could observe that both KIF2A and CEP170 antibodies produce diffuse staining in the soma, in dendrites and in the axon. More strikingly was the fact that a subset, but not all, axonal tips had an enrichment of KIF2A and CEP170 staining in the region preceding and including the central part of the growth cone (**Figure 30**). Since both KIF2A and CEP170 antibodies are raised in rabbit, it was not possible to co-stain neurons with both KIF2A and CEP170 antibodies. Therefore, it remains to be proven that both proteins colocalize in these structures. Furthermore, it remains to be proven that the signal observed is specific. Still, these results are in agreement the known functions of in negatively regulating growth of axonal collateral branches and could mean that KIF2A and CEP170 interact and cooperate at this subcellular region.

CEP170 depletion induces elongation of axonal branches

The role of CEP170 in neuronal development and homeostasis has never been characterized. Therefore, we decided to evaluate the effect of CEP170 depletion in cultured mouse hippocampal neurons. With this purpose we generated two pll3.7 expression plasmids expressing GFP and different shRNAs against CEP170. To test the efficiency of these plasmids in depleting CEP170, 1DIV neurons were infected with lentivirus expressing either CEP170 shRNA #1 or #2. Three days later, cells were lysed and neuronal extracts analysed by westernblot, which revealed that infected neurons showed ~68% and ~88% reduction in CEP170 protein levels, respectively (**Figure 31a**). These data demonstrate the efficacy of the generated shRNA expressing plasmids.

In order to evaluate the role of CEP170 during axonal development, mouse hippocampal neurons were transfected at 2DIV with pll3.7 plasmids expressing shRNAs #1 and #2 against CEP170. Five days later, 7DIV neurons were fixed, GFP expressing cells were detected by immunofluorescence and neuronal morphology was analysed using Fiji's plugin NeuronJ. We observed that depletion of CEP170 with shRNA#1, but not shRNA#2, caused a significative ~65% increase in the total axonal length (**Figure 31c**). CEP170 depletion did not cause any effect on the total axonal branching using either of the

shRNAs (**Figure 31d**). However, when we focused on long axonal branches (> 100 µm of length), we observed that both shRNAs caused an increase in the number of long axonal branches, corresponding to a ~21% and ~39% more long branches per 100 µm of axon (**Figure 31e**).

These results are in agreement with the described phenotypes caused by KIF2A depletion in neurons, which suggest that CEP170 and KIF2A could act together in inhibiting the growth of newly formed axonal collateral branches.

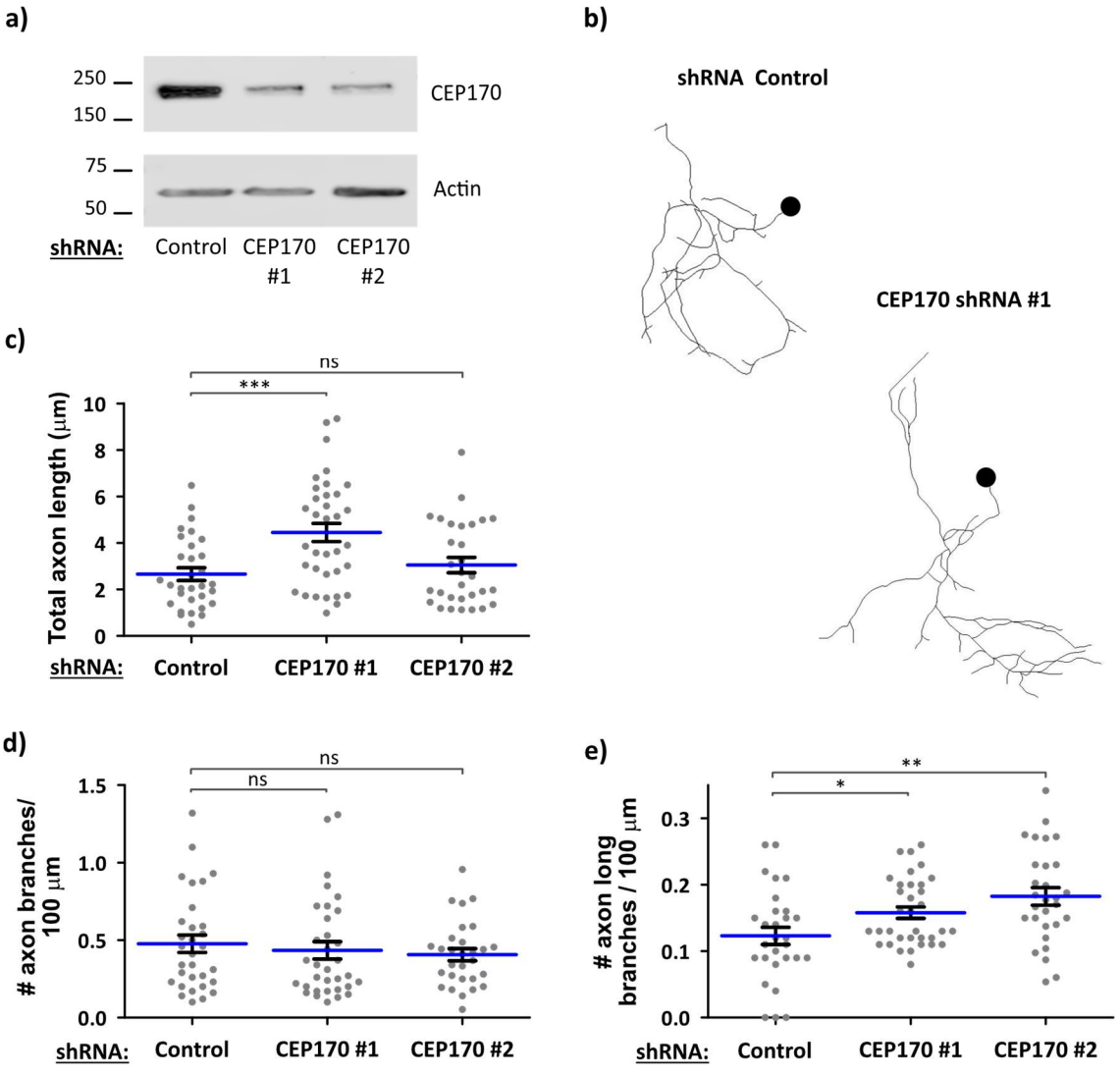

Figure 31 – CEP170 depletion induces growth of axonal collateral branches. (a) Immunoblot showing CEP170 levels in cellular extracts obtained from 4DIV neurons infected at 1DIV with lentivirus expressing either a shRNA control (against luciferase) or two different shRNAs (#1 and #2) against CEP170. **(b)** Axonal tracing of 7DIV control neurons and CEP170 depleted neurons (using shRNA#1) **(c,d,e)** Quantification of **(c)** total axonal length, **(d)** number of axon branches normalised

to axon length and **(e)** number of long axon branches (>100 µm) per 100 µm normalised to axon length. N=29-32 different neurons from a total of three individual experiments. Dotplots show averages (blue bars) +/- SEM. *P<0.05, **p<0.01 and ***p>0.001 from t-tests.

DISCUSSION

Role of augmin-mediated microtubule nucleation in establishing the uniform axonal microtubule polarity

Neurons display a very complex MT network which is essential to ensure proper neuronal development and homeostasis. Despite the importance of the MT cytoskeleton, little is known about how new MTs are originated during neuronal development. Generation of new MTs can be accomplished by two main mechanisms: (1) severing of pre-existing MTs or (2) MT nucleation at the centrosome and at non-centrosomal sites. Different studies show a clear role of MT severing enzymes like spastin or katanin during axonal and dendritic development[155,162,163]. However, until recently, the role of MT nucleation by the γTuRC in the context of neuronal development was poorly understood.

Results obtained by a former postdoc in our laboratory (Carlos Sanchez) show that γ-tubulin depletion in cultured mouse hippocampal neurons impairs primary neurite outgrowth and axon specification[175]. Furthermore, once the axon has been specified, γ-tubulin depletion leads to a decrease in axonal growth and branching. The observed defects are caused by a weakening in the axonal MT network (as observed by a reduction in the total amount of MTs) and include impaired mitochondrial transport along the axon. Furthermore, a previous study showed that γ-tubulin, in cooperation with the (-)-end capping protein CAMSAP2, is required for axonal specification and for dendritic development[178]. Both studies show, for the first time, a key role of the MT nucleator γTuRC in promoting neuronal differentiation and ensuring the formation of a proper MT network in neurons.

An important limitation in studying the mechanisms involved in MT nucleation in the context of cells is the lack of tools to detect nucleation events within complex MT arrays. One technique commonly known as “microtubule regrowth assay” is used in cultured cell lines to evaluate MT nucleation from MTOCs (e.g. centrosome or Golgi) and analyses the recovery of the MT network after complete depolymerisation. However, it is not suitable to use this strategy to study microtubule nucleation in axons and dendrites as, in these cellular compartment, the highly stable MT network is resistant to treatments

commonly used to depolymerise MTs (exposure to MT-depolymerising drugs, incubation on ice, or combination of the former two treatments). Indeed, unpublished data from our laboratory and examples found in the literature[226] show that, even after depolymerisation treatments like the ones described, non-depolymerised MTs could be observed in axons and dendrites. Therefore, analysis of MT regrowth under these conditions can be quite misleading as it is impossible to distinguish between nucleation events and repolymerisation of small MT seeds which haven't been completely depolymerised.

Instead, in this thesis I used another technique known as "EB-comets" technique, which relies on the analysis of growing MT (+)-ends in living cells. End-binding (EB) proteins, or EBs, are members of a protein family that specifically bind to MT (+)-ends, modulating MT polymerisation. Time-lapse imaging of cells expressing fluorescent protein-tagged EBs allows to visualise and measure both the density and directionality of growing MT (+)-ends (also known as "EB-comets" due to their comet-like shape)[158]. Even though this technique doesn't directly image MT (-)-ends we consider that, given the critical role of MT nucleation in MT formation, it can give us a good read out of the MT number and an approximation on the MT nucleation activity in axons and dendrites. One of the limitations of this assay is that, since it only recognises the actively growing pool of dynamic MTs, changes in (+)-tip dynamics like increase/decrease in the duration or speed of MT growth can also influence the results obtained. As I will discuss in the next paragraphs, this doesn't seem to be the case in our experimental model.

Still, the development of a MT nucleation sensor would be very important as a tool to study regulation and localisation of nucleation events in different cell types and in different stages of development.

Despite its limitations, we consider that, as other groups have done in the past, quantifying "EB-comets" is the best available tool to access MT organisation in non-fixed cultured neurons[178,180,291]. Therefore, in this thesis, we take the quantification of EB-comets as a readout of MT nucleation events.

Using this strategy, we showed that γ-tubulin depletion in mouse hippocampal neurons leads to a decrease in the density of EB-comets in the axon (**Figure 12d**). Whereas in Drosophila S2 cells γ-tubulin was proposed to have a role in regulation of (+)-end dynamics (which could have an influence in the interpretation of our EB-comets results), data from our laboratory show that, in the axon, γ-tubulin depletion has no effect in the duration and speed of EB-comets[62,175].

Together with the fact that γ-tubulin depletion causes a reduction in the total MT density in axons, our data supports the role of the γTuRC in promoting MT nucleation in the axonal compartment. One main question is where are these neuronal MTs nucleated.

Different studies show that, during neuronal maturation, γ-tubulin and γTuRC associated proteins (GCPWD/NEDD1 and CDK5RAP2) are depleted from the centrosome, causing this cellular organelle to lose its MTOC function[173–176]. This is due to a specific reduction in the centrosomal pool of γ-tubulin and does not involve a reduction in the overall expression levels of γTuRC subunits[175]. In one of these studies it is shown that, whereas in young 2DIV rat hippocampal neurons most MT regrow from the centrosome, in the soma of more mature 9 and 14DIV neurons, MT regrowth occurs almost entirely from non-centrosomal locations[173]. Furthermore, laser ablation of the centrosome in 2DIV neurons has no effect on axonal extension showing that, even in young neurons where the centrosome is still an active MTOC, it is not required for the generation of MTs that ensure proper axonal development. Together with the data presented in this thesis, this supports that during neuronal maturation, MT nucleation mediated by the γTuRC suffers a displacement from centrosomal to acentrosomal subcellular localisations. This is not the first case where, during cellular differentiation, a transition from centrosomal to acentrosomal MT network is reported. For example, in several animal epithelial cells MTOC function localises apically leading to the formation of a parallel MT array that concentrates along the apical-basal axis. Another example are mammalian muscle cells, where MTOC activity occurs at the nuclear envelope (revised in [292]).

In the case of neurons, it is still unclear if another subcellular structure can act as an acentrosomal MTOC. Two different studies using class IV *Drosophila* neurons, show that

at dendritic branching points γ-tubulin nucleates MTs and that this activity is important for establishing dendritic development and dendritic MT polarity[179,180]. However, the requirement of Golgi outpost for nucleation at these subcellular locations is not clear with conflicting results between the two studies.

In our model, staining of neurons with a γ-tubulin specific antibodies showed that: (1) γ-tubulin specifically localises throughout the cytoplasm; (2) and no accumulation of γ-tubulin was observed in another subcellular localisation [175]. In this thesis we propose that, in neurons, MT nucleation takes place from the lattice of pre-existing MTs, in a process mediated by the augmin complex.

The augmin complex is known to promote γTuRC-dependent MT nucleation from the lattice of pre-existing MTs in a process where the new MT displays the same polarity as the template one. Therefore, we hypothesised that augmin could be the mechanism used by neurons to nucleate new MTs independently of the centrosome. Furthermore, since in the axon MTs are organised into dense bundles of parallel MTs with their (+)-ends growing towards the axonal growth cone, we also hypothesised that augmin could have a role in maintaining this uniform MT polarity.

Our data show that, in contrast with γ-tubulin depletion, augmin depletion causes a disruption in the typical uniform axonal MT polarity with an increase in the amount of MTs growing towards the soma of the neuron (**Figure 12c,e**). Axonal MT polarity defects caused by augmin depletion were rescued by co-depletion of γ-tubulin, proving that these wrong-polarity MTs are nucleated by the γTuRC and that augmin acts as a targeting factor of the γTuRC, restraining MT polarity. Interestingly, and in clear contrast with γ-tubulin depletion (which causes a decrease in the density of EB-comets), augmin depletion had no effect on the density of EB-comets (**Figure 12d**). From these results one could hypothesise that, in the axon, targeting of the γTuRC to the lattice of pre-existing MTs by augmin and γTuRC activation are independent events. Furthermore, we show that depletion of augmin-mediated MT nucleation impairs axonal growth (**Figure 12f,g**). Recent studies where MT regrowth is analysed in the soma of 3, 5 and 7DIV cultured mouse hippocampal neurons show that as neuron maturation proceeds,

the amount of MTs nucleated at the soma considerably decreases[226]. These data support our hypothesis that MT nucleation can occur in the axonal compartment.

According to our model we propose that augmin is required to properly target the γTuRC to axonal MTs and that this is the mechanism through which cells ensure that MT nucleation occurs with the right parallel, (+)-end-out orientation, maintaining axonal uniform MT polarity. To further test our model, we induced ectopic MT nucleation through overexpression of the small γTuNA domain of CDK5RAP2, previously shown to activate the nucleation activity of the γTuRC at the cytoplasm[65]. Similar to augmin depletion, expression of the γTuNA of CDK5RAP2, disrupted the uniform MT polarity found in the axon (**Figure 13**). This last piece of data corroborates our model showing that active control of nucleation events is required to ensure the formation of a correct axonal MT network. Furthermore, it shows that, like in human cell lines, the γTuNA of CDK5RAP2 can induce MT nucleation by the γTuRC. From these data one could hypothesise that CDK5RAP2 may have an important role in the establishment of neuronal MT network. Still, whereas CDK5RAP2 plays a critical role in division of neural progenitors as shown by the association between mutations in its gene and the development of primary microcephaly (reviewed in [199]), its role in neuronal cells remains to be studied. CDK5RAP2 is strongly downregulated during brain development and in the mouse cortex it is only detectable in young developing neurons (that co-stain for β3-tubulin) but not in more mature neurons (that stain for the neuronal marker NeuN)[293]. Therefore, in case there is any role of CDK5RAP2 in regulating the neuronal MT network, it is most likely restrained to early stages of neuronal development.

An interesting difference between the mechanism of augmin-mediated MT nucleation identified in the axon and the one previously described in the mitotic spindle is the requirement of the γTuRC subunit GCP-WD/NEDD1 for augmin-γTuRC interaction. In mitotic cells, targeting of the γTuRC to the lattice of pre-existing MTs requires interaction between the augmin subunit HAUS6 with NEDD1[105,121,294]. In contrast, work from our laboratory shows that, in neurons, NEDD1 plays no role in augmin-mediated nucleation at the axon[175]. This is not unexpected as NEDD1 (which stands for Neural Precursor Cell Expressed Developmentally Down-Regulated Protein 1) is strongly

downregulated during neuronal maturation. Interestingly, work performed in *Arabidopsis* showed that, in the cortical MT array of interphase cells, depletion of GCP-WD/NEDD1 strongly favours the formation of MT branches with a decreased angle (more parallel)[295]. Based on these experiments, I hypothesise that, in neurons, downregulation of GCP-WD/NEDD1 may favour the formation of shallow branch angles, further promoting the formation of highly bundled MT arrays in axons and dendrites. Still, it remains a puzzle how, in the absence of NEDD1, the augmin complex recruits the γTuRC to the lattice of pre-existing MTs.

In the future, it would also be interesting to test if augmin has any role in the establishment of the original uniform MT polarity of primary neurites or if it is also involved in axon specification.

Role of augmin-mediated microtubule nucleation in the establishment of the dendritic microtubule network

In this thesis I show that the role of the augmin complex in establishing the neuronal MT network is not restricted to the axon but is also relevant in the context of dendritic development.

Our data show that augmin depletion in 4DIV neurons causes, not only a decrease in the total MT density in young dendrites, but also a decrease in stable MTs, as seen by a reduction in the fluorescence intensity of acetylated-α-tubulin **(Figure 14a,b,c)**. Finally, these MT defects cause a delay in the development of these young dendrites and a reduction in dendritic arborization **(Figure 15)**.

Whereas in the axon almost all MTs are arranged with their (+)-ends towards the tip, in dendrites there is a mixed MT polarity. Therefore, we were interested in studying if augmin would be involved in mediating the generation of MTs of either orientation. With that purpose, and similarly to the experiments performed in the axon, we took advantage of the EB-comet assay to access MT polarity in augmin-depleted dendrites. We observed that depletion of either HAUS7 or HAUS1 did not cause any significant

effect on the dendritic MT polarity **(Figure 14d,f)**. On the other hand, a reduction in the density of EB-comets (which we take as a readout for reduction in nucleation events) was observed when either of the shRNAs were used **(Figure 14d,e)**. These results are in agreement with a study published last year in *Cell Reports* showing that, in more mature 12DIV neurons, HAUS6 depletion doesn't have any effect on MT polarity at the dendrites but causes a reduction in the amount of dynamic MTs (EB-comets) and a reduction in total MT density and dendritic growth[291]. In both axons and dendrites, augmin depletions led to a reduction in the total MT density. However, whereas in axons augmin depletion had no effect on the density of EB-comets and on the density of stable acetylated-MTs, in dendrites, augmin depletion caused a decrease in both. One possibility is that in axons, where MTs stabilization is overall more stable, augmin depletion activates the MT stabilising machinery (like MT stabilization by tau), counteracting the reduction in the total amount of MTs observed in this condition. Despite these differences, our data support that, in both axon and dendrites, augmin acts by amplifying a pre-existing MT polarity.

Several studies have implicated augmin in the establishment of MT bundles of uniform polarity[118,296]. One possible consequence of the mechanism proposed in this thesis is that, in dendrites, augmin-mediated MT nucleation leads to the formation of individual bundles of uniform MT polarity with either their (+)-ends pointing towards the soma or the tip of the dendrites. Indeed, this hypothesis is sustained by recent advances in the ultrastructure of the dendritic MT architecture showing that, in this cellular compartment, MTs associate into individual uniform polarity bundles with either their (+)-ends oriented towards the tip of the dendrite or with their (+)-ends oriented towards the soma. Interestingly, bundles with MTs of opposite orientation carry different posttranslational modifications (PTMs) that mediate the binding of motor proteins only to MT bundles with a specific oritentation[161].

However, it remains unclear how, during dendritic development, the initially uniform (+)-end out MT polarity in young primary neurites is disrupted and what is the origin of the soma-directed (+)-end dendritic MTs. One possibility is that MTs nucleated in the soma, in the centrosome or at the cytosol (depending on whether the centrosome is still

an active MTOC) are subsequently released from their nucleation site and transported into dendrites with their (-)-ends leading by motor proteins like KIF23[297,298].

Our data brings new insights into how neurons maintain their acentrosomal MT network by amplifying pre-existing MTs in a mechanism mediated by augmin. However, there are still many unresolved questions regarding the mechanisms underlying augmin-mediated MT nucleation, for example: (1) how does the augmin complex target the γTuRC in the absence of GCP-WD/NEDD1; (2) how is the binding of augmin to pre-existing MTs and to the γTuRC regulated and (3) which molecular players are involved in γTuRC activation in these cells?

Results obtained from Xenopus egg extracts show that RanGTP and its effector TPX2 can induce augmin-dependent MT branching[111,115]. Indeed, recent studies in young hippocampal neurons show that TPX2 depletion inhibits neurite growth and that there is RanGTP accumulation at the soma and at the tip of young neurites[299]. Therefore, the authors hypothesised that RanGTP accumulation induces TPX2 activation and consequently induction of MT nucleation at specific subcellular locations in post-mitotic neurons. However, whether this mechanism is dependent on the augmin complex and how is this RanGTP accumulation achieved in a context where the nucleus is intact is still unclear.

In addition, different studies show that binding of the augmin complex to pre-existing MTs can be regulated by phosphorylation of HAUS subunits. For example, phosphorylation of HAUS8 by Aurora-A has an impact on the capacity of the augmin complex to bind to pre-existing MTs[300]. Similarly, phosphorylation of HAUS6 by Plk1 promotes binding of the augmin complex to spindle MTs[294]. Indeed, data from our lab show that in WB using neuronal and brain lysates, a HAUS6-specific antibody show multiple specific bands with different sizes[175]. This can also be seen in **Figure 12b**. Interestingly, these bands are differentially expressed during development. One possibility is that these different bands correspond to different phosphorylation forms of HAUS6. However, this hypothesis remains to be tested. In the future it would be

interesting to study whether regulation of augmin-dependent MT nucleation in axons and dendrites can also occur through phosphorylation of HAUS subunits.

The augmin complex is essential for division in neuroprogenitors during mouse brain development

Proper brain development requires tight control of rapid division of neural progenitors and neuronal differentiation, migration and maturation, among other processes. This complex succession of events makes the brain a very good model to study the requirement of specific proteins for both mitotic and post-mitotic processes in the context of a tissue.

Augmin-dependent MT nucleation is important for mitotic spindle assembly and, as shown in the first chapter of this thesis, it plays a critical role in neuronal development *in vitro*. Therefore, we decided to evaluate if augmin plays a similar role during mouse brain development. With that purpose we generated three cKO mouse strains where *Haus6* gene deletion is triggered under control of different gene promotors expressed at specific stages of brain development. In this thesis, I focused on the study of Nestin-Cre and Baf53b-Cre *Haus6* cKO mice with a stronger emphasis on the first one.

The *Nestin* gene encodes for an intermediate filament protein that is expressed during early mouse brain development in neuroepithelial cells and radial glial cells and, after birth, in neural stem cells[301]. Therefore, mice expressing the Cre-recombinase under the control of a *Nestin* gene promotor are widely used to induce cKO in neuroepithelial cells and all its progeny in the brain. Different studies show that the *Tg(Nes-cre)1Kln* mouse strain used in this thesis induces Cre/LoxP recombination in the neuroepithelia of the prosencephalon, mesencephalon, rhombencephalon and spinal cord from ~e10. At e15.5, it has been shown that recombination has occurred in cells from all cortical layers[302–304]. Still, another study proposes that in these mice recombination occurs at much lower rates during embryogenesis[305]. Furthermore, one should take into account that analysis of this and other Nestin-Cre mouse strains reveals that Cre/LoxP

recombination under control of *Nestin* promotor can also occur in other tissues, like progenitor cells of the kidney or in the germline[214,219]. Indeed, we obtained some *Haus6*$^{fl/ko}$ Cre^{-} and *Haus6*$^{wt/ko}$ Cre^{-} mice (this is, mice where full recombination has occurred in one allele even though Cre-recombinase was not expressed) (**Table 3 – other genotypes**) as a result of crosses between *Haus6*$^{fl/wt}$ Cre^{-} and *Haus6*$^{fl/wt}$ Cre^{+} animals. These unexpected genotypes confirm that, in our mouse model, Cre/LoxP recombination can also occur in the germline of mice carrying both floxed *Haus6* and Cre-recombinase alleles. Animals carrying these unexpected genotypes were discarded from the study.

One of the main obstacles that I experienced in this project was to validate HAUS6 depletion in *Haus6* cKO mice. Our main strategy was to validate HAUS6 depletion by immunofluorescence (IF) with antibodies raised against HAUS subunits in brain sections from cKO mice. Firstly, tests in mouse cell lines showed that, amongst the antibodies we had available against HAUS subunits, only the HAUS6 specific antibody works for IF experiments in mouse samples. Still, we observed that this antibody only gives a specific signal when samples are fixed in cold methanol. During this thesis I tried several fixation/histological procedures with brain e13 embryonic samples: (1) fixation with PFA followed by OCT embedding and cryosectioning; (2) methanol fixation followed by OCT embedding and crysectioning; (3) whole mount IF in methanol fixed brain explants as described in[306]; (4) tissue "snap-freezing" followed by OCT embedding and cryosectioning. By the time the present thesis was written, none of these techniques revealed satisfactory results, being impossible to visualise the spindle localisation of HAUS6 using two different antibodies against this augmin subunit. In the future, other strategies will be tested like WB or quantitative real time PCR. Still, and as shown in **Figure 16b-*4th lane***, Cre/LoxP recombination is observed in adult mice carrying both floxed *Haus6* and Cre-recombinase alleles. Similarly, Cre/LoxP recombination has also been observed in e13 embryos carrying these genotypes (data not shown). Furthermore, most of the phenotypes here described in neuroprogenitors of Nestin-Cre *Haus6* cKO mice (mitotic delay, mitotic spindle abnormalities, centrosome fragmentation and loss of the γ-tubulin signal at the mitotic spindle) are in agreement

with augmin-depletion phenotypes described in cell lines[104,105]. Therefore, we conclude that HAUS6 is being depleted in the brain of these mice.

The only study where the role of augmin during mammalian development was addressed shows that full *Haus6* KO mice are not viable, with augmin being required to cluster the multiple acentrosomal MTOCs found in the first rounds of mitosis of mouse development[99]. Therefore, our study is the first to reveal the in vivo role of augmin in mitotic spindle assembly and progression in the presence of centrosomes.

We observed that Nestin-Cre *Haus6* cKO embryos are not viable (**Table 3**) with the few newborn cKO mice identified at P0 being already dead. However, at embryonic day 17 these embryos were still alive. Therefore, Nestin-Cre *Haus6* cKOs most likely die either in the last days of gestation or at/right after birth.

The fact that at embryonic day 17 cKOs are still alive is quite surprising considering their major brain defects. In these mice, agenesis of the forebrain (including the cortex, thalamus and hypothalamus) and of the cerebellum **(Figure 17)** is observed at this time of embryogenesis. In contrast with the severe brain defects found in cKOs, no apparent defects in body size were identified in these mice. Still, and considering that Cre-recombinase expression in Nestin-Cre mice can also occur in other organs like the kidney, it would be interesting in the future to confirm if malformations are observed elsewhere.

A bibliographic research for mouse models with congenital brain malformations revealed very few cases where the severity of brain defects is comparable to those observed in Nestin-Cre *Haus6* cKO mice. Indeed, the majority of cases where most brain structures fail to form, resulting in severe anencephaly, derive from defects in neural tube closure[307]. However, this is not the case in our mouse model as neural tube closure occurs properly (**Figures 17 and 18**). Interestingly, the only example which I identified where agenesis of most brain structures is not linked to neural tube defects is a mouse model where the apoptosis inhibitory gene *Survivin* is deleted by crossing floxed *Survivin* mice with Nestin-Cre transgenic mice[308]. Whereas most brain structures initially form, at e13 *Survivin* cKO brains display massive levels of apoptosis and tissue disruption.

Similarly, impairment in forebrain development in Nestin-Cre *Haus6* cKO mice was already evident early during embryogenesis. At 13 days of gestation, lateral cortexes in cKO mice are not properly developed. Furthermore, a high amount of pyknotic nuclei is observed in the structures that would give rise to the cortical tissue **(Figure 18)**. At this embryonic stage, in cKOs, structures that will give rise to the thalamus and hypothalamus (and that surround the third ventricle of the brain) are present but show a delay in development and an increase in the amount of pyknotic nuclei when compared to controls **(Figure 18)**. Skull formation follows the increase in brain mass that occurs during neuronal development. However, in e17.5 cKO mice the skull appears larger than the defective brain structures (**Figure 17c,d**). Together with the fact that a high amount of pyknotic nuclei is observed in cKO brain tissue, these data already suggest that failure in brain development due to loss of augmin in neuroprogenitors and its progeny is most likely accompanied by massive apoptosis and loss of brain mass embryonically.

In the work presented in this thesis we found that *Haus6* deletion caused an accumulation of mitotic neuroprogenitors at the ventricular zone of the third ventricle **(Figure 19a,b)**. In these neuroprogenitors we observed an increase pre-metaphase mitotic stages with a strong accumulation of cells in prometaphase **(Figure 19c,d)**. Therefore, we conclude that there is a mitotic delay in neuroprogenitors dividing in the absence of augmin. Our data suggest that this mitotic delay is, at least at some extent, caused by defects in spindle bipolarity in dividing neuroprogenitors (**Figure 20d,3**). However, considering the described role of augmin in k-fiber formation[123], it is also possible that, even in metaphasic neuroprogenitors presenting proper bipolar spindles, SAC is not satisfied causing a delay in anaphase onset.

In agreement with the described functions of augmin in ensuring spindle pole integrity during mitosis[104], most of the mitotic *Haus6* KO neuroprogenitors displayed centrosomal PCM fragmentation **(Figure 20)**. It has been proposed that in the absence of augmin, mitotic centrosomes fragment due to an imbalance of forces generated at the level of spindle microtubules. However, and considering that augmin also localises to centrioles, one cannot discard that augmin may also have a more direct role in

centriole/centrosome integrity. Centrosomes and cilia (both centriole-dependent structures) are thought to be important for basal-apical polarity of radial glial cells (RGCs). This idea is supported by the fact that in mouse models with centrosomal or ciliary defects in neuroprogenitors (such as *Sas4* cKO or *Cep63*, *Eml1* or *Arl13b* KO mice[129,200,309–311]), these cells show increased detachment from the ventricular surface, loss of basal-apical polarity and cell division in more basal layers of the cortex. Similar to these studies, in our Nestin-Cre *Haus6* cKO, apart from centrosome fragmentation during mitosis, there is also an increase in neuroprogenitors dividing in outer cortical layers, far from the VZ **(Figure 19 and 20)**.

The severity of the phenotypes observed in Nestin-Cre *Haus6* cKO were quite stunning considering that analysis of augmin mutants by other groups *in vivo* in flies and zebrafish has only revealed relatively milder defects. Indeed, in studies with *Drosophila*, null mutants for two different augmin subunits (Wac and Msd1) don't cause any apparent developmental defects apart from female infertility. However, and as mentioned in the introduction of this thesis, the requirement of augmin for female fertility may arise from the fact that in *Drosophila* oocytes meiosis-I takes place in the absence of centrosomes. Comparison between these *Drosophila* mutants and our Nestin-Cre cKOs would suggest that the mechanisms involved in spindle assembly are different between these species. However, similarly to expression of augmin mutants, centrosome loss doesn't cause major brain defects[177] in *Drosophila* suggesting that the centrosome doesn't play a critical in spindle assembly in neuroprogenitors this species. One possibility is that, in clear contrast to observations in *Drosophila* S2 cells where TPX2 doesn't play a major role in spindle assembly in mitosis[116], the major spindle assembly pathway in *Drosophila* neuroprogenitors is the chromatin-mediated pathway. Another possibility is that, in opposition to what happens in mice, there is a strong redundancy between spindle assembly pathways in *Drosophila* neuroprogenitors.

Previously published mouse models show that both reduced and increased[87] centrosome number in neuroprogenitors lead to microcephaly but not forebrain agenesis. In one study, centrioles were depleted from neuroprogenitors by deletion of the centriole-biogenesis gene *Sas4* under control of a *Nestin* promotor[200], as in my thesis

work. Nestin-Cre *Sas4* cKO mice developed microcephaly, due to prolonged mitosis and apoptosis in neuroprogenitors. Similarly to *Sas4* cKO mice, full *Cep63* KO mice also develop microcephaly[309]. CEP63 is required for timely centriole duplication and *Cep63* KO mice have neuroprogenitors displaying monopolar spindles and acentriolar spindle poles, leading to a delay in mitosis and triggering of p53-dependent cell death. The fact that *Haus6* deletion in neuroprogenitors leads to more severe proliferation defects than centrosome loss may suggest that the augmin pathway is crucial for spindle assembly in these cells and cannot be compensated for by chromatin or centrosome-mediated nucleation. Alternatively, we can also hypothesise that the differences in the severity of the phenotypes observed with the two models (*Haus6* and *Sas4* cKO) are due to differences in the kinetics of augmin and centrosome loss in the tissue.

The critical role of γ-tubulin and other γTuRC subunits for proper human brain development has been revealed by the fact that individuals carrying mutations in TUBG1, TUBGCP2, TUBGCP4, TUBGCP5, and TUBGCP6 genes display a wide-spectrum of congenital malformations of cortical development including microcephaly and lissencephaly-pachygyria syndrome. In contrast, to my knowledge, there is no case where human patients carrying mutations in genes encoding for augmin subunits present similar phenotypes. Therefore, and considering the severe brain development phenotypes observed in Nestin-Cre *Haus6* cKO mouse models, it would be very interesting to perform a study where the presence of mutations in augmin subunits is evaluated from samples from patients suffering from malformations of cortical development.

Another interesting questions that arises from this mouse model is why the forebrain and cerebellum are particularly affected by *Haus6* deletion in comparison to other brain structures of the mid and hindbrain. Whereas to my knowledge there is no bibliographic data to support it, one could hypothesise that Cre/LoxP recombination occurs at different rates in different brain regions during brain development. Another possibility is that progenitors from different brain regions are differentially susceptive to spindle defects or to *Haus6* deletion. In the future it would be interesting to address this issue

by analysing if mitotic defects can also be found in neuroprogenitors from other regions of the brain of cKO embryos.

Haus6 deletion leads to mitotic delay and induction of the p53 pathway in neuroprogenitors

p53 is a well-known tumour suppressor gene involved in inducing cell cycle arrest and apoptosis in response to abnormal proliferative signals or stress signals (e.g. DNA damage). The pathway through which p53 promotes apoptosis involves transcriptional regulation of target genes as well as transcription-independent functions of p53 that culminates, in some cases, in activation of the Bax/Apaf-1/caspase-9/caspase-3 mitochondrial death pathway[312,313].

A recent study showed that, by increasing mitotic duration using drugs that interfere with spindle assembly, both cell fate and survival of cycling radial glial cells are affected[222]. In this study authors used organotypic brain slices and *in vitro* cultured neuroprogenitors and proved that induction of mitotic delay leads to an increase in neurogenic cell divisions (both symmetric and asymmetric) and to an increase in apoptosis in the progeny of these divisions. Their results suggest that whereas a mild increase in the mitotic duration simply induces neurogenic division, longer mitotic duration lead to both neurogenic division and apoptosis in daughter cells. Furthermore, it was observed that p53 KO was sufficient to prevent apoptosis. While the molecular pathway that link mitotic duration to differentiation or apoptotic cell death are not very clear, these findings provide new insights into the mechanisms involved in the development of microcephaly in patients with mutations in centrosomal and spindle-associated proteins. In fact, in both microcephaly mouse models described earlier (Nestin-Cre *Sas4* cKO and *Cep63* KO mice) p53 KO is sufficient to rescue both cell death and microcephaly phenotypes. However, *Sas4* cKO mice develop hydrocephaly due to the complete lack of centrioles (and thus cilia) in multi-ciliated ependymal cells, responsible for moving the cerebrospinal fluid.

Like in these other mouse models, Nestin-Cre *Haus6* cKO showed an increase in cells with increased p53 and cleaved caspase-3 expression **(Figure 21a,b,c)**. Compared to the referred studies, in our mouse model the increase in the amount of p53 and cleaved caspase-3 positive cells was much higher, with massive cell death taking place in the tissues surrounding the third ventricle. Most of these p53 and cleaved caspase-3 positive cells lie in apical regions of the tissues that would give rise to the thalamus and hypothalamus. Indeed, p53 and cleaved caspase-3 positive cells are mostly found in regions that don't show immunofluorescence staining for the neuronal marker β3-tubulin and are not found in mitotic cells. This suggests that *Haus6* depleted neuroprogenitors can complete mitosis and only then activate the apoptotic cell death program through a p53-dependent pathway. Indeed, we have observed that almost all cells overexpressing p53 also express the neural progenitor marker PAX6, proving that most of the p53-dependent cell death occurs in neural progenitors **(Figure 21d,e)**. Still, we cannot discard that, at least to some extent, cell death in post-mitotic neurons might occur.

In the future it would be interesting to perform experiments to properly trace the progeny of neuroprogenitors dividing in the absence of *Haus6*. This would allow us to address if there is still neurogenesis in the forebrain of cKO embryos at e13.5 or if all the neuroprogenitors that divide in the absence of *Haus6* undergo apoptosis. Furthermore, it remains to be tested if deletion of p53 in nestin-Cre *Haus6* cKO mice is also sufficient to rescue the cell death phenotype and potentially brain development and lethality.

Haus6 deletion under control of a *Baf53b* promotor leads to mild brain phenotypes but a strong impairment in the development of the exocrine pancreas

In order to study the role of augmin during neuronal differentiation we decided to cross floxed *Haus6* mice with mice expressing Cre recombinase under control of the *Baf53b* gene[217]. Among the commercially available Cre-expressing transgenic mouse strains we chose this one as it was shown to induce strong Cre-induced genomic recombination in

the developing brain, embryonically and very specifically in neurons. Furthermore, it was shown to induce recombination in neurons of the peripheral nervous system in the eye, olfactory epithelium, tongue and skin and of the enteric nervous system in the intestine[217].

Interestingly, Cre-induced recombination was also present in the pancreatic islets. This is not the first example of a neuron-specific gene which is also expressed in pancreatic islets and, more specifically, in β-cells (the most abundant cell type of pancreatic islets, which is responsible for insulin production). Indeed, even though neurons and β-cells arise from different germ layers, they both express a similar subset of differentiation markers[314,315]. This similarity in gene expression was shown in a genome-wide mRNA expression screening performed in humans and rodents where it was found that 15% of the cell-specific genes expressed in β-cells are also expressed in neuronal tissues where they code for proteins involved in neurotransmitter transport, synaptic vesicle formation and brain development[316].

Analysis of the brain of 2-month-old Baf53b-Cre *Haus6* cKO mice didn't reveal any major brain abnormality but a small but significative reduction in brain size (measured by brain weight) and in cortical thickness when compared to controls (**Figure 24b,c,d,**). We hypothesized that this small decrease in brain weight and cortical size could be caused by an increase in apoptosis in cKO brains. Nevertheless, preliminary data obtained by me showed no increase in cells expressing the apoptotic marker cleaved caspase 3 in brain sections from both 2-month-old and newborn cKO mice. One hypothesis is that, by limiting dendritic and axonal growth (as we have seen in our *in vitro* studies), *Haus6* deletion may cause a reduction in the neuronal mass, leading to a reduction in both brain weight and size. Still, further experiments would be needed to validate this hypothesis.

A recent study shows that injection of a shRNA against HAUS6 into the ventricle of the developing mouse brain causes mild defects in neuronal polarization and, consequently, on radial migration of cortical neurons *in vivo*[291]. However, analysis of Baf53b-Cre *Haus6* cKO mice did not reveal any significative differences in the formation of neuronal cortical

layers (**Figure 24e,f**). Still, the use neuronal markers for specific cortical layers would be required to confirm these results.

One possible interpretation of our results is that proper depletion of HAUS6 levels in *Haus6* deleted neurons only occurs once cells have already polarised and started migrating or have finished migrating towards their final destinations in the cortex. Therefore, it would be important to determine the exact timing of HAUS6 depletion and weather it occurs, before, during or after neuronal migration. For that, confirming Haus6 deletion at a single cell levels in IF experiments would be very useful.

However, it is very important to be cautious when interpreting the results obtained in the brain of Baf53b-Cre *Haus6* cKO mice. These cKO mice present: (1) strongly decreased growing curves after weaning (**Figure 22a,b,c**); (2) increase in water consumption; (3) severe atrophy in pancreatic islets (**Figure 23a**) where insulin production takes place and (4) severe hyperglycaemia (**Figure 23b**). All these symptoms support that Baf53b-Cre *Haus6* cKO mice develop diabetes type-1 where insulin production is impaired by defects/disruption of pancreatic islets[317]. Several studies have reported a correlation between de-regulation of blood glucose levels and small brain atrophy in patients suffering from type 1 diabetes[318–321]. Therefore, one must consider the hypothesis that the small but significant brain atrophy found in Baf53b-Cre *Haus6* cKO mice is not caused by *Haus6* deletion in the brain *per se* but is rather a side effect of abnormal glucose levels in these diabetic mice.

How may *Haus6* deletion affect pancreatic islet formation?

Formation of the endocrine pancreas starts around day e12.5-e13.5 with endocrine progenitors giving rise to the different cell populations that will compose the future pancreatic islets (α-cells, β-cells, PP-cells and δ-cells)[322,323]. Then, differentiated endocrine cells migrate towards the mesenchyme of the pancreas, where they cluster and give rise to proto-islets. It is important to mention that in these proto-islets endocrine cells already express differentiation markers like insulin (in β-cells) and glucagon (in α-cells)[324,325]. During the late stages of embryogenesis and in neonatal stages differentiated β-cell found in proto-islets can also re-enter the cell cycle

promoting expansion of the β-cell population in these pancreatic structures.[326–329]. Indeed, it has been shown that in the developmental stages proliferation of differentiated β-cells is the major mechanism contributing to pancreatic islet growth[330].

Consequently, it is not unlikely that perturbances in mitotic progression in these cells would strongly affect the formation of pancreatic islets and lead to deficits in insulin production. Here, I hypothesize that *Haus6* deletion in differentiated β-cells of Baf53b-Cre cKO may lead to mitotic defects once these cells re-enter the cell cycle during late embryogenesis and neonatal stages. Strong mitotic defects as the ones observed in *Haus6* KO neuroprogenitors would cause failure in islet expansion and consequently affect insulin production, culminating in the development of diabetes in the cKO mice.

Therefore, in the future it would be very important to test this hypothesis and evaluate if in newborn mice mitotic and cell survival defects are found in the pancreatic islets of Baf53b-Cre *Haus6* cKO mice. These results would have a strong implication in our study since they would show a clear mitotic requirement of augmin *in vivo* in other cell types rather than neuroprogenitors, which are known to be particularly sensitive to spindle defects.

Apart from defects in pancreatic islet development other tissues were also severely affected in Baf53b-Cre *Haus6* cKO (**Figure 25**). Some of the observed phenotypes (reduction in hepatocyte size and muscle atrophy) may be explained by the development of diabetes in these mice and consequent impairment in glucose uptake by these tissues. On the other hand, a direct link between diabetes and other phenotypes (spleen atrophy, hydronephrosis, cecum enlargement and disruption of the mucosa in the cecum) is less clear.

Hydronephrosis is characterised by an enlargement of the kidney as a result of urine accumulation in the renal pelvis or calyces. In contrast with other types of nephropathies, hydronephrosis has not been implicated as a side effect of diabetes[331]. Hydronephrosis is often caused by static anatomic occlusion (e.g., by stones) or by failure in peristaltic mechanism, responsible for propelling urine in the kidney pelvis and ureter[332]. Whereas different studies show that peristalsis in the ureter can occur in the

absence of neural innervation, activity of the autonomous nervous system has been implicated in modulation of peristaltic movements in this organ[333]. Furthermore, bladder disfunctions have also been linked to the development of hydronephrosis[334]. One of the hallmarks of diabetic patients is the development of neuropathy in neurons from the autonomous nervous system (which is essential for bladder function)[335]. Therefore, we hypothesize that hydronephrosis may arise from disruption of the autonomous nervous system in the urinary tract of Baf53-Cre *Haus6* cKO mice because of diabetes.

Similarly, diabetic neuropathy can also result in abnormalities in intestinal motility due to disruption of reflex and sensory pathways that control gastric and intestinal function. In the intestine it can result in diarrhoea, constipation, intestinal distention and abdominal pain[336]. Therefore, distention and enlargement of the cecum (and consequent atrophy of the mucosa of the cecum) may also be a consequence of loss of motility due to diabetic autonomic neuropathy in Baf53b-Cre *Haus6* cKO mice.

To distinguish between neuronal dysfunction caused by *Haus6* deletion in the autonomic nervous system and neuropathy caused by diabetes, an important experiment would be to determine which of these phenotypes can be rescued by administration of insulin to Baf53b-Cre Haus6 cKO mice, to promote glucose uptake by the different tissues and restore normal blood glucose levels.

Analysis of the γTuRC interactome by performing a GCP3 pulldown followed by MS

Considering that MT nucleation in neurons is still poorly characterized, an additional goal in this thesis was to identify the γTuRC-associated proteome in neurons, with the hope of discovering potential regulators.

Among the 54 proteins significantly enriched in GCP3 immunoprecipitates were the γTuRC subunits γ-tubulin, GCP2, GCP3, GCP4 and MZT2/GCP8 as high confidence interactors, which validated my approach (**Table 4**). While GCP5 and GCP6 were not identified in the MS data, the γTuRC subunit GCP4 was present suggesting that the samples indeed contained γTuRC and not only γTuSC subcomplexes.

Curiously, and even though we had previously identified HAUS6 in GCP3 IPs from lysates of mouse neuron primary cultures[175], none of the augmin subunits was included in the candidate list obtained by mass spectrometry. A possible explanation may be the technical differences in the experiments: (1) the lysis buffers used were considerably different; (2) the elution techniques used were also different: in the IP performed in this thesis, GCP3 interactors were eluted with high pH ammonium buffer instead of sample buffer. Sample buffer has a high concentration of SDS and reducing agent and thus is incompatible with MS analysis, but elutes proteins more efficiently.

A Gene Ontology (GO) analysis was performed in order to obtain a better understanding of the types of proteins identified by MS. Not surprisingly, we observed enrichment in proteins that form part of the γTuRC and localise to the spindle or to MTOCs like the centrosome (**Table 5 and 6**). Considering the localisation of GCP3 at these subcellular localisations, this piece of data confirms that our IP worked well and may give us reliable results on GCP3 interactor candidates.

Interestingly, we observed an enrichment in proteins that localise to pre and postsynaptic compartments (**Table 5**). Evidence of MTs playing a role in the development and function of dendritic spines is quite recent. It has been shown that dynamic (tyrosinated) MTs are able to invade dendritic spines and that an increase in MT invasion correlates with an increase in neuronal activity, spine formation and

synaptic plasticity[337,338]. Whereas several MAPs like EBs and MAP6 have been found to localise to dendritic spines, no function of the γTuRC has ever been reported in these structures[339,340]. While these results may look interesting one needs to consider that these IP experiments were performed with lysates from 7DIV primary cortical cultures, a stage where neurons present little amounts of dendritic spines[134]. Even though I did not further develop this subject in my thesis, it would be very interesting to test if MT nucleation occurs in pre and/or postsynaptic compartments at dendritic spines and axonal boutons. One possible experiment to validate these proteins as specific γTuRC interactors in pre and postsynaptic structures would be to repeat these IP experiments in more mature neurons, where a higher density of these structures have already been formed.

14-3-3 proteins are a family of conserved multifunctional regulatory molecules able to interact with many signalling proteins. These proteins are highly expressed during brain development and have been implicated in several signalling events taking place during neurogenesis, neuronal migration and neuromorphogenesis[341,342]. Amongst the list of putative GCP3 interactors identified by MS I found six members of the 14-3-3 family (*Ywhaz*, *Ywhag*, *Ywhal*, *Ywhaq*, *Ywhah*, *Ywhab*) as high confidence interactors. Due to lack of time, I was not able to validate these candidates as γTuRC interactors. Still, one could hypothesise that 14-3-3 proteins could be involved in γTuRC regulation and link γTuRC activity to other intracellular cell signalling pathways.

KIF2A and CEP170 interact with γTuRC in cellular extracts from cortical neurons

Amongst the GCP3 interactors identified by MS, I decided to focus my study on KIF2A and CEP170. KIF2A is a member of the kinesin-13 protein family which is characterised by promoting microtubule depolymerisation at MT ends. What could be the significance of the interaction of KIF2A with γTuRC? One possibility is that it is an inhibitory factor for MT nucleation similar to the role of the microtubule depolymerase MCAK in promoting catastrophe in small MT seeds *in vitro*[69]. Another possibility is that KIF2A

interacts with γTuRC capped MTs, promoting depolymerization at the (-)-end. These hypotheses will be discussed further below.

CEP170 has been identified as a targeting factor for kinesin-13 protein KIF2B to the mitotic spindle during mitosis and, more recently, as targeting factor for KIF2A to the centrosome during cilia disassembly[343,344]. Consequently, we wanted to test if it could play a role in targeting KIF2A to specific subcellular locations or be involved in γTuRC/KIF2A interaction in neurons. Furthermore, CEP170 was one of the GCP3 interactor candidates with the highest peptide count in the obtained MS list, making it a high confidence hit.

In this thesis I was able to validate both KIF2A and CEP170 as γTuRC interactors in neurons with both proteins co-immunoprecipitating with endogenous GCP3 and GCP8 in 7DIV mouse neuronal extracts **(Figure 28a)**. In the future it would be interesting to test if KIF2A and/or CEP170 form stable complexes with the γTuRC. For that, we could test if KIF2A and CEP170 co-fractionate with γ-tubulin complexes in a sucrose gradient.

KIF2A interacts with the C-terminal region of GCP8 and with CEP170

In order to better understand the interaction between CEP170, KIF2A and the γTuRC we performed immunoprecipitation experiments from HEK cells expressing GFP-tagged versions of KIF2A, CEP170 and different constructs of GCP8. Unpublished data from Sabine Klischies, a former PhD student in the lab, had shown that GCP8 binds to the γTuRC through interaction between GCP2 and the N-terminal region of GCP8 (aa 1-111). On the other hand, the C-terminal region of GCP8 (aa 112-158) alone was not able to bind to the γTuRC.

The experiments presented in this thesis show that KIF2A interacts with CEP170 in cellular extracts from HEK cells **(Figure 29)**. At the time when these experiments were performed, the CEP170 function in targeting KIF2A to the centrosome during cilia disassembly had not yet been described. Preliminary experiments performed with help of an Erasmus student at our laboratory (Chiara Paolantoni) showed that in U2OS cell

lines CEP170 is required for targeting of KIF2A, but not γ-tubulin, to the interphase centrosome.

We also observed that KIF2A interacts with GCP8 and, more specifically, with the GCP8 C-terminal region (which does not bind to γTuRC) **(Figure 29)**. Further experiments are required to test if the interaction between KIF2A and GCP8 occur in a direct or indirect manner. Interestingly, CEP170 was not immunoprecipitated with GCP8 constructs suggesting that interaction between CEP170 and the γTuRC occurs through a different mechanism than KIF2A-γTuRC interaction. Unexpectedly, neither GFP-KIF2A, nor GFP-CEP170 were able to pulldown γ-tubulin. Since in these experiments overexpression of protein tagged versions were used, we could hypothesise that the GFP tag of these constructs may interfere with KIF2A and CEP170 interaction with the γTuRC. In order to test this hypothesis, it would be interesting to test different KIF2A and CEP170 antibodies and try to perform IP experiments against endogenous KIF2A and CEP170 proteins. Another possibility is that, in the cytosol, only a small fraction of KIF2A and CEP170 is bound to the γTuRC. In the case of KIF2A this is quite likely as it has also been shown to interact with MT (+)-ends.

In his thesis Artur Ezquerra performed experiments where he depleted either GCP8 or KIF2A from RPE1 cells and performed MT regrowth experiments to analyse MT nucleation in the absence of these proteins. He observed that after MT depolymerisation using a cold treatment, MTs regrow faster from both the centrosome and Golgi Apparatus in cells lacking GCP8 or KIF2A. These data suggest that both GCP8 and KIF2A act as negative regulators of MT nucleation at both the centrosome and the Golgi apparatus.

During MT nucleation *in vitro*, MCAK functions as negative regulator by promoting catastrophe events in small MT seeds[69]. However, it is still unclear whether it also has this function in the context of nucleation by γTuRC. In addition, this same study shows that TPX2 and XMAP215, due to their activities as anti-catastrophe factor and MT polymerase, respectively, stimulate templated MT nucleation. I propose that KIF2A may act, like the proposed function of MCAK, as a negative regulator of MT nucleation by

γTuRC. On the other hand, CEP170 may act as a targeting factor of KIF2A to different subcellular locations where inhibition of MT nucleation is required. However, to confirm these hypotheses, further experiments are required.

Structurally, kinesin-13 proteins are characterised by the presence of a NECK domain (comprising aa 153-223 in human KIF2A) and a degenerated motor domain (comprising aa 553-706 in human KIF2A). Both domains are required for efficient MT depolymerisation activity of KIF2A[345]. Crystal structure of monomeric KIF2A in complex with α/β-tubulin heterodimers show that both NECK and motor domains interact with the lattice of consecutive tubulin heterodimers[346]. It was proposed that this interaction promotes the insertion of the loop L2 region (which constitutes the ATPase domain of the motor domain) between the two α/β-tubulin dimers and promotes MT bending and consequent depolymerisation in an ATP-dependent manner. As future perspectives for this project, it would be interesting to map the region (or regions) of KIF2A that interact with the γTuRC. Ideally, these data would allow us to generate a KIF2A mutant which can induce MT depolymerisation at the (+)-end but is unable to interact with the γTuRC. Testing if this mutant can rescue MT regrowth phenotypes observed after KIF2A depletion would be very informative to understand the relevance of γTuRC/KIF2A interaction for MT formation.

Role of KIF2A and CEP170 in neuronal development

Whereas different studies have shown the relevance of KIF2A during neuronal development, CEP170 has never been described in this cell type. In this thesis we show that, like KIF2A, CEP170 is expressed during early stages of development of mouse hippocampal neurons (from 1 to 7 DIV) **(Figure 28b)**. Curiously, the immunoblot against KIF2A showed the expression of bands with different sizes that are differentially expressed during neuron differentiation. This observation could be explained by differential expression of different KIF2A isoforms. This is the case, for example, for the KIF2Aβ isoform which was shown to be expressed during specific stages of hippocampal development[347]. On the other hand, these different band sizes could also be explained

by differential phosphorylation which, depending on the amino acid where the posttranslational modification occurs, were shown to either induce or decrease KIF2A activity and, consequently neurite outgrowth[348]. However, both hypotheses were not tested in this thesis.

When performing an immunostaining with specific antibodies against CEP170 and KIF2A we observed that, in young 2DIV neurons both proteins localise to the centrosome and give a diffuse staining in the soma, dendrites and axon. Interestingly, both antibodies stained a subset of axonal growth cones, showing an enrichment of both CEP170 and KIF2A in the region preceding and at the central region of the growth cone **(Figure 30)**. As mentioned during the introduction of this thesis, MTs at the central zone of the growth cone are highly tyrosinated and dynamic. On the other hand, very stable MTs are found in the region preceding the central region of the growth cone. Previous studies showed that KIF2A localises to the tip of neurites in mouse cortical neurons[349,350]. Furthermore some studies suggest that KIF2A is able to bind to tyrosinated MTs[351]. Since dynamic tyrosinated MTs are particularly enriched at the growth cone[352], the mechanism through which KIF2A slows down axonal growth may be trough inducing MT depolymerization at these cellular locations. This mechanism becomes particularly important for controlling extension of axon collateral branches.

During axonal development, neurons extend long primary axons toward targets in order to form appropriate neuronal connections. Apart from the primary axon, neurons also establish connections with multiple targets by growing axonal collateral branches. However, while the growth cone of the primary axon is actively extending, growth of small collateral branches is inhibited until conditions require them to extend (discussed in [251]). KIF2A activity has been strongly implicated in this process since *Kif2a* KO neurons show aberrant axonal branching due to overextension of collateral branches[251,349]. *Kif2a* KO mice are not viable and die early after birth presenting defects in migration of cortical neurons and overextension of axonal extensions[251]. A recent study shows that cKO of *Kif2a* induced by tamoxifen administration leads to dendro-axonal conversion and development of aberrant axonal extensions in hippocampal neurons. This leads to defects in hippocampal wiring with cKO mice presenting signs of epileptic hippocampus[253].

In order to understand what the role of CEP170 for axonal development is we designed two different shRNAs against the mouse CEP170 **(Figure 31a)**. Interestingly, we observed that, similarly to *Kif2a* KO neurons described in the literature, CEP170 depleted neurons presented an increase in axonal growth (with one of the shRNAs used) and an increase in the amount of long axonal collateral branches **(Figure 31b,c,d,e)**. Therefore, since both CEP170 and KIF2A show similar subcellular localisations and its depletion show similar phenotypes, I speculate that the role of KIF2A in controlling growth of axon collateral branches could be linked to CEP170. Considering that CEP170 is a KIF2A interactor and that, in mitotic cells, it is able to target another kinesin-13 protein (KIF2B) to spindle MTs, one can even speculate that CEP170 could be the targeting factor of KIF2A to the growth cone of axon collateral branches. In order to test this hypothesis, it would be crucial to test if there is any displacement of KIF2A from the growth cone in CEP170 depleted neurons.

Another question that remains to be answered is whether the phenotypes observed for KIF2A and CEP170 depletion are linked to regulation of γTuRC nucleation activity or are simply caused by regulation of MT plus-ends. We have never observed accumulation of γTuRC at the growth cone in neurons. However, advances in the field have shown that regulation of MT nucleation is far more complex than simply concentrating γTuRCs at MTOCs and involve, for example, specific regulation by activating factors such asMT polymerases of the XMAP215 family[67]. In analogy to such observations negative regulation of γTuRC by KIF2A is equally plausible.

As a final summary, in this thesis we were able to establish augmin-mediated MT nucleation as an essential factor for maintaining a proper MT network in both axons and dendrites *in vitro* and for neural progenitor division during mammalian brain development *in vivo*. Furthermore, our data provides new insights into the regulation of MT nucleation in neurons by proposing KIF2A and CEP170 as two new γTuRC interactors (and potential regulators), which repress the growth of axonal collateral branches.

CONCLUSIONS

The major conclusions of this thesis are the following:

- Depletion of γ-tubulin in cultured mouse hippocampal neurons causes a reduction in the amount of actively growing dynamic microtubules in the axon.
- Depletion of augmin in cultured mouse hippocampal neurons impairs axonal uniform microtubule polarity with an increase in retrograde microtubules in a process dependent on γ-tubulin.
- Proper targeting of microtubule nucleation in the axon is required to ensure a correct microtubule polarity in this cellular compartment
- Augmin depletion in cultured mouse hippocampal neurons leads to a decrease in the amount of dendritic microtubules, including a reduction in the density of stable microtubules.
- Augmin depletion in cultured mouse hippocampal neurons impairs dendritic growth and arborisation.
- Augmin depletion in cultured mouse hippocampal neurons leads to a decrease in the amount of actively growing dynamic microtubules in dendrites, with no effect on their overall polarity.
- KO of *Haus6* in neuroprogenitors *in vivo* aborts brain development embryonically.
- KO of *Haus6* in neuroprogenitors *in vivo* causes a mitotic delay in these cells.
- *Haus6* KO causes centrosome fragmentation and spindle defects in mitotic neuroprogenitors *in vivo*.
- KO of *Haus6* in neuroprogenitors leads to induction of the p53 pathway and apoptosis.

- KO of Haus6 under control of the Baf53b promotor causes atrophy of pancreatic islets and development of diabetes type 1 in a mouse model
- In cultured neurons, CEP170 and KIF2A interact with the γ-TuRC.
- CEP170 is an interactor of KIF2A.
- KIF2A interacts with the C-terminal region of the γTuRC subunit MZT2/GCP8.
- CEP170 depletion in hippocampal neurons leads to an increase in size of axonal branches

REFERENCES

1. Huber, F., Boire, A., López, M. P. & Koenderink, G. H. Cytoskeletal crosstalk: when three different personalities team up. Curr. Opin. Cell Biol. 32, 39–47 (2015).

2. Coles, C. H. & Bradke, F. Coordinating Neuronal Actin–Microtubule Dynamics. Current Biology 25, R677–R691 (2015).

3. Hu, J. et al. Septin-driven Coordination of Actin and Microtubule Remodeling Regulates the Collateral Branching of Axons. Curr Biol 22, 1109–1115 (2012).

4. Pacheco, A. & Gallo, G. Actin Filament-Microtubule Interactions in Axon Initiation and Branching. Brain Res Bull 126, 300–310 (2016).

5. Borisy, G. et al. Microtubules: 50 years on from the discovery of tubulin. Nat Rev Mol Cell Biol 17, 322–328 (2016).

6. Chrétien, D. & Wade, R. H. New data on the microtubule surface lattice. Biology of the Cell 71, 161-174 (1991)

7. Tilney, L. G. et al. MICROTUBULES: EVIDENCE FOR 13 PROTOFILAMENTS. J Cell Biol 59, 267–275 (1973).

8. Akhmanova, A. & Hoogenraad, C. C. Microtubule minus-end-targeting proteins. Curr. Biol. 25, R162-171 (2015).

9. Burns, R. G. Alpha-, beta-, and gamma-tubulins: sequence comparisons and structural constraints. Cell Motil. Cytoskeleton 20, 181–189 (1991).

10. Downing, K. H. & Nogales, E. New insights into microtubule structure and function from the atomic model of tubulin. Eur. Biophys. J. 27, 431–436 (1998).

11. Desai, A. & Mitchison, T. J. Microtubule Polymerization Dynamics. Annual Review of Cell and Developmental Biology 13, 83–117 (1997).

12. Mitchison, T. & Kirschner, M. Dynamic instability of microtubule growth. Nature 312, 237–242 (1984).

13. Akhmanova, A. & Hoogenraad, C. C. Microtubule plus-end-tracking proteins: mechanisms and functions. Curr. Opin. Cell Biol. 17, 47–54 (2005).

14. Roll-Mecak, A. & McNally, F. J. Microtubule-severing enzymes. Curr. Opin. Cell Biol. 22, 96–103 (2010).

15. Akhmanova, A. & Steinmetz, M. O. Microtubule +TIPs at a glance. J. Cell. Sci. 123, 3415–3419 (2010).

16. Bu, W. & Su, L. K. Regulation of microtubule assembly by human EB1 family proteins. Oncogene 20, 3185–3192 (2001).

17. Hayward, D., Metz, J., Pellacani, C. & Wakefield, J. G. Synergy between Multiple Microtubule-Generating Pathways Confers Robustness to Centrosome-Driven Mitotic Spindle Formation. Dev Cell 28, 81–93 (2014).

18. Maurer, S. P., Fourniol, F. J., Bohner, G., Moores, C. A. & Surrey, T. EBs recognize a nucleotide-dependent structural cap at growing microtubule ends. Cell 149, 371–382 (2012).

19. Maurer, S. P. et al. EB1 accelerates two conformational transitions important for microtubule maturation and dynamics. Curr. Biol. 24, 372–384 (2014).

20. Zanic, M., Widlund, P. O., Hyman, A. A. & Howard, J. Synergy between XMAP215 and EB1 increases microtubule growth rates to physiological levels. Nat. Cell Biol. 15, 688–693 (2013).

21. Al-Bassam, J. & Chang, F. Regulation of microtubule dynamics by TOG-domain proteins XMAP215/Dis1 and CLASP. Trends Cell Biol. 21, 604–614 (2011).

22. Aher, A. et al. CLASP Suppresses Microtubule Catastrophes through a Single TOG Domain. Dev. Cell 46, 40-58.e8 (2018).

23. Al-Bassam, J. et al. CLASP promotes microtubule rescue by recruiting tubulin dimers to the microtubule. Dev. Cell 19, 245–258 (2010).

24. Walczak, C. E., Gayek, S. & Ohi, R. Microtubule-Depolymerizing Kinesins. Annual Review of Cell and Developmental Biology 29, 417–441 (2013).

25. Hunter, A. W. et al. The kinesin-related protein MCAK is a microtubule depolymerase that forms an ATP-hydrolyzing complex at microtubule ends. Mol. Cell 11, 445–457 (2003).

26. Wittmann, T. & Waterman-Storer, C. M. Spatial regulation of CLASP affinity for microtubules by Rac1 and GSK3beta in migrating epithelial cells. J. Cell Biol. 169, 929–939 (2005).

27. Goodwin, S. S. & Vale, R. D. Patronin regulates the microtubule network by protecting microtubule minus ends. Cell 143, 263–274 (2010).

28. Mayr, M. I. et al. The Human Kinesin Kif18A Is a Motile Microtubule Depolymerase Essential for Chromosome Congression. Current Biology 17, 488–498 (2007).

29. Chen, Y. & Hancock, W. O. Kinesin-5 is a microtubule polymerase. Nature Communications 6, 8160 (2015).

30. Freixo, F. et al. NEK7 regulates dendrite morphogenesis in neurons via Eg5-dependent microtubule stabilization. Nat Commun 9, 2330 (2018).

31. Gadadhar, S., Bodakuntla, S., Natarajan, K. & Janke, C. The tubulin code at a glance. J. Cell. Sci. 130, 1347–1353 (2017).

32. Lewis, S. A., Lee, M. G. & Cowan, N. J. Five mouse tubulin isotypes and their regulated expression during development. J. Cell Biol. 101, 852–861 (1985).

33. Lewis, S. A., Gu, W. & Cowan, N. J. Free intermingling of mammalian beta-tubulin isotypes among functionally distinct microtubules. Cell 49, 539–548 (1987).

34. Vemu, A., Atherton, J., Spector, J. O., Moores, C. A. & Roll-Mecak, A. Tubulin isoform composition tunes microtubule dynamics. Mol. Biol. Cell 28, 3564–3572 (2017).

35. Ti, S.-C., Alushin, G. M. & Kapoor, T. M. Human β-Tubulin Isotypes Can Regulate Microtubule Protofilament Number and Stability. Dev. Cell 47, 175-190.e5 (2018).

36. Janke, C. & Bulinski, J. C. Post-translational regulation of the microtubule cytoskeleton: mechanisms and functions. Nat. Rev. Mol. Cell Biol. 12, 773–786 (2011).

37. Valenstein, M. L. & Roll-Mecak, A. Graded Control of Microtubule Severing by Tubulin Glutamylation. Cell 164, 911–921 (2016).

38. Voter, W. A. & Erickson, H. P. The kinetics of microtubule assembly. Evidence for a two-stage nucleation mechanism. J. Biol. Chem. 259, 10430–10438 (1984).

39. Roostalu, J. & Surrey, T. Microtubule nucleation: beyond the template. Nature Reviews Molecular Cell Biology 18, 702–710 (2017).

40. Oakley, C. E. & Oakley, B. R. Identification of γ-tubulin, a new member of the tubulin superfamily encoded by mipA gene of Aspergillus nidulans. Nature 338, 662–664 (1989).

41. Findeisen, P. et al. Six Subgroups and Extensive Recent Duplications Characterize the Evolution of the Eukaryotic Tubulin Protein Family. Genome Biol Evol 6, 2274–2288 (2014).

42. Oakley, B. R., Paolillo, V. & Zheng, Y. γ-Tubulin complexes in microtubule nucleation and beyond. Mol Biol Cell 26, 2957–2962 (2015).

43. Farache, D., Emorine, L., Haren, L. & Merdes, A. Assembly and regulation of γ-tubulin complexes. Open Biol 8, (2018).

44. Yuba-Kubo, A., Kubo, A., Hata, M. & Tsukita, S. Gene knockout analysis of two γ-tubulin isoforms in mice. Developmental Biology 282, 361–373 (2005).

45. Oegema, K. et al. Characterization of Two Related Drosophila γ-tubulin Complexes that Differ in Their Ability to Nucleate Microtubules. J Cell Biol 144, 721–733 (1999).

46. Teixidó-Travesa, N., Roig, J. & Lüders, J. The where, when and how of microtubule nucleation - one ring to rule them all. J. Cell. Sci. 125, 4445–4456 (2012).

47. Kollman, J. M., Merdes, A., Mourey, L. & Agard, D. A. Microtubule nucleation by γ-tubulin complexes. Nature Reviews Molecular Cell Biology 12, 709–721 (2011).

48. Gunawardane, R. N. et al. Characterization and reconstitution of Drosophila gamma-tubulin ring complex subunits. J. Cell Biol. 151, 1513–1524 (2000).

49. Murphy, S. M. et al. GCP5 and GCP6: Two New Members of the Human γ-Tubulin Complex. Mol Biol Cell 12, 3340–3352 (2001).

50. Guillet, V. et al. Crystal structure of γ-tubulin complex protein GCP4 provides insight into microtubule nucleation. Nature Structural & Molecular Biology 18, 915–919 (2011).

51. Greenberg, C. H. et al. Structure of γ-tubulin small complex based on a cryo-EM map, chemical cross-links, and a remotely related structure. J Struct Biol 194, 303–310 (2016).

52. Teixidó-Travesa, N. et al. The gammaTuRC revisited: a comparative analysis of interphase and mitotic human gammaTuRC redefines the set of core components and identifies the novel subunit GCP8. Mol. Biol. Cell 21, 3963–3972 (2010).

53. Cota, R. R. et al. MZT1 regulates microtubule nucleation by linking γTuRC assembly to adapter-mediated targeting and activation. J Cell Sci 130, 406–419 (2017).

54. Lüders, J., Patel, U. K. & Stearns, T. GCP-WD is a gamma-tubulin targeting factor required for centrosomal and chromatin-mediated microtubule nucleation. Nat. Cell Biol. 8, 137–147 (2006).

55. Manning, J. A., Shalini, S., Risk, J. M., Day, C. L. & Kumar, S. A direct interaction with NEDD1 regulates gamma-tubulin recruitment to the centrosome. PLoS ONE 5, e9618 (2010).

56. Gomez-Ferreria, M. A. et al. Novel NEDD1 phosphorylation sites regulate γ-tubulin binding and mitotic spindle assembly. J. Cell. Sci. 125, 3745–3751 (2012).

57. Scrofani, J., Sardon, T., Meunier, S. & Vernos, I. Microtubule nucleation in mitosis by a RanGTP-dependent protein complex. Curr. Biol. 25, 131–140 (2015).

58. Lin, T.-C. et al. MOZART1 and γ-tubulin complex receptors are both required to turn γ-TuSC into an active microtubule nucleation template. J. Cell Biol. 215, 823–840 (2016).

59. Masuda, H., Mori, R., Yukawa, M. & Toda, T. Fission yeast MOZART1/Mzt1 is an essential γ-tubulin complex component required for complex recruitment to the microtubule organizing center, but not its assembly. Mol. Biol. Cell 24, 2894–2906 (2013).

60. Wiese, C. & Zheng, Y. A new function for the gamma-tubulin ring complex as a microtubule minus-end cap. Nat. Cell Biol. 2, 358–364 (2000).

61. Anders, A. & Sawin, K. E. Microtubule stabilization in vivo by nucleation-incompetent γ-tubulin complex. J. Cell. Sci. 124, 1207–1213 (2011).

62. Bouissou, A. et al. γ-Tubulin ring complexes regulate microtubule plus end dynamics. The Journal of Cell Biology 187, 327–334 (2009).

63. Evans, L., Mitchison, T. & Kirschner, M. Influence of the centrosome on the structure of nucleated microtubules. J. Cell Biol. 100, 1185–1191 (1985).

64. Moudjou, M., Bordes, N., Paintrand, M. & Bornens, M. gamma-Tubulin in mammalian cells: the centrosomal and the cytosolic forms. Journal of Cell Science 109, 875–887 (1996).

65. Choi, Y.-K., Liu, P., Sze, S. K., Dai, C. & Qi, R. Z. CDK5RAP2 stimulates microtubule nucleation by the γ-tubulin ring complex. J Cell Biol 191, 1089–1095 (2010).

66. Alfaro-Aco, R., Thawani, A. & Petry, S. Structural analysis of the role of TPX2 in branching microtubule nucleation. J Cell Biol 216, 983–997 (2017).

67. Thawani, A., Kadzik, R. S. & Petry, S. XMAP215 is a microtubule nucleation factor that functions synergistically with the γ-tubulin ring complex. Nat. Cell Biol. 20, 575–585 (2018).

68. Chen, G.-Y. et al. Kinesin-5 Promotes Microtubule Nucleation and Assembly by Stabilizing a Lattice-Competent Conformation of Tubulin. Curr. Biol. 29, 2259-2269.e4 (2019).

69. Wieczorek, M., Bechstedt, S., Chaaban, S. & Brouhard, G. J. Microtubule-associated proteins control the kinetics of microtubule nucleation. Nat Cell Biol 17, 907–916 (2015).

70. O'Toole, E., Greenan, G., Lange, K. I., Srayko, M. & Müller-Reichert, T. The Role of γ-Tubulin in Centrosomal Microtubule Organization. PLOS ONE 7, e29795 (2012).

71. Strome, S. et al. Spindle dynamics and the role of gamma-tubulin in early Caenorhabditis elegans embryos. Mol. Biol. Cell 12, 1751–1764 (2001).

72. Sampaio, P., Rebollo, E., Varmark, H., Sunkel, C. E. & González, C. Organized microtubule arrays in gamma-tubulin-depleted Drosophila spermatocytes. Curr. Biol. 11, 1788–1793 (2001).

73. Nakaoka, Y., Kimura, A., Tani, T. & Goshima, G. Cytoplasmic Nucleation and Atypical Branching Nucleation Generate Endoplasmic Microtubules in Physcomitrella patens[OPEN]. Plant Cell 27, 228–242 (2015).

74. Rogers, G. C., Rusan, N. M., Peifer, M. & Rogers, S. L. A multicomponent assembly pathway contributes to the formation of acentrosomal microtubule arrays in interphase Drosophila cells. Mol. Biol. Cell 19, 3163–3178 (2008).

75. Scheer Ulrich. Historical roots of centrosome research: discovery of Boveri's microscope slides in Würzburg. Philosophical Transactions of the Royal Society B: Biological Sciences 369, 20130469 (2014).

76. Winey Mark & O'Toole Eileen. Centriole structure. Philosophical Transactions of the Royal Society B: Biological Sciences 369, 20130457 (2014).

77. Tsou, M.-F. B. & Stearns, T. Mechanism limiting centrosome duplication to once per cell cycle. Nature 442, 947–951 (2006).

78. Nigg, E. A. & Stearns, T. The centrosome cycle: Centriole biogenesis, duplication and inherent asymmetries. Nat Cell Biol 13, 1154–1160 (2011).

79. Wang, G., Jiang, Q. & Zhang, C. The role of mitotic kinases in coupling the centrosome cycle with the assembly of the mitotic spindle. J. Cell. Sci. 127, 4111–4122 (2014).

80. Kuriyama, R. & Borisy, G. G. Centriole cycle in Chinese hamster ovary cells as determined by whole-mount electron microscopy. J. Cell Biol. 91, 814–821 (1981).

81. Plotnikova, O. V., Pugacheva, E. N. & Golemis, E. A. Primary Cilia and the Cell Cycle. Methods Cell Biol 94, 137–160 (2009).

82. Satir, P., Pedersen, L. B. & Christensen, S. T. The primary cilium at a glance. J Cell Sci 123, 499–503 (2010).

83. Mirvis, M., Stearns, T. & Nelson, W. J. Cilium structure, assembly, and disassembly regulated by the cytoskeleton. Biochemical Journal 475, 2329–2353 (2018).

84. Mercey, O. et al. Dynamics of centriole amplification in centrosome-depleted brain multiciliated progenitors. bioRxiv 503730 (2018) doi:10.1101/503730.

85. Bettencourt-Dias, M., Hildebrandt, F., Pellman, D., Woods, G. & Godinho, S. Centrosomes and Cilia in Human Disease. Trends Genet 27, 307–315 (2011).

86. Nano, M. & Basto, R. The Janus soul of centrosomes: a paradoxical role in disease? Chromosome Res 24, 127–144 (2016).

87. Marthiens, V. et al. Centrosome amplification causes microcephaly. Nature Cell Biology 15, 731–740 (2013).

88. Wu, J. & Akhmanova, A. Microtubule-Organizing Centers. Annual Review of Cell and Developmental Biology 33, 51–75 (2017).

89. Wu, J. et al. Molecular Pathway of Microtubule Organization at the Golgi Apparatus. Dev. Cell 39, 44–60 (2016).

90. Meunier, S. & Vernos, I. Acentrosomal Microtubule Assembly in Mitosis: The Where, When, and How. Trends Cell Biol. 26, 80–87 (2016).

91. Sánchez-Huertas, C. & Lüders, J. The augmin connection in the geometry of microtubule networks. Curr. Biol. 25, R294-299 (2015).

92. Dumont, S. & Mitchison, T. J. Force and Length in the Mitotic Spindle. Curr Biol 19, R749–R761 (2009).

93. Prosser, S. L. & Pelletier, L. Mitotic spindle assembly in animal cells: a fine balancing act. Nat. Rev. Mol. Cell Biol. 18, 187–201 (2017).

94. Maiato, H., DeLuca, J., Salmon, E. D. & Earnshaw, W. C. The dynamic kinetochore-microtubule interface. Journal of Cell Science 117, 5461–5477 (2004).

95. Musacchio, A. The Molecular Biology of Spindle Assembly Checkpoint Signaling Dynamics. Current Biology 25, R1002–R1018 (2015).

96. Godek, K. M., Kabeche, L. & Compton, D. A. Regulation of kinetochore–microtubule attachments through homeostatic control during mitosis. Nat Rev Mol Cell Biol 16, 57–64 (2015).

97. Vallot, A. et al. Tension-Induced Error Correction and Not Kinetochore Attachment Status Activates the SAC in an Aurora-B/C-Dependent Manner in Oocytes. Curr. Biol. 28, 130-139.e3 (2018).

98. Khodjakov, A., Cole, R. W., Oakley, B. R. & Rieder, C. L. Centrosome-independent mitotic spindle formation in vertebrates. Current Biology 10, 59–67 (2000).

99. Watanabe, S., Shioi, G., Furuta, Y. & Goshima, G. Intra-spindle Microtubule Assembly Regulates Clustering of Microtubule-Organizing Centers during Early Mouse Development. Cell Rep 15, 54–60 (2016).

100. Bazzi, H. & Anderson, K. V. Acentriolar mitosis activates a p53-dependent apoptosis pathway in the mouse embryo. Proc Natl Acad Sci U S A 111, E1491–E1500 (2014).

101. Mahoney, N. M., Goshima, G., Douglass, A. D. & Vale, R. D. Making microtubules and mitotic spindles in cells without functional centrosomes. Curr. Biol. 16, 564–569 (2006).

102. Goshima, G. et al. Genes required for mitotic spindle assembly in Drosophila S2 cells. Science 316, 417–421 (2007).

103. Goshima, G., Mayer, M., Zhang, N., Stuurman, N. & Vale, R. D. Augmin: a protein complex required for centrosome-independent microtubule generation within the spindle. J. Cell Biol. 181, 421–429 (2008).

104. Lawo, S. et al. HAUS, the 8-subunit human Augmin complex, regulates centrosome and spindle integrity. Curr. Biol. 19, 816–826 (2009).

105. Uehara, R. et al. The augmin complex plays a critical role in spindle microtubule generation for mitotic progression and cytokinesis in human cells. Proc. Natl. Acad. Sci. U.S.A. 106, 6998–7003 (2009).

106. McKinley, K. L. & Cheeseman, I. M. Large-Scale Analysis of CRISPR/Cas9 Cell-Cycle Knockouts Reveals the Diversity of p53-Dependent Responses to Cell-Cycle Defects. Dev. Cell 40, 405-420.e2 (2017).

107. Meireles, A. M., Fisher, K. H., Colombié, N., Wakefield, J. G. & Ohkura, H. Wac: a new Augmin subunit required for chromosome alignment but not for acentrosomal microtubule assembly in female meiosis. J. Cell Biol. 184, 777–784 (2009).

108. Du, L. et al. Rumba and Haus3 are essential factors for the maintenance of hematopoietic stem/progenitor cells during zebrafish hematopoiesis. Development 138, 619–629 (2011).

109. Ho, C.-M. K. et al. Augmin plays a critical role in organizing the spindle and phragmoplast microtubule arrays in Arabidopsis. Plant Cell 23, 2606–2618 (2011).

110. Petry, S., Pugieux, C., Nédélec, F. J. & Vale, R. D. Augmin promotes meiotic spindle formation and bipolarity in Xenopus egg extracts. Proc. Natl. Acad. Sci. U.S.A. 108, 14473–14478 (2011).

111. Petry, S., Groen, A. C., Ishihara, K., Mitchison, T. J. & Vale, R. D. Branching microtubule nucleation in Xenopus egg extracts mediated by augmin and TPX2. Cell 152, 768–777 (2013).

112. Savoian, M. S. & Glover, D. M. Differing requirements for Augmin in male meiotic and mitotic spindle formation in Drosophila. Open Biol 4, 140047 (2014).

113. Edzuka, T., Yamada, L., Kanamaru, K., Sawada, H. & Goshima, G. Identification of the augmin complex in the filamentous fungus Aspergillus nidulans. PLoS ONE 9, e101471 (2014).

114. Wainman, A. et al. A new Augmin subunit, Msd1, demonstrates the importance of mitotic spindle-templated microtubule nucleation in the absence of functioning centrosomes. Genes Dev. 23, 1876–1881 (2009).

115. Thawani, A., Stone, H. A., Shaevitz, J. W. & Petry, S. Spatiotemporal organization of branched microtubule networks. Elife 8, (2019).

116. Goshima, G. Identification of a TPX2-like microtubule-associated protein in Drosophila. PLoS ONE 6, e28120 (2011).

117. Verma, V. & Maresca, T. J. Direct observation of branching MT nucleation in living animal cells. J. Cell Biol. (2019) doi:10.1083/jcb.201904114.

118. Hsia, K.-C. et al. Reconstitution of the augmin complex provides insights into its architecture and function. Nat Cell Biol 16, 852–863 (2014).

119. Song, J.-G. et al. Mechanism of how augmin directly targets the γ-tubulin ring complex to microtubules. J. Cell Biol. 217, 2417–2428 (2018).

120. Zhu, H., Coppinger, J. A., Jang, C.-Y., Yates, J. R. & Fang, G. FAM29A promotes microtubule amplification via recruitment of the NEDD1-gamma-tubulin complex to the mitotic spindle. J. Cell Biol. 183, 835–848 (2008).

121. Zhu, H., Fang, K. & Fang, G. FAM29A, a target of Plk1 regulation, controls the partitioning of NEDD1 between the mitotic spindle and the centrosomes. J. Cell. Sci. 122, 2750–2759 (2009).

122. Lecland, N. & Lüders, J. The dynamics of microtubule minus ends in the human mitotic spindle. Nat. Cell Biol. 16, 770–778 (2014).

123. David, A. F. et al. Augmin accumulation on long-lived microtubules drives amplification and kinetochore-directed growth. J. Cell Biol. 218, 2150–2168 (2019).

124. Megraw, T. L. & Kaufman, T. C. The centrosome in Drosophila oocyte development. Curr. Top. Dev. Biol. 49, 385–407 (2000).

125. Chen, V. S. et al. Histology Atlas of the Developing Prenatal and Postnatal Mouse Central Nervous System, with Emphasis on Prenatal Days E7.5 to E18.5. Toxicol Pathol 45, 705–744 (2017).

126. Götz, M. & Huttner, W. B. The cell biology of neurogenesis. Nat. Rev. Mol. Cell Biol. 6, 777–788 (2005).

127. Agirman, G., Broix, L. & Nguyen, L. Cerebral cortex development: an outside-in perspective. FEBS Lett. 591, 3978–3992 (2017).

128. Chenn, A., Zhang, Y. A., Chang, B. T. & McConnell, S. K. Intrinsic polarity of mammalian neuroepithelial cells. Mol. Cell. Neurosci. 11, 183–193 (1998).

129. Higginbotham, H. et al. Arl13b-regulated cilia activities are essential for polarized radial glial scaffold formation. Nat. Neurosci. 16, 1000–1007 (2013).

130. Lepanto, P., Badano, J. L. & Zolessi, F. R. Neuron's little helper: The role of primary cilia in neurogenesis. Neurogenesis (Austin) 3, e1253363 (2016).

131. Ohtsuka, T. & Kageyama, R. Regulation of temporal properties of neural stem cells and transition timing of neurogenesis and gliogenesis during mammalian neocortical development. Semin. Cell Dev. Biol. (2019).

132. Heng, J. I.-T., Chariot, A. & Nguyen, L. Molecular layers underlying cytoskeletal remodelling during cortical development. Trends Neurosci. 33, 38–47 (2010).

133. Noctor, S. C., Martínez-Cerdeño, V., Ivic, L. & Kriegstein, A. R. Cortical neurons arise in symmetric and asymmetric division zones and migrate through specific phases. Nat. Neurosci. 7, 136–144 (2004).

134. Barnes, A. P. & Polleux, F. Establishment of axon-dendrite polarity in developing neurons. Annu. Rev. Neurosci. 32, 347–381 (2009).

135. Umeshima, H., Hirano, T. & Kengaku, M. Microtubule-based nuclear movement occurs independently of centrosome positioning in migrating neurons. Proc. Natl. Acad. Sci. U.S.A. 104, 16182–16187 (2007).

136. Distel, M., Hocking, J. C., Volkmann, K. & Köster, R. W. The centrosome neither persistently leads migration nor determines the site of axonogenesis in migrating neurons in vivo. J. Cell Biol. 191, 875–890 (2010).

137. Bekkers, J. M. Pyramidal neurons. Curr. Biol. 21, R975 (2011).

138. Dotti, C. G., Sullivan, C. A. & Banker, G. A. The establishment of polarity by hippocampal neurons in culture. J. Neurosci. 8, 1454–1468 (1988).

139. Baas, P. W., Black, M. M. & Banker, G. A. Changes in microtubule polarity orientation during the development of hippocampal neurons in culture. J. Cell Biol. 109, 3085–3094 (1989).

140. Witte, H., Neukirchen, D. & Bradke, F. Microtubule stabilization specifies initial neuronal polarization. J. Cell Biol. 180, 619–632 (2008).

141. de Anda, F. C. et al. Centrosome localization determines neuronal polarity. Nature 436, 704–708 (2005).

142. Calderon de Anda, F., Gärtner, A., Tsai, L.-H. & Dotti, C. G. Pyramidal neuron polarity axis is defined at the bipolar stage. J. Cell. Sci. 121, 178–185 (2008).

143. Barnes, A. P., Solecki, D. & Polleux, F. New insights into the molecular mechanisms specifying neuronal polarity in vivo. Curr. Opin. Neurobiol. 18, 44–52 (2008).

144. Baas, P. W., Deitch, J. S., Black, M. M. & Banker, G. A. Polarity orientation of microtubules in hippocampal neurons: uniformity in the axon and nonuniformity in the dendrite. Proc Natl Acad Sci U S A 85, 8335–8339 (1988).

145. Conde, C. & Cáceres, A. Microtubule assembly, organization and dynamics in axons and dendrites. Nat. Rev. Neurosci. 10, 319–332 (2009).

146. Dehmelt, L. & Halpain, S. The MAP2/Tau family of microtubule-associated proteins. Genome Biol. 6, 204 (2005).

147. Méphon-Gaspard, A. et al. Role of tau in the spatial organization of axonal microtubules: keeping parallel microtubules evenly distributed despite macromolecular crowding. Cell Mol Life Sci 73, 3745–3760 (2016).

148. Qiang, L., Yu, W., Andreadis, A., Luo, M. & Baas, P. W. Tau protects microtubules in the axon from severing by katanin. J. Neurosci. 26, 3120–3129 (2006).

149. Baas, P. W. & Mozgova, O. I. A novel role for retrograde transport of microtubules in the axon. Cytoskeleton (Hoboken) 69, 416–425 (2012).

150. Rao, A. N. & Baas, P. W. Polarity Sorting of Microtubules in the Axon. Trends Neurosci. 41, 77–88 (2018).

151. Poulain, F. E. & Sobel, A. The microtubule network and neuronal morphogenesis: Dynamic and coordinated orchestration through multiple players. Mol. Cell. Neurosci. 43, 15–32 (2010).

152. Rochlin, M. W., Wickline, K. M. & Bridgman, P. C. Microtubule stability decreases axon elongation but not axoplasm production. J. Neurosci. 16, 3236–3246 (1996).

153. Williamson, T., Gordon-Weeks, P. R., Schachner, M. & Taylor, J. Microtubule reorganization is obligatory for growth cone turning. Proc. Natl. Acad. Sci. U.S.A. 93, 15221–15226 (1996).

154. Yu, W., Ahmad, F. J. & Baas, P. W. Microtubule fragmentation and partitioning in the axon during collateral branch formation. J. Neurosci. 14, 5872–5884 (1994).

155. Yu, W. et al. The microtubule-severing proteins spastin and katanin participate differently in the formation of axonal branches. Mol. Biol. Cell 19, 1485–1498 (2008).

156. Dent, E. W. & Kalil, K. Axon branching requires interactions between dynamic microtubules and actin filaments. J. Neurosci. 21, 9757–9769 (2001).

157. Homma, N. et al. Kinesin superfamily protein 2A (KIF2A) functions in suppression of collateral branch extension. Cell 114, 229–239 (2003).

158. Stepanova, T. et al. Visualization of microtubule growth in cultured neurons via the use of EB3-GFP (end-binding protein 3-green fluorescent protein). J. Neurosci. 23, 2655–2664 (2003).

159. Yau, K. W. et al. Dendrites In Vitro and In Vivo Contain Microtubules of Opposite Polarity and Axon Formation Correlates with Uniform Plus-End-Out Microtubule Orientation. J Neurosci 36, 1071–1085 (2016).

160. Lin, S., Liu, M., Mozgova, O. I., Yu, W. & Baas, P. W. Mitotic motors coregulate microtubule patterns in axons and dendrites. J. Neurosci. 32, 14033–14049 (2012).

161. Tas, R. P. et al. Differentiation between Oppositely Oriented Microtubules Controls Polarized Neuronal Transport. Neuron 96, 1264-1271.e5 (2017).

162. Jinushi-Nakao, S. et al. Knot/Collier and cut control different aspects of dendrite cytoskeleton and synergize to define final arbor shape. Neuron 56, 963–978 (2007).

163. Mao, C.-X. et al. Microtubule-severing protein Katanin regulates neuromuscular junction development and dendritic elaboration in Drosophila. Development 141, 1064–1074 (2014).

164. Hu, X., Viesselmann, C., Nam, S., Merriam, E. & Dent, E. W. Activity-dependent dynamic microtubule invasion of dendritic spines. J. Neurosci. 28, 13094–13105 (2008).

165. Jaworski, J. et al. Dynamic microtubules regulate dendritic spine morphology and synaptic plasticity. Neuron 61, 85–100 (2009).

166. Gu, J., Firestein, B. L. & Zheng, J. Q. Microtubules in dendritic spine development. J. Neurosci. 28, 12120–12124 (2008).

167. Hoogenraad, C. C. & Bradke, F. Control of neuronal polarity and plasticity-a renaissance for microtubules? Trends Cell Biol. 19, 669–676 (2009).

168. Yu, W., Centonze, V. E., Ahmad, F. J. & Baas, P. W. Microtubule nucleation and release from the neuronal centrosome. J. Cell Biol. 122, 349–359 (1993).

169. Yu, W., Schwei, M. J. & Baas, P. W. Microtubule transport and assembly during axon growth. J. Cell Biol. 133, 151–157 (1996).

170. Ahmad, F. J., Yu, W., McNally, F. J. & Baas, P. W. An essential role for katanin in severing microtubules in the neuron. J. Cell Biol. 145, 305–315 (1999).

171. Karabay, A., Yu, W., Solowska, J. M., Baird, D. H. & Baas, P. W. Axonal growth is sensitive to the levels of katanin, a protein that severs microtubules. J. Neurosci. 24, 5778–5788 (2004).

172. Zheng, Y. et al. Dynein is required for polarized dendritic transport and uniform microtubule orientation in axons. Nat. Cell Biol. 10, 1172–1180 (2008).

173. Stiess, M. et al. Axon extension occurs independently of centrosomal microtubule nucleation. Science 327, 704–707 (2010).

174. Nguyen, M. M., Stone, M. C. & Rolls, M. M. Microtubules are organized independently of the centrosome in Drosophila neurons. Neural Dev 6, 38 (2011).

175. Sánchez-Huertas, C. et al. Non-centrosomal nucleation mediated by augmin organizes microtubules in post-mitotic neurons and controls axonal microtubule polarity. Nat Commun 7, 12187 (2016).

176. Yonezawa, S., Shigematsu, M., Hirata, K. & Hayashi, K. Loss of γ-tubulin, GCP-WD/NEDD1 and CDK5RAP2 from the Centrosome of Neurons in Developing Mouse Cerebral and Cerebellar Cortex. Acta Histochem Cytochem 48, 145–152 (2015).

177. Basto, R. et al. Flies without centrioles. Cell 125, 1375–1386 (2006).

178. Yau, K. W. et al. Microtubule Minus-End Binding Protein CAMSAP2 Controls Axon Specification and Dendrite Development. Neuron 82, 1058–1073 (2014).

179. Ori-McKenney, K. M., Jan, L. Y. & Jan, Y.-N. Golgi outposts shape dendrite morphology by functioning as sites of acentrosomal microtubule nucleation in neurons. Neuron 76, 921–930 (2012).

180. Nguyen, M. M. et al. Γ-tubulin controls neuronal microtubule polarity independently of Golgi outposts. Mol. Biol. Cell 25, 2039–2050 (2014).

181. Pirozzi, F., Nelson, B. & Mirzaa, G. From microcephaly to megalencephaly: determinants of brain size. Dialogues Clin Neurosci 20, 267–282 (2018).

182. Parrini, E., Conti, V., Dobyns, W. B. & Guerrini, R. Genetic Basis of Brain Malformations. Mol Syndromol 7, 220–233 (2016).

183. Bahi-Buisson, N. & Cavallin, M. Tubulinopathies Overview. in GeneReviews® (eds. Adam, M. P. et al.) (University of Washington, Seattle, 1993).

184. Brock, S. et al. Tubulinopathies continued: refining the phenotypic spectrum associated with variants in TUBG1. Eur. J. Hum. Genet. 26, 1132–1142 (2018).

185. Breuss, M. & Keays, D. A. Microtubules and neurodevelopmental disease: the movers and the makers. Adv. Exp. Med. Biol. 800, 75–96 (2014).

186. Breuss, M. et al. Mutations in the β-tubulin gene TUBB5 cause microcephaly with structural brain abnormalities. Cell Rep 2, 1554–1562 (2012).

187. Poirier, K. et al. Mutations in TUBG1, DYNC1H1, KIF5C and KIF2A cause malformations of cortical development and microcephaly. Nat. Genet. 45, 639–647 (2013).

188. Ivanova, E. L. et al. TUBG1 missense variants underlying cortical malformations disrupt neuronal locomotion and microtubule dynamics but not neurogenesis. Nat Commun 10, 2129 (2019).

189. Yuen, Y. T. K., Guella, I., Roland, E., Sargent, M. & Boelman, C. Case reports: novel TUBG1 mutations with milder neurodevelopmental presentations. BMC Med. Genet. 20, 95 (2019).

190. Mitani, T. et al. Bi-allelic Pathogenic Variants in TUBGCP2 Cause Microcephaly and Lissencephaly Spectrum Disorders. Am. J. Hum. Genet. 105, 1005–1015 (2019).

191. Scheidecker, S. et al. Mutations in TUBGCP4 alter microtubule organization via the γ-tubulin ring complex in autosomal-recessive microcephaly with chorioretinopathy. Am. J. Hum. Genet. 96, 666–674 (2015).

192. Martin, C.-A. et al. Mutations in PLK4, encoding a master regulator of centriole biogenesis, cause microcephaly, growth failure and retinopathy. Nat. Genet. 46, 1283–1292 (2014).

193. Maver, A., Čuturilo, G., Kovanda, A., Miletić, A. & Peterlin, B. Rare missense TUBGCP5 gene variant in a patient with primary microcephaly. Eur J Med Genet (2018) doi:10.1016/j.ejmg.2018.12.003.

194. Chen, C.-P. et al. Prenatal diagnosis of a familial 15q11.2 (BP1-BP2) microdeletion encompassing TUBGCP5, CYFIP1, NIPA2 and NIPA1 in a fetus with ventriculomegaly, microcephaly and intrauterine growth restriction on prenatal ultrasound. Taiwan J Obstet Gynecol 57, 730–733 (2018).

195. Puffenberger, E. G. et al. Genetic mapping and exome sequencing identify variants associated with five novel diseases. PLoS ONE 7, e28936 (2012).

196. Buchman, J. J. et al. Cdk5rap2 interacts with pericentrin to maintain the neural progenitor pool in the developing neocortex. Neuron 66, 386–402 (2010).

197. Lizarraga, S. B. et al. Cdk5rap2 regulates centrosome function and chromosome segregation in neuronal progenitors. Development 137, 1907–1917 (2010).

198. Lancaster, M. A. et al. Cerebral organoids model human brain development and microcephaly. Nature 501, 373–379 (2013).

199. Nano, M. & Basto, R. Consequences of Centrosome Dysfunction During Brain Development. Adv. Exp. Med. Biol. 1002, 19–45 (2017).

200. Insolera, R., Bazzi, H., Shao, W., Anderson, K. V. & Shi, S.-H. Cortical neurogenesis in the absence of centrioles. Nat. Neurosci. 17, 1528–1535 (2014).

201. Zempel, H. & Mandelkow, E.-M. Linking amyloid-β and tau: amyloid-β induced synaptic dysfunction via local wreckage of the neuronal cytoskeleton. Neurodegener Dis 10, 64–72 (2012).

202. Dubey, J., Ratnakaran, N. & Koushika, S. P. Neurodegeneration and microtubule dynamics: death by a thousand cuts. Front Cell Neurosci 9, 343 (2015).

203. Watanabe, S., Shioi, G., Furuta, Y. & Goshima, G. Intra-spindle Microtubule Assembly Regulates Clustering of Microtubule-Organizing Centers during Early Mouse Development. Cell Rep 15, 54–60 (2016).

204. Lentiviral RNAi Protocols. https://www.sciencegateway.org/protocols/lentivirus/cloning.htm.

205. Sabine Klischies. The role of the gTuRC subunit GCP8 in microtubule regulation and cytoskeleton organization. (Tesi doctoral UPF/2015, 2015).

206. Rubinson, D. A. et al. A lentivirus-based system to functionally silence genes in primary mammalian cells, stem cells and transgenic mice by RNA interference. Nat. Genet. 33, 401–406 (2003).

207. Teixidó-Travesa, N. et al. The gammaTuRC revisited: a comparative analysis of interphase and mitotic human gammaTuRC redefines the set of core components and identifies the novel subunit GCP8. Mol. Biol. Cell 21, 3963–3972 (2010).

208. Cota, R. R. et al. MZT1 regulates microtubule nucleation by linking γTuRC assembly to adapter-mediated targeting and activation. J. Cell. Sci. 130, 406–419 (2017).

209. Ferreira, T. A. et al. Neuronal morphometry directly from bitmap images. Nat. Methods 11, 982–984 (2014).

210. Box, G. E. P. & Cox, D. R. An Analysis of Transformations. Journal of the Royal Statistical Society: Series B (Methodological) 26, 211–243 (1964).

211. Gelman, A. & Hill, J. Data Analysis Using Regression and Multilevel/Hierarchical Models by Andrew Gelman. Cambridge Core (2006) doi:10.1017/CBO9780511790942.

212. Hothorn, T., Bretz, F. & Westfall, P. Simultaneous inference in general parametric models. Biom J 50, 346–363 (2008).

213. Wang, Z. et al. Conserved Motif of CDK5RAP2 Mediates Its Localization to Centrosomes and the Golgi Complex. J Biol Chem 285, 22658–22665 (2010).

214. Dubois, N. C., Hofmann, D., Kaloulis, K., Bishop, J. M. & Trumpp, A. Nestin-Cre transgenic mouse line Nes-Cre1 mediates highly efficient Cre/loxP mediated recombination in the nervous system, kidney, and somite-derived tissues. Genesis 44, 355–360 (2006).

215. Mignone, J. L., Kukekov, V., Chiang, A.-S., Steindler, D. & Enikolopov, G. Neural stem and progenitor cells in nestin-GFP transgenic mice. Journal of Comparative Neurology 469, 311–324 (2004).

216. Isaka, F. et al. Ectopic expression of the bHLH gene Math1 disturbs neural development. European Journal of Neuroscience 11, 2582–2588 (1999).

217. Zhan, X. et al. Generation of BAF53b-Cre transgenic mice with pan-neuronal Cre activities. Genesis 53, 440–448 (2015).

218. Tg(Camk2a-cre)T29-1Stl - Nervous System Recombinase Activity Detail MGI Mouse. http://www.informatics.jax.org/recombinase/specificity?id=MGI:2177650&system=nervous+system#refSection.

219. Zhang, J. et al. Germ-Line Recombination Activity of the Widely Used hGFAP-Cre and Nestin-Cre Transgenes. PLOS ONE 8, e82818 (2013).

220. Fong, C. S. et al. 53BP1 and USP28 mediate p53-dependent cell cycle arrest in response to centrosome loss and prolonged mitosis. Elife 5, (2016).

221. Meitinger, F. et al. 53BP1 and USP28 mediate p53 activation and G1 arrest after centrosome loss or extended mitotic duration. J. Cell Biol. 214, 155–166 (2016).

222. Pilaz, L.-J. et al. Prolonged mitosis of neural progenitors alters cell fate in the developing brain. Neuron 89, 83–99 (2016).

223. Hankenson, F. C. Critical Care Management for Laboratory Mice and Rats - F. Claire Hankenson - Google Livros. (CRC Press - Taylor & Francis Group, 2014).

224. Steiner, D. J., Kim, A., Miller, K. & Hara, M. Pancreatic islet plasticity: Interspecies comparison of islet architecture and composition. Islets 2, 135–145 (2010).

225. Dráberová, E. et al. Differential expression of human γ-tubulin isotypes during neuronal development and oxidative stress points to a γ-tubulin-2 prosurvival function. FASEB J. 31, 1828–1846 (2017).

226. Yamada, M. & Hayashi, K. Microtubule nucleation in the cytoplasm of developing cortical neurons and its regulation by brain-derived neurotrophic factor. Cytoskeleton (Hoboken) 76, 339–345 (2019).

227. Dirk, B. S. et al. PACS-1 and adaptor protein-1 mediate ACTH trafficking to the regulated secretory pathway. Biochem. Biophys. Res. Commun. 507, 519–525 (2018).

228. Jenkins, P. M., Zhang, L., Thomas, G. & Martens, J. R. PACS-1 mediates phosphorylation-dependent ciliary trafficking of the cyclic-nucleotide-gated channel in olfactory sensory neurons. J. Neurosci. 29, 10541–10551 (2009).

229. Schuurs-Hoeijmakers, J. H. M. et al. Recurrent de novo mutations in PACS1 cause defective cranial-neural-crest migration and define a recognizable intellectual-disability syndrome. Am. J. Hum. Genet. 91, 1122–1127 (2012).

230. Stern, D. et al. Association of the missense variant p.Arg203Trp in PACS1 as a cause of intellectual disability and seizures. Clin. Genet. 92, 221–223 (2017).

231. Romaniello, R. et al. Tubulin genes and malformations of cortical development. Eur J Med Genet 61, 744–754 (2018).

232. Guarguaglini, G. et al. The forkhead-associated domain protein Cep170 interacts with Polo-like kinase 1 and serves as a marker for mature centrioles. Mol. Biol. Cell 16, 1095–1107 (2005).

233. Welburn, J. P. I. & Cheeseman, I. M. The microtubule-binding protein Cep170 promotes the targeting of the kinesin-13 depolymerase Kif2b to the mitotic spindle. Mol. Biol. Cell 23, 4786–4795 (2012).

234. Kanca, O. et al. De Novo Variants in WDR37 Are Associated with Epilepsy, Colobomas, Dysmorphism, Developmental Delay, Intellectual Disability, and Cerebellar Hypoplasia. Am. J. Hum. Genet. 105, 413–424 (2019).

235. Groeneweg, F. L., Trattnig, C., Kuhse, J., Nawrotzki, R. A. & Kirsch, J. Gephyrin: a key regulatory protein of inhibitory synapses and beyond. Histochem. Cell Biol. 150, 489–508 (2018).

236. Chen, T. et al. Homer1 knockdown protects dopamine neurons through regulating calcium homeostasis in an in vitro model of Parkinson's disease. Cell. Signal. 25, 2863–2870 (2013).

237. Beetz, C. et al. Inhibition of TFG function causes hereditary axon degeneration by impairing endoplasmic reticulum structure. Proc. Natl. Acad. Sci. U.S.A. 110, 5091–5096 (2013).

238. Watson, P., Townley, A. K., Koka, P., Palmer, K. J. & Stephens, D. J. Sec16 defines endoplasmic reticulum exit sites and is required for secretory cargo export in mammalian cells. Traffic 7, 1678–1687 (2006).

239. Guella, I. et al. De Novo Mutations in YWHAG Cause Early-Onset Epilepsy. Am. J. Hum. Genet. 101, 300–310 (2017).

240. Yu, S. et al. PACS2 is required for ox-LDL-induced endothelial cell apoptosis by regulating mitochondria-associated ER membrane formation and mitochondrial Ca2+ elevation. Exp. Cell Res. 379, 191–202 (2019).

241. Hinze, S. J. et al. Incorrect dosage of IQSEC2, a known intellectual disability and epilepsy gene, disrupts dendritic spine morphogenesis. Transl Psychiatry 7, e1110 (2017).

242. Shoubridge, C. et al. Mutations in the guanine nucleotide exchange factor gene IQSEC2 cause nonsyndromic intellectual disability. Nat. Genet. 42, 486–488 (2010).

243. Cornell, B., Wachi, T., Zhukarev, V. & Toyo-Oka, K. Regulation of neuronal morphogenesis by 14-3-3epsilon (Ywhae) via the microtubule binding protein, doublecortin. Hum. Mol. Genet. 25, 4405–4418 (2016).

244. Corda, D., Colanzi, A. & Luini, A. The multiple activities of CtBP/BARS proteins: the Golgi view. Trends Cell Biol. 16, 167–173 (2006).

245. Hu, K., Li, Y., Yu, H. & Hu, Y. CTBP1 Confers Protection for Hippocampal and Cortical Neurons in Rat Models of Alzheimer's Disease. Neuroimmunomodulation 1–14 (2019) .

246. Grover, D. et al. Family-based association of YWHAH in psychotic bipolar disorder. Am. J. Med. Genet. B Neuropsychiatr. Genet. 150B, 977–983 (2009).

247. Zhao, Y. et al. OTUD4 Is a Phospho-Activated K63 Deubiquitinase that Regulates MyD88-Dependent Signaling. Mol. Cell 69, 505-516.e5 (2018).

248. Lehrer, S., Rheinstein, P. H. & Rosenzweig, K. E. Loss of MycBP may be associated with the improved survival in 1P co-deletion of lower grade glioma patients. Clin Neurol Neurosurg 172, 112–115 (2018).

249. Walczak, C. E., Gayek, S. & Ohi, R. Microtubule-depolymerizing kinesins. Annu. Rev. Cell Dev. Biol. 29, 417–441 (2013).

250. Ganem, N. J. & Compton, D. A. The KinI kinesin Kif2a is required for bipolar spindle assembly through a functional relationship with MCAK. J. Cell Biol. 166, 473–478 (2004).

251. Homma, N. et al. Kinesin superfamily protein 2A (KIF2A) functions in suppression of collateral branch extension. Cell 114, 229–239 (2003).

252. Maor-Nof, M. et al. Axonal pruning is actively regulated by the microtubule-destabilizing protein kinesin superfamily protein 2A. Cell Rep 3, 971–977 (2013).

253. Homma, N. et al. KIF2A regulates the development of dentate granule cells and postnatal hippocampal wiring. Elife 7, (2018).

254. Hamada, T., Kurachi, S. & Kurachi, K. Heterogeneous nuclear ribonucleoprotein A3 is the liver nuclear protein binding to age related increase element RNA of the factor IX gene. PLoS ONE 5, e12971 (2010).

255. Roy, G. et al. Paip1 interacts with poly(A) binding protein through two independent binding motifs. Mol. Cell. Biol. 22, 3769–3782 (2002).

256. Di Paolo, G. et al. Decreased synaptic vesicle recycling efficiency and cognitive deficits in amphiphysin 1 knockout mice. Neuron 33, 789–804 (2002).

257. Abe, K., Chisaka, O., Van Roy, F. & Takeichi, M. Stability of dendritic spines and synaptic contacts is controlled by alpha N-catenin. Nat. Neurosci. 7, 357–363 (2004).

258. Quattrone, A. et al. Posttranscriptional regulation of gene expression in learning by the neuronal ELAV-like mRNA-stabilizing proteins. Proc Natl Acad Sci U S A 98, 11668–11673 (2001).

259. Ince-Dunn, G. et al. Neuronal Elav-like (Hu) proteins regulate RNA splicing and abundance to control glutamate levels and neuronal excitability. Neuron 75, 1067–1080 (2012).

260. Liu, Z.-Z. et al. CRMP2 and CRMP4 Are Differentially Required for Axon Guidance and Growth in Zebrafish Retinal Neurons. Neural Plast. 2018, 8791304 (2018).

261. Blasco, H. et al. A rare motor neuron deleterious missense mutation in the DPYSL3 (CRMP4) gene is associated with ALS. Hum. Mutat. 34, 953–960 (2013).

262. Ong Tone, S., Dayanandan, B., Fournier, A. E. & Mandato, C. A. GSK3 regulates mitotic chromosomal alignment through CRMP4. PLoS ONE 5, e14345 (2010).

263. Kim, H. et al. Identification of transketolase as a target of PARIS in substantia nigra. Biochem. Biophys. Res. Commun. 493, 1050–1056 (2017).

264. Dörr, A. et al. MYCBP2 Is a Guanosine Exchange Factor for Ran Protein and Determines Its Localization in Neurons of Dorsal Root Ganglia. J. Biol. Chem. 290, 25620–25635 (2015).

265. Smith, K. R. et al. Cadherin-10 Maintains Excitatory/Inhibitory Ratio through Interactions with Synaptic Proteins. J Neurosci 37, 11127–11139 (2017).

266. Elagabani, M. N. et al. Subunit-selective N-Methyl-d-aspartate (NMDA) Receptor Signaling through Brefeldin A-resistant Arf Guanine Nucleotide Exchange Factors BRAG1 and BRAG2 during Synapse Maturation. J. Biol. Chem. 291, 9105–9118 (2016).

267. Andrew, R. J. et al. Reduction of the expression of the late-onset Alzheimer's disease (AD) risk-factor BIN1 does not affect amyloid pathology in an AD mouse model. J. Biol. Chem. 294, 4477–4487 (2019).

268. D'Alessandro, M. et al. Amphiphysin 2 Orchestrates Nucleus Positioning and Shape by Linking the Nuclear Envelope to the Actin and Microtubule Cytoskeleton. Dev. Cell 35, 186–198 (2015).

269. Liu, Y. et al. Protein Phosphatase 2A (PP2A) Regulates EG5 to Control Mitotic Progression. Sci Rep 7, 1630 (2017).

270. Magnoni, R. et al. Late onset motoneuron disorder caused by mitochondrial Hsp60 chaperone deficiency in mice. Neurobiol. Dis. 54, 12–23 (2013).

271. Fanning, A. S. & Anderson, J. M. Zonula occludens-1 and -2 are cytosolic scaffolds that regulate the assembly of cellular junctions. Ann. N. Y. Acad. Sci. 1165, 113–120 (2009).

272. Malik, A. M. et al. Matrin 3-dependent neurotoxicity is modified by nucleic acid binding and nucleocytoplasmic localization. Elife 7, (2018).

273. Belzil, C., Ramos, T., Sanada, K., Colicos, M. A. & Nguyen, M. D. p600 stabilizes microtubules to prevent the aggregation of CaMKIIα during photoconductive stimulation. Cell. Mol. Biol. Lett. 19, 381–392 (2014).

274. Faller, E. M., Villeneuve, T. S. & Brown, D. L. MAP1a associated light chain 3 increases microtubule stability by suppressing microtubule dynamics. Mol. Cell. Neurosci. 41, 85–93 (2009).

275. Przedborski, S. Peroxiredoxin-2 links Cdk5 to neurodegeneration. Nature Medicine 13, 907–909 (2007).

276. Manojlovic, Z. & Stefanovic, B. A novel role of RNA helicase A in regulation of translation of type I collagen mRNAs. RNA 18, 321–334 (2012).

277. Korshunova, I. et al. Characterization of BASP1-mediated neurite outgrowth. J. Neurosci. Res. 86, 2201–2213 (2008).

278. Copic, A., Latham, C. F., Horlbeck, M. A., D'Arcangelo, J. G. & Miller, E. A. ER cargo properties specify a requirement for COPII coat rigidity mediated by Sec13p. Science 335, 1359–1362 (2012).

279. Damrath, E. et al. ATXN2-CAG42 Sequesters PABPC1 into Insolubility and Induces FBXW8 in Cerebellum of Old Ataxic Knock-In Mice. PLoS Genet 8, (2012).

280. Palmieri, F. The mitochondrial transporter family SLC25: identification, properties and physiopathology. Mol. Aspects Med. 34, 465–484 (2013).

281. Sokka, A.-L. et al. Bruce/apollon promotes hippocampal neuron survival and is downregulated by kainic acid. Biochem. Biophys. Res. Commun. 338, 729–735 (2005).

282. Beck, J. & Peter, M. Regulating PLK1 dynamics by Cullin3/KLHL22-mediated ubiquitylation. Cell Cycle 12, 2528–2529 (2013).

283. Chen, J. et al. KLHL22 activates amino-acid-dependent mTORC1 signalling to promote tumorigenesis and ageing. Nature 557, 585–589 (2018).

284. Wang, B. et al. PKM2 is involved in neuropathic pain by regulating ERK and STAT3 activation in rat spinal cord. J Headache Pain 19, 7 (2018).

285. Wu, Q., Ge, W., Chen, Y., Kong, X. & Xian, H. PKM2 Involved in Neuronal Apoptosis on Hypoxic-ischemic Encephalopathy in Neonatal Rats. Neurochem. Res. 44, 1602–1612 (2019).

286. Gene Ontology Resource. Gene Ontology Resource http://geneontology.org/.

287. Chatterjee, C. et al. Distinct Interaction Modes of the Kinesin-13 Motor Domain with the Microtubule. Biophys J 110, 1593–1604 (2016).

288. Broix, L. et al. Ciliogenesis and cell cycle alterations contribute to KIF2A-related malformations of cortical development. Hum. Mol. Genet. 27, 224–238 (2018).

289. Zhang, W. et al. Modeling microcephaly with cerebral organoids reveals a WDR62-CEP170-KIF2A pathway promoting cilium disassembly in neural progenitors. Nat Commun 10, 2612 (2019).

290. Dumoux, M., Menny, A., Delacour, D. & Hayward, R. D. A Chlamydia effector recruits CEP170 to reprogram host microtubule organization. J. Cell. Sci. 128, 3420–3434 (2015).

291. Cunha-Ferreira, I. et al. The HAUS Complex Is a Key Regulator of Non-centrosomal Microtubule Organization during Neuronal Development. Cell Rep 24, 791–800 (2018).

292. Sanchez, A. D. & Feldman, J. L. Microtubule-organizing centers: from the centrosome to non-centrosomal sites. Curr Opin Cell Biol 44, 93–101 (2017).

293. Issa, L. et al. CDK5RAP2 expression during murine and human brain development correlates with pathology in primary autosomal recessive microcephaly. Cereb. Cortex 23, 2245–2260 (2013).

294. Zhu, H., Coppinger, J. A., Jang, C.-Y., Yates, J. R. & Fang, G. FAM29A promotes microtubule amplification via recruitment of the NEDD1-gamma-tubulin complex to the mitotic spindle. J. Cell Biol. 183, 835–848 (2008).

295. Walia, A. et al. GCP-WD mediates γ-TuRC recruitment and the geometry of microtubule nucleation in interphase arrays of Arabidopsis. Curr. Biol. 24, 2548–2555 (2014).

296. Fishel, E. A. & Dixit, R. Role of nucleation in cortical microtubule array organization: variations on a theme. Plant J. 75, 270–277 (2013).

297. Lin, S., Liu, M., Mozgova, O. I., Yu, W. & Baas, P. W. Mitotic motors coregulate microtubule patterns in axons and dendrites. J. Neurosci. 32, 14033–14049 (2012).

298. Yamada, M. & Hayashi, K. Microtubule nucleation in the cytoplasm of developing cortical neurons and its regulation by brain-derived neurotrophic factor. Cytoskeleton (Hoboken) 76, 339–345 (2019).

299. Chen, W.-S. et al. Ran-dependent TPX2 activation promotes acentrosomal microtubule nucleation in neurons. Sci Rep 7, 42297 (2017).

300. Tsai, C. Y. et al. Aurora-A phosphorylates Augmin complex component Hice1 protein at an N-terminal serine/threonine cluster to modulate its microtubule binding activity during spindle assembly. J. Biol. Chem. 286, 30097–30106 (2011).

301. Bernal, A. & Arranz, L. Nestin-expressing progenitor cells: function, identity and therapeutic implications. Cell Mol Life Sci 75, 2177–2195 (2018).

302. Graus-Porta, D. et al. Beta1-class integrins regulate the development of laminae and folia in the cerebral and cerebellar cortex. Neuron 31, 367–379 (2001).

303. Daviaud, N., Chen, K., Huang, Y., Friedel, R. H. & Zou, H. Impaired cortical neurogenesis in plexin-B1 and -B2 double deletion mutant. Developmental Neurobiology 76, 882–899 (2016).

304. Shimada, I. S. et al. Derepression of sonic hedgehog signaling upon Gpr161 deletion unravels forebrain and ventricular abnormalities. Developmental Biology 450, 47–62 (2019).

305. Liang, H., Hippenmeyer, S. & Ghashghaei, H. T. A Nestin-cre transgenic mouse is insufficient for recombination in early embryonic neural progenitors. Biol Open 1, 1200–1203 (2012).

306. Rujano, M. A., Basto, R. & Marthiens, V. New insights into centrosome imaging in Drosophila and mouse neuroepithelial tissues. Methods Cell Biol. 129, 211–227 (2015).

307. Juriloff, D. M. & Harris, M. J. Mouse models for neural tube closure defects. Hum Mol Genet 9, 993–1000 (2000).

308. Jiang, Y. et al. Essential Role for Survivin in Early Brain Development. J. Neurosci. 25, 6962–6970 (2005).

309. Marjanović, M. et al. CEP63 deficiency promotes p53-dependent microcephaly and reveals a role for the centrosome in meiotic recombination. Nat Commun 6, 7676 (2015).

310. Uzquiano, A. et al. Mutations in the Heterotopia Gene Eml1/EML1 Severely Disrupt the Formation of Primary Cilia. Cell Rep 28, 1596-1611.e10 (2019).

311. Bizzotto, S. et al. Eml1 loss impairs apical progenitor spindle length and soma shape in the developing cerebral cortex. Sci Rep 7, 17308 (2017).

312. Benchimol, S. p53-dependent pathways of apoptosis. Cell Death & Differentiation 8, 1049-1051 (2001).

313. Jacobs, W. B., Kaplan, D. R. & Miller, F. D. The p53 family in nervous system development and disease. Journal of Neurochemistry 97, 1571–1584 (2006).

314. Eberhard, D. Neuron and beta-cell evolution: Learning about neurons is learning about beta-cells. BioEssays 35, 584–584 (2013).

315. Arntfield, M. E. & Kooy, D. van der. β-Cell evolution: How the pancreas borrowed from the brain. BioEssays 33, 582–587 (2011).

316. Martens, G. A. et al. Clusters of conserved beta cell marker genes for assessment of beta cell phenotype. PLoS ONE 6, e24134 (2011).

317. Information, N. C. for B., Pike, U. S. N. L. of M. 8600 R., MD, B. & Usa, 20894. Type 1 diabetes: Overview. (Institute for Quality and Efficiency in Health Care (IQWiG), 2017).

318. Brands, A. M. A., Kessels, R. P. C., de Haan, E. H. F., Kappelle, L. J. & Biessels, G. J. Cerebral dysfunction in type 1 diabetes: effects of insulin, vascular risk factors and blood-glucose levels. European Journal of Pharmacology 490, 159–168 (2004).

319. Šerbedžija, P. & Ishii, D. N. Insulin and insulin-like growth factor prevent brain atrophy and cognitive impairment in diabetic rats. Indian J Endocrinol Metab 16, S601–S610 (2012).

320. Ferguson, S. C. et al. Cognitive Ability and Brain Structure in Type 1 Diabetes: Relation to Microangiopathy and Preceding Severe Hypoglycemia. Diabetes 52, 149–156 (2003).

321. Wrighten, S. A., Piroli, G. G., Grillo, C. A. & Reagan, L. P. A look inside the diabetic brain: Contributors to diabetes-induced brain aging. Biochimica et Biophysica Acta (BBA) - Molecular Basis of Disease 1792, 444–453 (2009).

322. Nair, G. & Hebrok, M. Islet formation in mice and men: Lessons for the generation of functional insulin-producing β cells from human pluripotent stem cells. Curr Opin Genet Dev 32, 171–180 (2015).

323. Bastidas-Ponce, A., Scheibner, K., Lickert, H. & Bakhti, M. Cellular and molecular mechanisms coordinating pancreas development. Development 144, 2873–2888 (2017).

324. Hald, J. et al. Pancreatic islet and progenitor cell surface markers with cell sorting potential. Diabetologia 55, 154–165 (2012).

325. Lin, C.-L. V. & Vuguin, P. M. Determinants of Pancreatic Islet Development in Mice and Men: A Focus on the Role of Transcription Factors. HRP 77, 205–213 (2012).

326. O'Dowd, J. F. & Stocker, C. J. Endocrine pancreatic development: impact of obesity and diet. Front. Physiol. 4, (2013).

327. Miller, K. et al. Islet Formation during the Neonatal Development in Mice. PLOS ONE 4, e7739 (2009).

328. Diaferia, G. R. et al. β1 integrin is a crucial regulator of pancreatic β-cell expansion. Development 140, 3360–3372 (2013).

329. Qiu, W.-L. et al. Deciphering Pancreatic Islet β Cell and α Cell Maturation Pathways and Characteristic Features at the Single-Cell Level. Cell Metab. 25, 1194-1205.e4 (2017).

330. Georgia, S. & Bhushan, A. β cell replication is the primary mechanism for maintaining postnatal β cell mass. J Clin Invest 114, 963–968 (2004).

331. Lim, A. K. Diabetic nephropathy – complications and treatment. Int J Nephrol Renovasc Dis 7, 361–381 (2014).

332. Mendelsohn, C. Functional obstruction: the renal pelvis rules. J Clin Invest 113, 957–959 (2004).

333. Mulţescu, R., Georgescu, D., Geavlete, P. A. & Geavlete, B. Chapter 2 - Notions of Histology, Anatomy, and Physiology of the Upper Urinary Tract. in Retrograde Ureteroscopy (ed. Geavlete, P. A.) 7–19 (Academic Press, 2016). doi:10.1016/B978-0-12-802403-4.00002-4.

334. Zambon, J. P., Koslov, D. S., Mihai, B. & Badlani, G. H. Bladder and Ureteral Dysfunction Leading to Hydronephrosis and Hydroureteronephrosis in Adults. Urology 117, 1–8 (2018).

335. Vinik, A. I., Maser, R. E., Mitchell, B. D. & Freeman, R. Diabetic autonomic neuropathy. Diabetes Care 26, 1553–1579 (2003).

336. Azpiroz, F. & Malagelada, C. Diabetic neuropathy in the gut: pathogenesis and diagnosis. Diabetologia 59, 404–408 (2016).

337. Hu, X., Viesselmann, C., Nam, S., Merriam, E. & Dent, E. W. Activity-dependent dynamic microtubule invasion of dendritic spines. J. Neurosci. 28, 13094–13105 (2008).

338. Jaworski, J. et al. Dynamic microtubules regulate dendritic spine morphology and synaptic plasticity. Neuron 61, 85–100 (2009).

339. Gu, J., Firestein, B. L. & Zheng, J. Q. Microtubules in dendritic spine development. J. Neurosci. 28, 12120–12124 (2008).

340. Peris, L. et al. A key function for microtubule-associated-protein 6 in activity-dependent stabilisation of actin filaments in dendritic spines. Nat Commun 9, 3775 (2018).

341. Cornell, B. & Toyo-oka, K. 14-3-3 Proteins in Brain Development: Neurogenesis, Neuronal Migration and Neuromorphogenesis. Front. Mol. Neurosci. 10, (2017).

342. Foote, M. & Zhou, Y. 14-3-3 proteins in neurological disorders. Int J Biochem Mol Biol 3, 152–164 (2012).

343. Welburn, J. P. I. & Cheeseman, I. M. The microtubule-binding protein Cep170 promotes the targeting of the kinesin-13 depolymerase Kif2b to the mitotic spindle. Mol. Biol. Cell 23, 4786–4795 (2012).

344. Zhang, W. et al. Modeling microcephaly with cerebral organoids reveals a WDR62-CEP170-KIF2A pathway promoting cilium disassembly in neural progenitors. Nat Commun 10, 2612 (2019).

345. Moores, C. A. & Milligan, R. A. Lucky 13 - microtubule depolymerisation by kinesin-13 motors. Journal of Cell Science 119, 3905–3913 (2006).

346. Trofimova, D. et al. Ternary complex of Kif2A-bound tandem tubulin heterodimers represents a kinesin-13-mediated microtubule depolymerization reaction intermediate. Nat Commun 9, 2628 (2018).

347. Santama, N. et al. KIF2beta, a new kinesin superfamily protein in non-neuronal cells, is associated with lysosomes and may be implicated in their centrifugal translocation. EMBO J 17, 5855–5867 (1998).

348. Ogawa, T. & Hirokawa, N. Microtubule Destabilizer KIF2A Undergoes Distinct Site-Specific Phosphorylation Cascades that Differentially Affect Neuronal Morphogenesis. Cell Rep 12, 1774–1788 (2015).

349. Noda, Y. et al. Phosphatidylinositol 4-phosphate 5-kinase alpha (PIPKα) regulates neuronal microtubule depolymerase kinesin, KIF2A and suppresses elongation of axon branches. Proc Natl Acad Sci U S A 109, 1725–1730 (2012).

350. Seira, O., Liu, J., Assinck, P., Ramer, M. & Tetzlaff, W. KIF2A characterization after spinal cord injury. Cell. Mol. Life Sci. (2019) doi:10.1007/s00018-019-03116-2.

351. Peris, L. et al. Motor-dependent microtubule disassembly driven by tubulin tyrosination. J. Cell Biol. 185, 1159–1166 (2009).

352. Gordon-Weeks, P. R. & Lang, R. D. A. The α-tubulin of the growth cone is predominantly in the tyrosinated form. Developmental Brain Research 42, 156–160 (1988).